11-5-2020 5:00 PM

The Effect of Joint Alignment After a Wrist Injury on Joint Mechanics and Osteoarthritis Development

Puneet Kaur Ranota, *The University of Western Ontario*

Supervisor: Lalone, Emily, *The University of Western Ontario*
: Suh, Nina, *The University of Western Ontario*
A thesis submitted in partial fulfillment of the requirements for the Master of Engineering
Science degree in Biomedical Engineering
© Puneet Kaur Ranota 2020

Recommended Citation

Abstract

Wrist injuries are common and can lead to the development of post-traumatic osteoarthritis. For example, one major complication after a wrist fracture, is when the fractured bone heals in a mal-aligned position, called malunion. It has been assumed that a malunion after wrist fractures alters joint congruency and mechanics leading to the development of post-traumatic osteoarthritis and poor functional outcomes. It is unclear whether anatomical restoration is a key component for the management of wrist injuries and to limit the progression of post-traumatic osteoarthritis. However, the mechanistic pathways between joint structure (and mal-alignment) and patient outcomes, such as the development of osteoarthritis and joint function, are not clearly understood due to the limitations in current techniques. The present work advances our understanding of the relationship between joint structure (and mal-alignment) and joint contact mechanics using image-based 3D measurement tools. The purpose of the present work was to employ CT imaging and inter-bone distance mapping to determine the 3D implications of a wrist fracture on 3D joint space area (a measure of joint congruency). This image-based tool was then extended to 4DCT (3DCT and time) to examine the dynamic effects of wrist movement on joint contact mechanics, in the presence of a wrist injury. This research is an important step in the quest to determine a causal relationship between joint structure and patient function.

Keywords

Summary for Lay Audience

The wrist joint consists of eight articulating carpal bones that allow for complex motions while maintaining stability. The bones and ligaments of the wrist are critical to normal function and any damage to them requires prompt evaluation and proper treatment. When wrist fractures are undetected or improperly treated, the damaged bones can heal in the wrong positions leading to significant pain, stiffness, and progress to osteoarthritis; this is called a malunion. The pathomechanics of malunions are not well understood in the literature and the clinical consequences are controversial. This makes it difficult for surgeons to decide on the best treatment plan.

Furthermore, current imaging modalities are unable to reliably detect wrist injuries because of their static nature and some patients will go on to have lifelong wrist pain and stiffness. It is thought that wrist injuries can be better visualised by having patients replicate movements causing the discomfort. Recent advances in 4D (three dimensions and time) Computed Tomography can capture the mechanical abnormalities causing the patients' symptoms. The results from this work will help investigators gain a greater understanding of the biomechanical impact of wrist fractures.

Co-Authorship Statement

Chapter 1: Introduction

      Authorship: Puneet Ranota

      Chapter Review: Emily Lalone, Nina Suh

Chapter 2: The Effect of Scaphoid Malunion on Joint Congruency

      Study Design: Ruby Grewal, Joy MacDermid, Anna Seltser

      Data Collection: Anna Seltser

      Data Analysis: Puneet Ranota

      Statistical Analysis: Puneet Ranota

      Manuscript Preparation: Puneet Ranota

      Manuscript Review: Emily Lalone, Nina Suh, Anna Seltser, Ruby Grewal

Chapter 3: Four-Dimensional Computed Tomography to Measure Distal Radial-Ulnar and Radio-Carpal Joint Congruency After Distal Radius Fractures

      Study Design: Emily Lalone, Nina Suh

      Data Collection: Puneet Ranota, Michael Riddle, Sydney Robinson

      Data Analysis: Puneet Ranota

      Statistical Analysis: Puneet Ranota

      Manuscript Preparation: Puneet Ranota

      Manuscript Review: Emily Lalone, Nina Suh

Chapter 4: General Discussion and Conclusions

      Authorship: Puneet Ranota

      Chapter Review: Emily Lalone, Nina Suh

Acknowledgments

Table of Contents

List of Tables

List of Figures

Chapter 1 – Introduction

1   *Overview*

This chapter reviews the hand and wrist anatomy and wrist kinematics. The current understanding of injuries and complications of the wrist, joint biomechanics methods and imaging techniques are discussed. This chapter concludes with the rationale, objectives and hypotheses of this thesis.

1.1   The Structure and Function of the Wrist

1.1.1   Osseous Anatomy

The wrist connects the bones of the hand to the long bones of the forearm and enables a wide range of movements. [1] This functionality requires interactions between numerous bones, tendons and ligaments making the wrist an extremely complex joint in the human body. [1] The osseous framework of the wrist consists of the distal ends of the radius and ulna, eight small carpal bones, and the proximal portions of the five metacarpal bones. [2]

The wrist joint consists of articulations between the radius, ulna, carpal bones and metacarpals. The distal radius and ulna articulate with the proximal row of carpal bones. The bones within the proximal row are loosely joined while strong ligaments tightly bind the bones of the distal row in order to provide a rigid base for the articulations with the metacarpal bones. [3] Altogether, there are 27 bones that form the hand and the wrist (Figure 1.1).
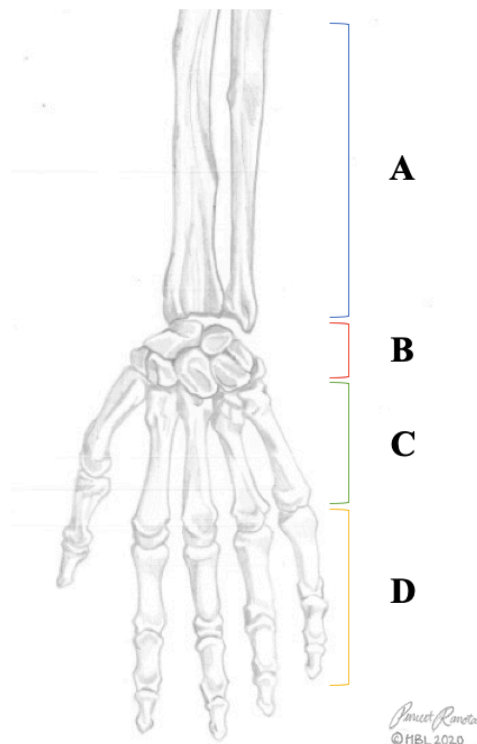
Figure 1.1: Forearm, Hand and Wrist Osseous Anatomy.
Bony anatomy of the right forearm, wrist and hand demonstrating groups of bones of interest.
(A) Radius and Ulna (B) Carpals (C) Metacarpals (D) Phalanges.

1.1.2 Forearm Anatomy

The forearm contains two long bones, the radius and the ulna that run parallel to each other. The radius is located on the lateral side of the forearm, while the ulna is on the medial side.

1.1.2.1 Radius Osteology

The radius is the first of the forearm bones (Figure 1.2). Distally, the radius articulates with the ulna, and the scaphoid and lunate carpal bones to form part of the wrist joint. The distal end of the radius consists of three articular surfaces: sigmoid notch, scaphoid facet and lunate facet. The sigmoid notch articulates with the distal ulnar forming the distal radioulnar joint. The scaphoid and lunate facet articulate with the scaphoid and lunate bones, respectively, forming the radiocarpal joint. The scaphoid and lunate fossae are separated by an interfacet prominence. [4] In addition, the lateral edge of the distal radius projects more distally forming the radial styloid process.
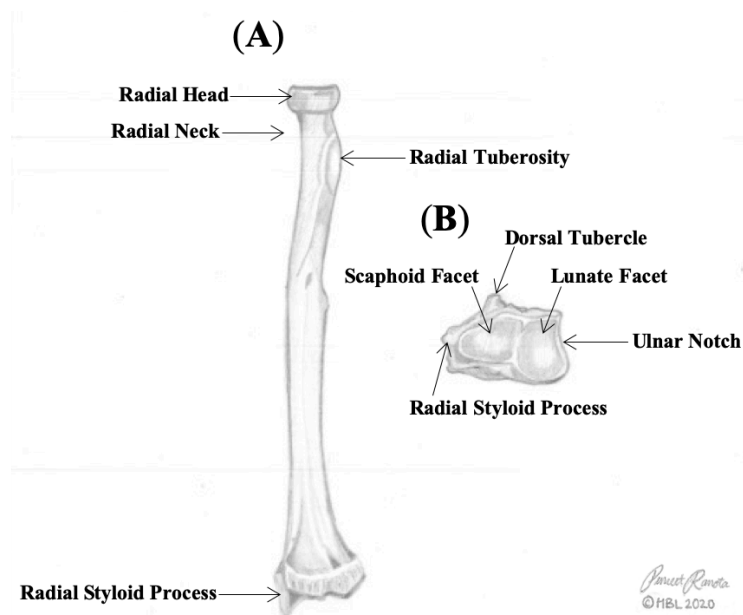
Figure 1.2: Distal Radius Osseous Anatomy.

(A) Anterior view (B) Distal articular surface

1.1.2.2 Ulna Osteology

The ulna is the second forearm bone (Figure 1.3). There are two important bone surfaces at the distal ulna: the head and the styloid process. [5] The ulnar head articulates with the radius

forming the distal radioulnar joint. The ulnar head also articulates with the triangular fibrocartilage complex, which stabilizes the ulnar aspect of the wrist. [5] The bone projection on the medial and posterior side of the distal ulna is the ulnar styloid process which is non-articular, and the origin point of the ulnar collateral ligament. [5]

(A)
Olecranon Process
Radial notch of the Ulna
Coronoid Process
Ulnar Tuberosity
Styloid Process
(B)
Ulnar Head
Ulnar Styloid Process
©HBL 2020
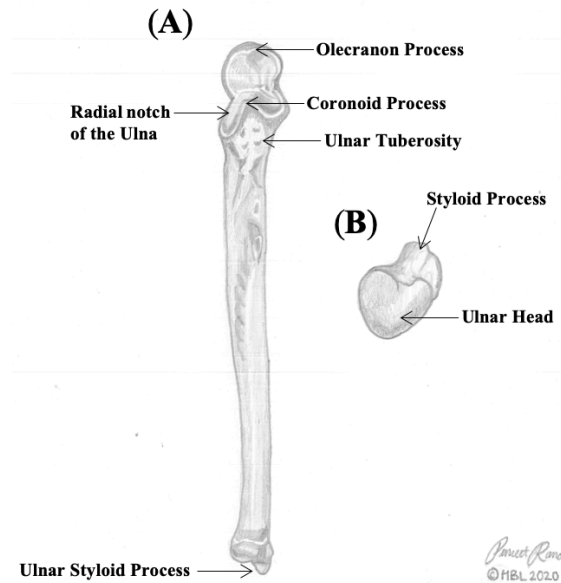
Figure 1.3: Distal Ulna Osseous Anatomy.
(A) Anterior view (B) Distal articular surface

1.1.3   Carpal Anatomy

The carpal bones connect the distal aspects of the long bones in the forearm to the bases of the metacarpal bones of the hand (Figure 1.4). [6] The eight carpal bones are divided into two rows forming a proximal row of four carpal bones and a distal row of four carpal bones. [6] The bones in the proximal carpal row are the scaphoid, lunate, triquetrum and pisiform. The carpal distal row bones are the trapezium, trapezoid, capitate, and hamate.
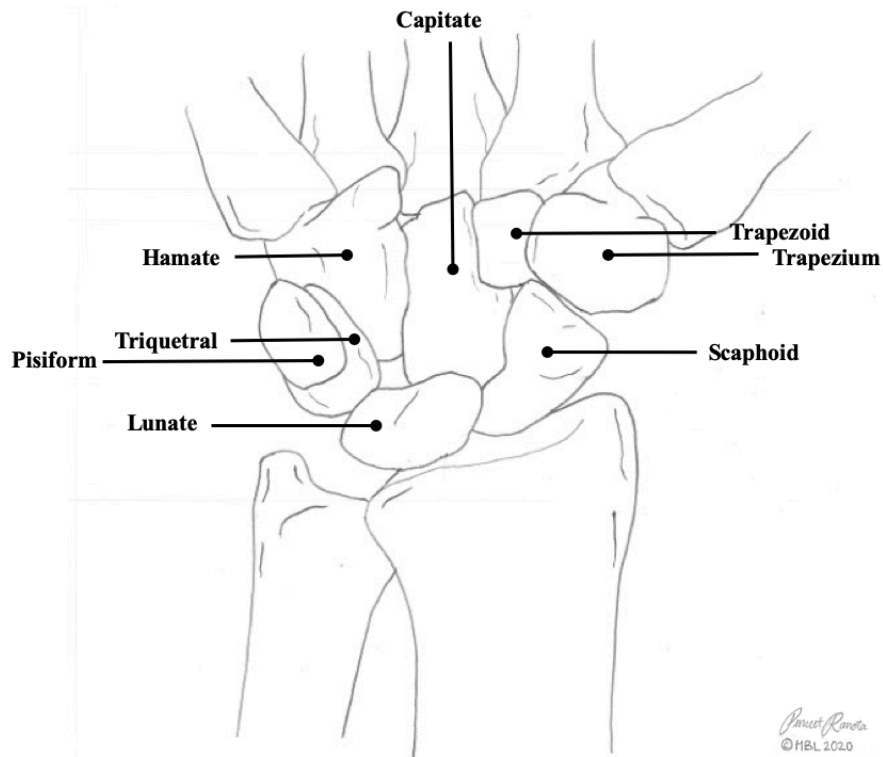
Figure 1.4: The Carpus Osseous Anatomy.
Anterior view of the carpus, with all eight carpal bones labeled.

1.1.3.1   Scaphoid Osteology

The scaphoid is the largest of the carpal bones in the proximal carpal and provides a stabilizing link between the proximal and distal carpal rows (Figure 1.5). [6] As a result, it receives most of the force transmitted through the radius and is frequently fractured in falls. [7] The scaphoid consists of cartilage forming an articular surface that covers 80% of its surface and allows it to facilitate articulations with five surrounding bones (distal radius, capitate, lunate, trapezium and trapezoid). [8] These articulations include: the proximal surface articulating with the scaphoid fossa of the distal radius forming the radioscaphoid joint; the ulnar facet of the scaphoid articulates with the lunate at the scapholunate joint; the distal ulnar aspect of the scaphoid articulates with the capitate forming the scaphocapitate joint; the distal aspect of the scaphoid is divided by a sagittal ridge separating the articulations between the trapezium laterally and trapezoid medially forming the scaphotrapeziotrapezoid joint. [8] On the palmar aspect of the bone between the proximal and distal articular surfaces, there is a rounded prominence called scaphoid tubercle that provides an attachment point for the radioscaphocapitate and scaphotrapezial trapezoid ligaments as well as a pivot point for the flexor carpi radialis tendon.
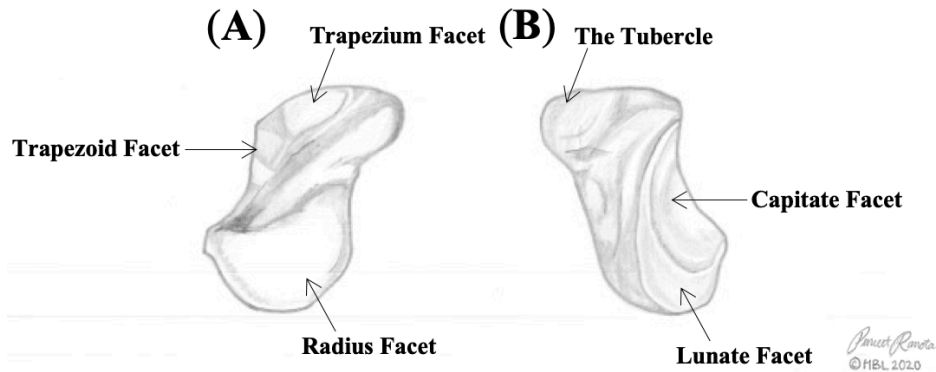
Figure 1.5: Scaphoid Anatomy.

Bony anatomy of the left scaphoid with associated landmarks. (A) Anterior View (B) Dorsal View

1.1.3.2   Lunate Osteology

The lunate has often been described as the keystone bone of the carpal bones (Figure 1.6). [8] It is located between the scaphoid and triquetrum in the proximal row and its ligamentous attachments play a critical role in stabilizing the proximal row. It has a moon-shaped configuration, where the palmar aspect is larger than the dorsal aspect. [8] Two types of lunates have been classified based on their midcarpal articulations. [9] The type I lunate has a single distal facet for the capitate and does not articulate with the hamate. [9] The type II lunate has two distal facets: the radial facet articulates with the capitate and the ulnar facet with the hamate. [9]
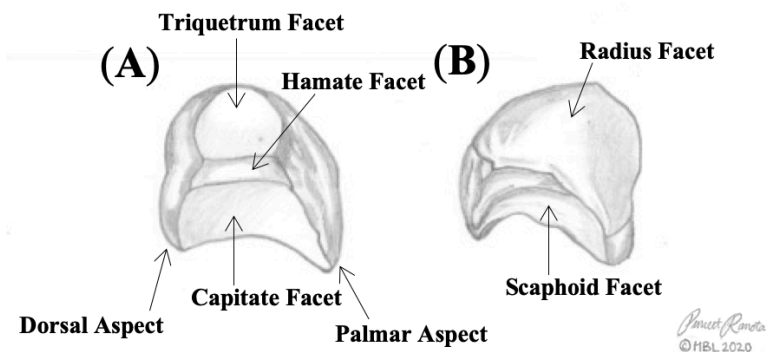
Figure 1.6: Lunate Anatomy

Bony anatomy of a left lunate with associated landmarks. (A) Inferomedial View (B) Superolateral View

1.1.3.3   Trapezium Osteology

The trapezium is on the radial side of distal carpal row, interposed between the scaphoid and the first metacarpal bone (Figure 1.7). [10] Its saddle-shaped surface articulates proximally with the scaphoid, medially with the trapezoid, and distally with the metacarpal of the thumb. [10]
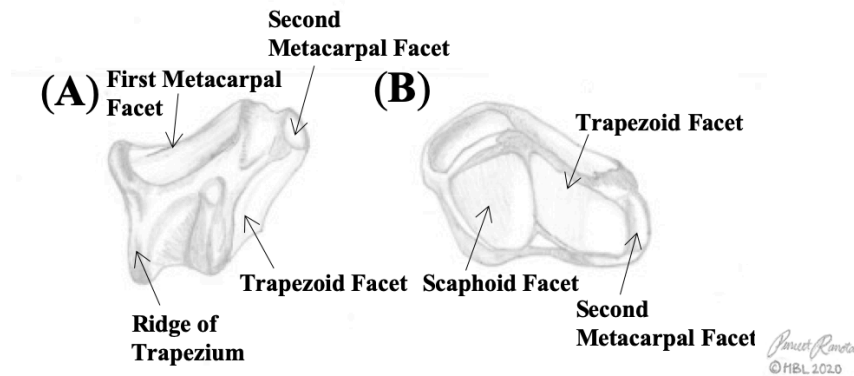
Figure 1.7: Trapezium Anatomy

Bony anatomy of a left trapezium with associated landmarks. (A) Palmar View (B) Superolateral View

1.1.3.4   Trapezoid Osteology

The trapezoid is the smallest bone in the distal carpal row, interposed between the trapezium and the capitate (Figure 1.8). Its wedge-shaped surface articulates with four bones: proximally with the scaphoid, distally with the second metacarpal, laterally with the trapezium, and medially with the capitate. [10]
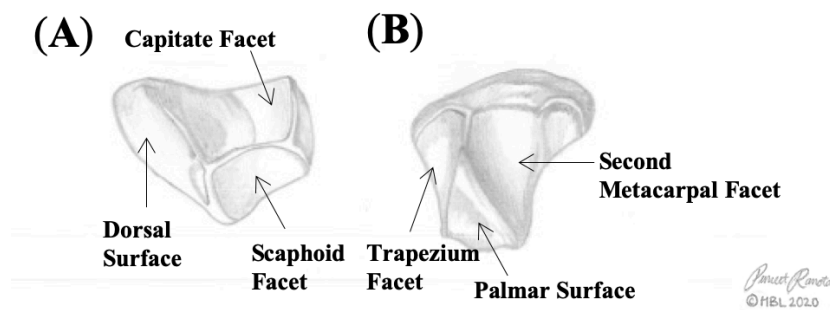
Figure 1.8: Trapezoid Anatomy

Bony anatomy of a left trapezoid with associated landmarks. (A) Superomedial View (B) Palmar View

1.1.3.5   Capitate Osteology

The capitate is the largest carpal bone and occupies the center of the wrist in the distal carpal row (Figure 1.9). [10] The axis of rotation for all wrist movements passes through the capitate. [3] The capitate articulates with eight surrounding bones: proximally with the scaphoid and lunate, distally with the second and third metacarpal and smaller articulations with the second and fourth metacarpal, laterally with the trapezoid, and medially with the hamate. [10]
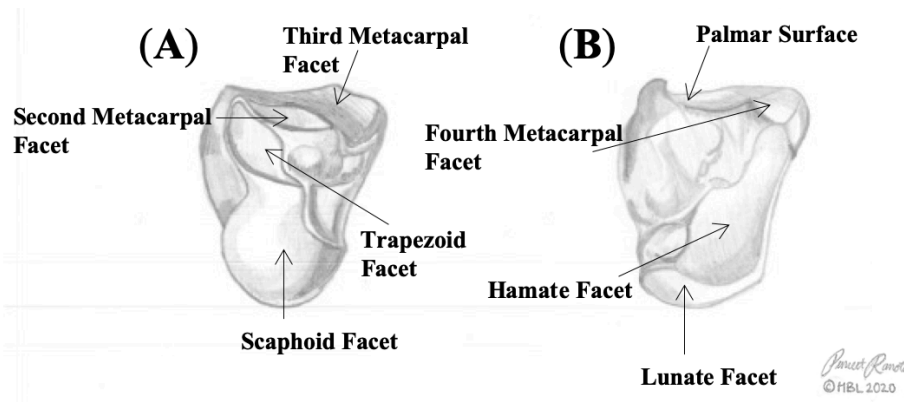
Figure 1.9: Capitate Anatomy

Bony anatomy of a left capitate with associated landmarks. (A) Lateral View (B) Medial View

1.1.4   Soft Tissue Anatomy

Wrist joint control and stability is ensured through the relationship between static and dynamic joint stabilizers. [11]

1.1.4.1   Static Stabilizers

The ligaments of the wrist are divided into extrinsic and intrinsic ligaments. Both the intrinsic and extrinsic wrist ligaments have a static function in joint stability. [11] The extrinsic ligaments are situated outside the carpus, attaching the distal radius and ulna to the carpal bones. Whereas, the intrinsic wrist ligaments are situated within the carpus, attaching the carpal bones to each other.

The extrinsic ligaments include volar radiocarpal ligaments, volar ulnocarpal ligaments, and dorsal radiocarpal ligaments (Figure 1.10). These ligaments connect the distal radius to the carpal bones which stabilize the radiocarpal joint. [12] The volar radiocarpal ligament complex is composed of the short radiolunate, long radiolunate, radioscaphocapitate, and radioscapholunate ligaments. The short and long radiolunate ligaments originate on the ulnar aspect of the radius and

insert onto the lunate. The role of the long radiolunate is to limit ulnar or distal translocation of the lunate. [12] The radioscaphocapitate ligament originates at the radial styloid and inserts on the scaphoid and proximal capitate. This ligament runs in parallel with the long radiolunate ligament, and forms an empty space, called the space of Poirier that may predispose the wrist joint to instability. [12] Lastly is the radioscapholunate ligament, which does not provide structural support, but it does serve as a channel for vasculature to the lunate, and damages may lead to avascular necrosis. [12]

The intrinsic ligaments include the proximal row ligaments (scapholunate, and lunotriquetral ligaments) and the distal row ligaments (trapeziotrapezoid, trapezocapitate, and capitohamate ligaments). [13] Injuries to the proximal row ligaments are a common cause of wrist pain and instability. [14] The radiocarpal joint is dorsally spanned by the dorsal radiocarpal ligament. [15] This ligament originates on the dorsal surface of the radius and inserts on the lunate and triquetrum. The role of this ligament is to provide dorsal stabilization to the scaphoid during normal carpal kinematics. [16]
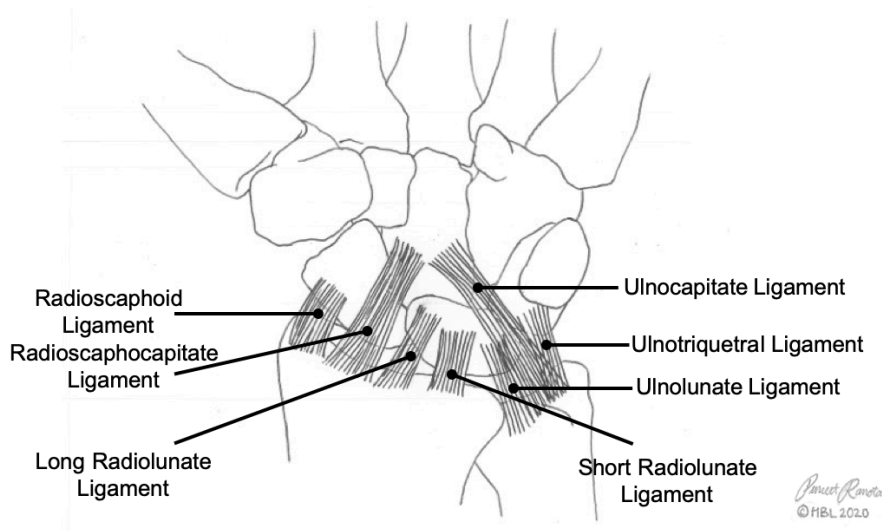
Figure 1.10. Extrinsic Ligaments of the Wrist.
Schematic of the extrinsic ligaments on the palmar side of the wrist.

1.1.4.2   Dynamic Stabilizers

Dynamic contribution towards joint stability includes the muscles and tendons that cross the wrist joint structures. [11] Many of the muscles of the flexor and extensor compartments of the forearm cross the radiocarpal joint and affect the motion and stability of the joint. [12] Wrist

extension is produced mainly by the dorsal muscles of the wrist which are the extensor carpi radialis longus and brevis, and extensor carpi ulnaris, with assistance from the extensor digitorum. [17] Wrist flexion is produced mainly by the dorsal muscles of the wrist which are the flexor carpi ulnaris, flexor carpi radialis, with assistance from the flexor digitorum superficialis. [17]

1.1.5   Joint Anatomy

A two-layered capsule covers the articulation of the osseous and soft tissue structures mentioned above. [18] The outer portion of the capsule is composed of fibrous connective tissue which provides structural support. [18] The inner layer is a synovial membrane that secretes synovial fluid to keep the joint lubricated. [18] When all the components are functioning in unison with the wrist joints, an ellipsoidal (condyloid) joint is formed allowing for varying degrees of flexion, extension, abduction, and adduction movements. [19] The three wrist joints of interest include the distal radioulnar, radiocarpal, midcarpal joints. The ulna articulates with the radius as the distal radioulnar joint (Figure 1.11). The scaphoid and lunate articulate with the radius as the radioscaphoid and radiolunate joints making up the radiocarpal joint (Figure 1.11). The midcarpal joint separates the proximal and distal rows of carpal bones. The trapezium and trapezoid articulate with the scaphoid as the scapho-trapezium and scapho-trapezoid joints, which are parts of the midcarpal joint. A large range of motions occur at the radiocarpal and midcarpal joints; the scaphoid and the lunate bones are both important members of both wrist articulations.
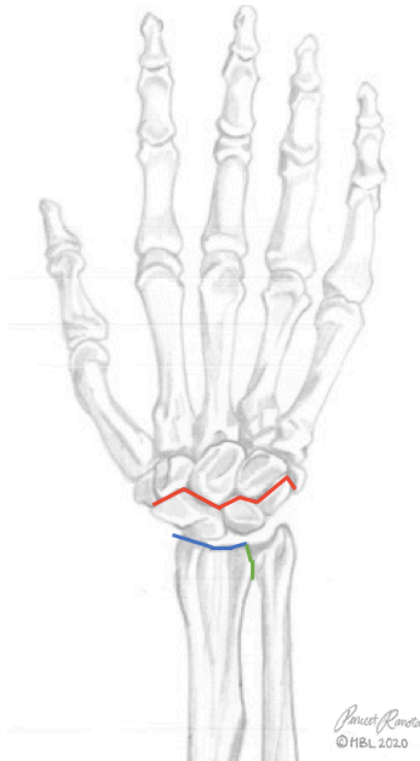
Figure 1.11. Radioulnar, Radiocarpal and Midcarpal Wrist Joints.

Dorsal view of the left wrist showing the distal radioulnar (green line), radiocarpal (blue line) and midcarpal (red line) joints.

1.1.6   Biomechanics

Studies investigating the force transmission across the wrist at neutral position and neutral forearm rotation, show that approximately 80% of the force is transmitted across the radiocarpal joint and 20% across the ulnocarpal joint. [20] The radiocarpal force can be further subdivided into that across the radioscaphoid joint (61.1%) and that across the radiolunate joint (38.9%). [21] Forces across the mid-carpal joint are estimated to be distributed at 23% through the scaphoid-trapezium-trapezoid joint, 28% through the scaphoid-capitate joint, 29% through the lunate-capitate joint, and 20% through the triquetrum-hamate joint. [22] Furthermore, wrist positions and movements influence load transmission across the wrist. However, wrist flexion has little impact on force transmission distribution across the wrist compared to the impact of forearm pronation/supination and ulnar deviation/radial deviation. [19]

11

1.1.7   Range of Motion

The wrist is capable of different range of motions such as wrist flexion and extension, wrist radial and ulnar deviation, forearm supination and pronation.

1.1.7.1   Wrist Extension and Flexion

One anatomically defined motion is wrist extension (raising the back of the hand) and flexion (bending the palm down) (Figure 1.12). Extension and flexion occur between the radiocarpal and midcarpal articulations and previous studies have demonstrated that more motion occurs at the radiocarpal articulation. [23,24] As the wrist extends, there is a tendency for the scaphoid to supinate and the lunate to pronate, which effectively separates the palmar surfaces of the 2 bones; the reverse phenomenon occurs during wrist flexion. [19] On average, from a neutral (0-degree) position, the wrist flexes approximately 70 to 80 degrees and extends approximately 60 to 75 degrees, for a total of approximately 130 to 155 degrees. [25] Total flexion normally exceeds extension by approximately 15 degrees. [25]
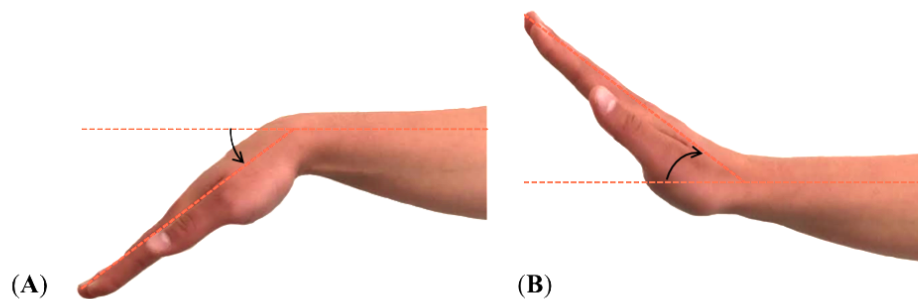
Figure 1.12. Extension/Flexion Range of Motion.

The wrist joint in flexion (A) and extension (B) motion (Image reproduced with permission from Clare Padmore).

1.1.7.2   Wrist Radial and Ulnar deviation

Another anatomically defined motion is wrist radial (bending the wrist to the thumb) and ulnar deviation (bending the wrist to the little finger) (Figure 1.13). The wrist joint is more ulnarly deviated during daily activities such as holding and carrying objects, and the lunate bears a greater load than the scaphoid. [26] A literature review found that the radial and ulnar deviations ranged from 14.5 – 50.9° and 25.0 – 66.1°, respectively, depending on the position of the arm. [27]

(A)   **(B)**
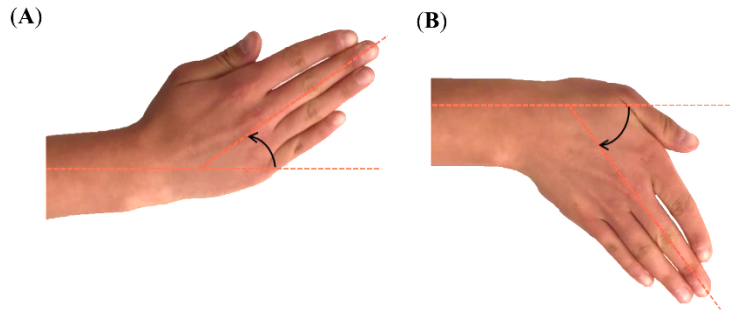
Figure 1.13. Radial/Ulnar Deviation Range of Motion.

The wrist joint in radial (A) and ulnar (B) deviation motion (Image reproduced with permission from Clare Padmore).

1.1.7.3   Forearm Pronation and Supination

Pronation (palm down) and supination (palm up) is a rotational motion that exist exclusively in the forearm (Figure 1.14). [28] Pronation and supination are achieved through the distal radioulnar joint (DRUJ), which allows the radius to rotate around a nearly fixed ulna. [28] The reported rotational range during pronation and supination is between 150° and 190°. [31,32] Additionally, the average rotation angle of the radius at maximum pronation is 66.1° and at maximum supination is 75°. [31,32]

(A)   **(B)**
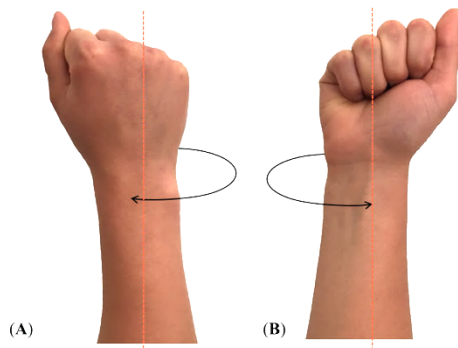
Figure 1.14. Pronation/Supination Range of Motion.

The wrist joint in pronation (A) and supination (B) motion (Image reproduced with permission from Clare Padmore).

1.1.7.4   Dart-Throwing Motion

The functional oblique motion of the wrist is the dart-throwing motion (DTM), from radial deviation-extension to ulnar deviation-flexion (Figure 1.15). [33] Most daily activities are performed using a DTM involving tool use, throwing, and weaponry that also may have played an important role in human evolution. [33] This motion is called DTM because it is similar to the act of throwing a dart, and was stated to be functional and natural. [34] The range during the DTM depends on the motion planes, with a maximum at around the motion plane of 45° from the sagittal plane (45° of pronation). [35] Most of the carpal kinematic data, however, has been measured, *in vitro* or *in vivo*, during pure wrist flexion/extension or pure wrist radial/ulnar deviation. [23,36,37] The movement of the scaphoid and lunate during a dart throw motion are poorly understood. [33]

(A)   (B)
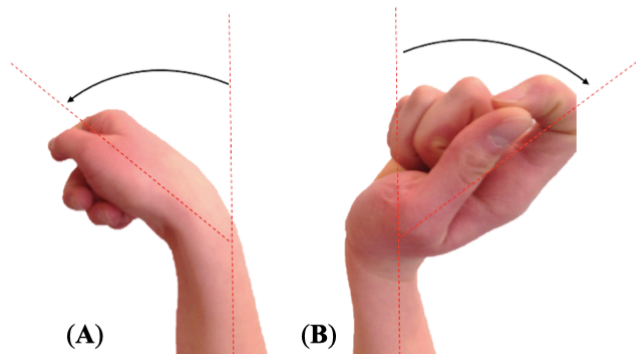
Figure 1.15. Dart-Throwing Range of Motion.
The wrist joint in forward dart-thrower (A) and reverse dart-thrower (B) motion (Image reproduced with permission from Clare Padmore).

1.2   Injuries and Complications of the Wrist

1.2.1   Scaphoid Fractures

The scaphoid plays a major role in maintaining carpal stability. [38] It provides a mechanical link between the distal and proximal carpal rows and transfers compression loads from the hand to the forearm. [38] Scaphoid fractures are the most common carpal bone fracture, representing 60-70% of carpal bone fractures and 2-7% of all fractures. [39] Scaphoid fractures can escape early detection because in many cases they are subtle, and the initial symptoms are minimal. Missed scaphoid fractures have a high risk of non-union or malunion. [40]

1.2.1.1   Mechanism of Fracture

A scaphoid fracture occurs most often after a fall onto an outstretched hand which forces the wrist into hyperextension and radial deviation and applies an axial load on the wrist. [41] Most of the force transmits through the scaphoid making it prone to injury since the scaphoid acts as a hinge in stabilizing the wrist joint. [42] Athletic injuries and motor vehicle accidents are also common causes of scaphoid fractures. [41]

1.2.1.2   Demographics

Scaphoid fractures predominantly affect young active individuals, with a mean age of 29 years. [43] The incidence of scaphoid fractures is higher in males compared to females. [44] Scaphoid fractures are rare in the pediatric and elderly populations where the distal radius is more likely to fracture. [45]

1.2.1.3   Diagnosis

One indication of a possible scaphoid fracture is anatomic snuffbox tenderness, which is a highly sensitive (85.71%), but it is nonspecific (29.62%). [46] Another indication is the scaphoid tubercle tenderness, which provides more diagnostic information with a similar sensitivity (95.23%) to the anatomic snuffbox tenderness test, but it is more specific (74.07%). [46] The lack of tenderness of the anatomic snuffbox and scaphoid tubercle makes a scaphoid fracture highly unlikely. [47]

There are several diagnostic modalities to assess a patient with a suspected scaphoid fracture. These include radiographs, computed tomography (CT), magnetic resonance imaging, bone scintigraphy and sonograms. [48–51] Scaphoid fractures are often missed with the use of radiographs alone and suspected scaphoid fractures are confirmed with CT scans, which are used in the decision-making process concerning whether to operate on scaphoid fractures. [50,52]

1.2.1.4   Treatment

The aim of the treatment is to achieve anatomical restoration and functional recovery while avoiding complications such as non- or mal-union. [53] Treatment options consist of a splint, cast immobilisation, and operative treatment depending on the fracture's severity and location. [53]

1.2.1.5   Complications

Displaced or unstable fractures are prone to non-union and mal-union if not reduced and stabilized. [54] This can lead to instability, arthrosis and collapse of the carpal joint. [53] Other potential complications include limited mobility, decreased grip strength, avascular necrosis, and osteoarthritis. [53] Scaphoid non-union advanced collapse (SNAC) and scapholunate advanced collapse (SLAC) are common patterns of post-traumatic wrist arthritis which are the end-stage result of progressive instability and abnormal joint kinematics. [55,56]

1.2.1.5.1   Scapholunate advanced collapse

Scapholunate advanced collapse (SLAC) is a common degenerative condition of the wrist. [57] SLAC wrist is often the terminal result from an untreated dorsal intercalated segment instability (DISI) deformity as a result of a long-standing scapholunate ligament injury. [56] Watson and colleagues described a four-stage progressive pattern of arthrosis. [56] Stage 1 demonstrates radial styloid degenerative changes. Stage 2 is represented by degenerative changes that involve the scaphoid fossa and the styloid. Stage 3 includes lunocapitate degenerative changes. Lastly, stage 4 is represented by pancarpal arthrosis with preservation of the radiolunate joint, but the degenerative changes in this stage are debated.

1.2.1.5.2   Scaphoid non-union advanced collapse

Scaphoid non-union advanced collapse (SNAC) are arthritic changes in the wrist that develop after a scaphoid fracture that has progressed to a scaphoid non-union. [58] SNAC is initially limited to the radial styloid and then it affects the radius scaphoid fossa and the midcarpal joint, but the radioulnar joint is spared due to its relatively spherical shape. [59] Vender and his colleagues discovered that the degenerative changes occur in a different pattern from the SLAC wrist and coined the term SNAC. [60] Vender and his colleagues described the arthritic changes in three stages. [60] The first stage is represented by degenerative changes at the interface between the radius scaphoid fossa and the fractured scaphoid distal fragment interface. The second stage is represented by degenerative changes at the interface between the fractured scaphoid proximal fragment and the capitate. The third stage is represented by degenerative changes at the radius-scaphoid, scaphoid-capitate and lunate-capitate interfaces. Additionally, the interface between the fractured scaphoid proximal pole and radius is often spared. The difference

between SNAC and SLAC wrist is that the articulation between the proximal pole of the scaphoid and the radius is spared in SNAC wrists. [61]

1.2.2 Scaphoid Malunions

A scaphoid malunion results when a scaphoid fracture heals in a flexed position or when a scaphoid non-union with carpal collapse is grafted without correction of the angular deformity. [62] Unstable fractures at the waist of the scaphoid may fall into a 'humpback' deformity which occurs when the distal segment flexes and the proximal segment extends. [63] The humpback deformity of the scaphoid can cause dorsal rotation of the lunate together with the proximal scaphoid fragment which is referred to as the dorsal intercalated segment instability (DISI). [64] The resulting scaphoid height loss, flexion, and potential DISI deformity can lead to abnormal wrist biomechanics. [65–67]

1.2.2.1 Scaphoid 'Humpback' Deformity Measurements

Radiographs are commonly used by clinicians to assess the scaphoid 'humpback' deformity, but it can be difficult to visualize and thus radiographs are not a reliable diagnostic approach. [68,69] Computerized axial tomography (CT scans) through the longitudinal axis of the scaphoid are used to measure the humpback deformity. The three measuring techniques are the following: lateral intrascaphoid angle, the dorsal cortical angle, and the height-to-length ratio. The intra- and interobserver reliability was the best for the height-to-length ratio and worst for the intrascaphoid angle. [70] Therefore, the height-to-length ratio is the most reproducible method of assessing the humpback deformity. [70] The ratio was calculated by dividing the height by the length. [70] The length of the scaphoid was measured from the most proximal to the most distal aspect of the scaphoid using a baseline along the volar aspect of the scaphoid. [70] The maximum height of the scaphoid was measured on a line perpendicular to the baseline (Figure 1.16). [70] The height-to-length ratio, however, has not been shown to be correlated with clinical outcome measures of scaphoid fractures. [70]
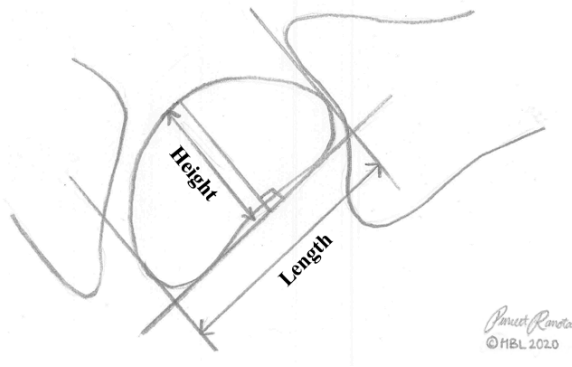
Figure 1.16. Height-to-Length Ratio.
A baseline is drawn along the volar aspect of the scaphoid. The length of the scaphoid is parallel to the baseline and the height is perpendicular to the baseline.

1.2.2.2   Long-Term Outcomes of Scaphoid Malunion

The pathomechanics of scaphoid malunions are not well understood and the clinical consequences are controversial. As the carpal bones are closely inter-connected, the alignment of one, in theory, can affect the kinematics and joint loading of the adjacent carpal bones. This occurrence can potentially lead to pain, limited range of motion, and abnormal cartilage wear. A review study confirmed that patients with scaphoid malunions seem to have a higher likelihood of post-traumatic arthritis, but the clinical implications of malunion are not completely understood. [71] Furthermore, Amadio et al. used trispiral tomography and reported that 27% of patients with a lateral intrascaphoid angle (LISA) greater than 45° had satisfactory outcome, but 54% of cases in the malunion group demonstrated post-traumatic arthritis. [72] Additionally, Jiranek et al. found that patients who healed with a LISA greater than 45° had high subjective functional scores, but low objectives scores based on radiographs (range of motion and grip strength). [73] The validity of these findings is questionable because of the poor reproducibility of using LISA to assess a scaphoid malunion. [63,74,75]

Studies have found that the scaphoid alignment assessed by the H/L ratio demonstrated little effect on clinical outcomes. [76,77] More specifically, Forward et al. identified scaphoids treated conservatively for 1 year with a H/L ratio greater than 0.6 as the malunion group, and compared them to a group with an H/L ratio of less than 0.6; they found no significant difference in the clinical outcomes between the groups. [76] While this relationship has been investigated in the biomechanical literature, previous studies describing the clinical impact of malunion are controversial.

Patients with scaphoid malunion present with limited wrist extension due to the flexion and shortening of the malunited scaphoid ('humpback' deformity) and require a corrective osteotomy procedure. [78] Multiple case reports have indicated good outcomes after a corrective osteotomy procedure [72,79–83]; however, these studies were limited to a small case series and had short follow-ups. [72,79–83] Other studies have found no correlation between scaphoid malunion and clinical outcomes. [63,76,84–86] There is no clear consensus in the literature, therefore, regarding what degree of scaphoid deformity or carpal malalignment can be tolerated without clinically compromising wrist function.

1.2.3 Distal Radius Fractures

Distal radius fractures are common upper extremity fractures accounting for 75% of all forearm fractures. [87] The two common types of distal radius fractures are Colles' and Smith's fractures which are characterized by the forces applied to the wrist during the injury. [88] The Colles' fracture occurs when the hand is extended backward on the wrist with characteristic dorsal tilt, dorsal shift, radial tilt and radial shift of the distal fragment. [89] The Smith's fractures, also referred to as a "reverse Colles' fracture", occurs when the hand is flexed forward under the wrist with characteristic palmar tilt of the distal fragment. [89]

1.2.3.1 Mechanism of Fracture

A distal radius fracture occurs most often after a fall onto an outstretched hand. Older adults with osteoporotic bone and poor postural stability suffer from these fractures after a low-energy fall onto an outstretched hand from a standing or seated position. [90] Children and young adults suffer from these fractures after a high energy falls on the playground or at sporting events. [91] Furthermore, distal radius fractures account for 23% of all sports-related fractures in adolescents. [92]

1.2.3.2 Demographics

Distal radius fractures accounting for approximately 25% of fractures in the pediatric population and approximately 18% of fractures in the senior population. [87,93] The incidence of distal radius fractures has increased worldwide over the past 40 years, almost doubling in certain populations. [87] The increase in the prevalence of this injury may be due to the growth of the elderly population or a greater number of active seniors. [94]

1.2.3.3   Diagnosis

A physical exam, patient history, and imaging are typically utilized to diagnose a distal radius fracture. The physical exam evaluates the gross deformity (general appearance of the distal extremity) and focuses on ruling out complications such as compartment syndrome or neurovascular issues. [88] Imaging includes initial and follow-up x-rays and CT scans for complex or occult fractures to assess the alignment or fragmentation of the joint surface. [88,95] The x-ray examinations include evaluating the radial height, radial inclination, radial shift, volar tilt, ulnar variance, ulnar styloid fracture, and DRUJ widening. [88]

1.2.3.4   Treatment

Closed reduction (plaster splint or cast) and cast immobilization is the primary management strategy for DRFs. [96] In unstable fracture patterns, where fracture reduction cannot be maintained with cast immobilization and thus leads to malunion in more than 50%, additional fixation is recommended (plates, screws, pins). [97,98]

1.2.3.5   Complications

The type and frequency of complications differs among variants of distal radius fractures. McKay et al. found overall complication rates vary from 6% to 80% and rates of post-traumatic arthritis ranging from 7% to 65%. [99] The most frequent complication after distal radius fractures is malunion. [100] Other complications include tendon irritation and rupture, nerve injury, non-union, pain syndromes, loss of reduction, and post-traumatic osteoarthritis. [101]

1.2.4   Distal Radius Malunion

Malunion of the radius is defined as a mal-alignment associated with dysfunction. [102] More specifically, malunion occurs when a fracture heals with improper alignment, articular incongruity, incorrect length, or a combination of these elements leading to deformity, motion range limitation, pain and loss of strength. [103–105] A malunited distal radius fracture can be extra-articular or intra-articular and can cause severe functional impairments. [104] Extra-articular malunions are commonly the result of non-operative management and are characterized by a loss of the normal palmar tilt of the articular surface in the sagittal plan, a loss of ulnar inclination in the frontal plane, and a loss of length relative to the ulna. [104,106] Whereas, intra-articular malunions are associated with a step-off or a gap at the radiocarpal joint and/or the distal

radioulnar joint as a result of insufficient reduction and fixation in surgical treatment. [104,106] Therefore, early surgical correction of an intra-articular malunion should be pursued to restore the integrity of the joint before the onset cartilage damage. [106]

1.2.4.1   Radiographic Evaluation

A suspected malunion is confirmed using radiographs and verified with specific criteria used to define a malunion. The guidelines written by the American Society for Surgery of the Hand (ASSH) [107] used to designate radiographic alignment as unacceptable are:

1. Radial inclination <15 degrees

2. Volar tilt > 20 degrees, dorsal tilt > 10 degrees

3. Ulnar variance ≥ 3 mm

Surgical correction is strongly recommended for patients presenting with both clinical and radiographic symptoms of a malunion. [103]. A corrective osteotomy is strongly considered for patients presenting with angulation of the distal articular surface of the radius greater than 25 degrees in the sagittal plane. [108]

1.2.4.2   Long-Term Outcomes of Distal Radius Malunion

Previous studies that have examined the relationship between a distal radius malunion and functional outcomes demonstrate conflicting results. Some authors have produced evidence supporting a link between anatomic restoration and function after fracture [109–111], but other authors have shown that precision of fracture reduction has no predictive value on post-fracture wrist function. [112,113] Studies even demonstrated satisfactory function regardless of radiographic deformity, commonly seen in the elderly. [114–116] A previous study reported that patients have a higher risk of prolonged disability (arm-related) when mal-alignment and degenerative changes occur [117]; conversely, another study has indicated that a large amount of radiographic deformity is required before functional impairment occurs. [118] Consequently, the clinical evidence linking incongruity to post-traumatic arthritis is inconclusive.

Radiographic degenerative changes are frequently reported in patients who have suffered a DRF. Previous studies have shown no correlation between anatomically reduced fractures (according to standard radiographic measures on the radial height, radial inclination, volar tilt, etc.) and good functional outcomes or increased patient satisfaction. [119,120] Alternatively, other

studies have indicated that radiographic measurements do correlate with functional outcomes. [121–123] The long-term clinical impact of distal radius fractures, therefore, has not been clearly defined in the literature.

Distal radius fractures that heal with a positive ulnar variance alter joint loading of the wrist and has been shown to affect subjective outcome, grip strength, and ROM. [124,125] Dorsal tilt may alter the force distribution in the radiocarpal joint, increasing the load through the ulna, and may result in midcarpal instability. [126] Furthermore, dorsal tilt has been associated with decreased grip strength, persistent pain, and increased difficulties with daily activities. [110,111] Another study suggests that the combination of a substantial dorsal tilt and positive ulnar variance appears to cause the persistent disability. [127] The relationship between distal radius malunions and persistent long-term pain and disability, however, needs to be further examined.

1.3   Joint Contact Mechanics of the Wrist

1.3.1   Joint Surface Area in Normal Wrists

Previous studies have shown that changes in the joint contact mechanics are closely associated with the motion of carpal bones. [36,128–130] At all wrist positions, *in vivo* and *in vitro* studies have found that the scaphoid contributed a greater extent to wrist motion compared to the lunate. [131–133] But there is still no consensus regarding the role of each joint to the wrist motion. A more detailed understanding of normal carpal kinematics during continuous wrist motion is necessary.

1.3.2   Joint Surface Area in Malunited Scaphoid Wrists

The biomechanical understanding of scaphoid malunions is not extensively investigated. To examine the effects of scaphoid malunion on wrist motion, a single in vitro cadaveric study had been performed. [134] The authors analyzed simulated scaphoid malunions in four cadaveric specimens [134]. This study found that the loss of wrist extension was proportional to the angular deformity, where the loss of radiocarpal extension occurred at 15° of angulation and loss of midcarpal extension occurred at 30° of angulation. [134] Other studies have measured *in vivo* kinematics after a scaphoid non-union using static three-dimensional (3D) and dynamic four-dimensional (4D) imaging. [135–137] An *in vivo* study is necessary to further investigate into joint mechanics during wrist motion after a scaphoid malunion.

1.3.3   Joint Surface Area in Malunited Distal Radius Wrists

In vivo studies demonstrate conflicting results on the effect of distal radius malunion on the kinematics of DRUJ during forearm rotation. One study demonstrated that distal radius malunion did not alter the kinematic pattern of the DRUJ during forearm rotation, and the range of motion was not limited by bony impingements at the sigmoid notch. [138] This study concluded that altered DRUJ kinematics was not the primary cause of distal radioulnar dysfunction. [138] Another study demonstrated that joint space area (JSA) at the DRUJ was significantly smaller and located more proximally in the malunited wrists compared to contralateral uninjured wrists. This study concluded that DRUJ congruency and mechanics were altered in patients with malunited distal radius fractures. [29] Another study revealed no change in the JSA and locations of contacting regions at the radiocarpal joints when comparing the injured and non-injured wrists. [139] These previous studies were limited to static 3D imaging and a small case series. Additionally, it is still unclear whether altered congruency and mechanics of the DRUJ and radiocarpal joints is a major contributor to early signs of wrist osteoarthritis. A previous study also demonstrated the extension-flexion arc of motion can be limited due to the osseous deformity seen in distal radius mal-alignment that results in abnormal load transmission. [140] Future work investigating the mechanism of joint mechanics in patients with distal radius malunion during functional range of motions using dynamic 4DCT imaging is required.

1.4   Experimental Methods of Assessing Joint Contact

1.4.1   Direct Methods

Initial techniques for evaluating and quantifying the contact area in articulating joints were direct approaches. Such approaches rely on invasive procedures and are limited to inferring motion from static positions. Three techniques will be discussed: first, the silicone casting technique is known as the gold standard by which to study joint contact area. [141] This technique consists of a cement injection within the articular surface, and the areas lacking the dried cement are the joint contact areas; the injection of cement is invasive, since it requires sectioning of the surrounding capsule and soft tissue. While directly accessing the joint, the magnitude and orientation of contact can alter, resulting in an inaccurate representation of native joint contact mechanics. This procedure is also time-consuming, due to the setting time of cement; second, pressure-sensitive films involve the insertion of a film into the joint, whereby the joint is loaded in a single position that applies pressure and produces a stain; the intensity of the stain is then

calibrated to the magnitude of pressure. Previous studies have used this technique to assess the distribution and magnitude of pressures in the radiocarpal joint [142,143]; third, dynamic pressure-sensitive film provides real-time contact data throughout a range of motion. Previous studies have examined real-time contact data in the radiocarpal joint [144] and DRUJ. [145,146] The second and third techniques are limited by the invasive introduction of the film that can produce overestimated pressure recordings due to artifacts (crinkling, sliding and shear stress) and inherent thickness of the film.

1.4.2   Indirect Methods

Indirect approaches non-invasively study joint contact area using Computed Tomography (CT) and Magnetic Resonance (MR) imaging volumetric datasets. [147,148] This approach involved identifying overlapping pixels in each slice in order to measure the contact area [149]; it was not only time-consuming, but also used two-dimensional (2D) slices which can introduce errors when anatomically complex structures are examined. Proximity mapping was then introduced to measure 3D joint congruency and mechanics. The volumetric data acquired from CT imaging are used to generate 3D bone reconstructions of the articulating joints and create proximity maps using software algorithms. [150] The joint contact mechanics are defined by the Joint Space Area (JSA) measurements based on the assumption that regions at a lower inter-bone distance are the same regions that are most likely in contact (high proximity). This previously developed inter-bone distance algorithm was initially developed for *in vitro* cadaveric testing and has been validated against a gold standard. [151] This algorithm has been used in several subsequent *in vitro* and *in vivo* studies investigating shoulder, elbow, and wrist contact mechanics. [30,151,152]

1.5   Imaging Techniques

Imaging techniques play an important role in accurately diagnosing wrist injuries and prescribing adequate treatments. Previous studies examining carpal contact mechanics have relied on static radiographs and Computed Tomography (CT) imaging.

1.5.1   Radiographs

Radiographs (x-rays) are the first line of investigation to assess suspected fractures and fracture healing and alignment. The x-rays are produced by the bombardment of accelerated electrons to a metal anode in tubes, and the transmitted x-rays are detected by phosphor screen or a film combination. This two-dimensional (2D) projection image has intensity proportional to the

amount by which the x-rays are attenuated as they pass through the body. The x-rays passing through an object experience exponential attenuation proportional to the linear attenuation coefficient of the object. The resulting image provides important diagnostic information due to differences in the attenuation coefficients of bone, muscle, fat, and other tissues in the 40–120 keV range used in clinical radiography. [153] Radiographs are cost-effective and have excellent contrast for bone applications.

Literature shows that there is a discrepancy between radiographic and clinical results, which may be due to its inability to accurately detect articular incongruity using conventional 2D radiography. It has been shown that conventional radiography can underestimate the presence of intra-articular distal radius fractures. [154] Additionally, fractures of the scaphoid and other carpal bones are often unnoticed on radiographs. [53] Moreover, patients with wrist injuries continue to experience wrist pain or a snapping sensation in the joint with motion with no bone position abnormalities on static radiographs. [155] The challenge is that the wrist is very complex and relying on 2D projection-based images limits the clinician in assessing the extent of the mal-alignment and the consequences of mal-alignment on the surrounding joints in the wrist.

1.5.2   Fluoroscopy

Fluoroscopy is used as a diagnostic tool to guide instruments through the internal structures of a patient for certain medical procedures. Fluoroscopy (X-ray "movie") allows for real-time kinematics to be assessed. Fluoroscopy involves an injection of a contrast agent ("X-ray dye"), and its movement is tracked through the body producing a moving image of the body's functioning organs. During a fluoroscopy procedure, X-rays are passed through the body and received by an image intensifier which converts x-rays to moving images played on a monitor. Fluoroscopic techniques overcome the limitation of static studies. [156] Fluoroscopic techniques have been utilized to dynamically analyze movement of joints that mainly occur about a single axis, but this technique is limited by the unavailability of 3D imaging and the use of active motion. The 2D nature of fluoroscopy makes it difficult to detect complex and subtle musculoskeletal abnormalities, such as wrist joint instabilities. [155]

Recently developed 3D fluoroscopy is used to measure *in vivo* joint kinematics based on 3D models of bones matched to the 2D features of the acquired radiographic images. [157] 3D fluoroscopy can accurately monitor real-time complex motions and joint forces under dynamic *in vivo* conditions. The outcome of the procedure remains strongly operator dependent; it requires the user to align the 3D model of the segment to the relevant fluoroscopic projections and to get

as close as possible to the real pose. This is time-consuming and pose estimations can be inaccurate. Moreover, fluoroscopic images obtained with this instrument are geometrically distorted and unsuitable for a quantitative analysis, unless a careful correction procedure is performed.

Videofluoroscopy allows for a real dynamic investigation in which the wrist is moved through a full range of movement to reproduce the stresses and positions which may be causing the pain or instability seen in patients. [158] This dynamic method has been used to diagnose midcarpal and ligament instability, but its diagnostic ability is limited due to its relatively low resolution. [159,160] This can be problematic because subtle dynamic changes cannot be identified as it is a projectional technique and the carpal bones may overlap. [161] Therefore, dynamic imaging with good spatial and temporal resolution is required.

1.5.3   Computed Tomography

Computed tomography (CT) has a superior performance compared to radiography for detecting carpal and distal forearm fractures. It has been clearly shown that CT can provide more accurate and detailed information for quantifying the displacement and deformity of these fractures. [162–164] More specifically, CT has been found to have a higher sensitivity for carpal bone fractures. [165,166] Gilley et al. found that up to 33% of scaphoid fractures were judged nondisplaced on radiograph but displaced on CT scan. [167] Welling et al. also found that many carpal bone fractures are radiographically occult and detectable only on CT. More specifically, it demonstrated that radiographs failed to detect 30% of wrist fractures identified at CT and suggested the importance of future studies using advanced imaging to improve fracture detection in clinical settings. [165]

The advantage of using CT to diagnose acute wrist injury is the visualization of anatomic structures without the overlap of other structures that confounds radiographic interpretation. [165] The main drawback of CT is the higher amount of radiation. However, some authors argue that despite the increased radiation exposure, early evaluation of clinically suspected fractures should be performed with CT if the radiograph appears normal. [168] This would avoid unnecessary immobilization and prevent the delayed diagnosis of fractures which reduces the risk for complications such as non-union or malunion. [169]

In displaced fractures, recognizing the deformities is important when deciding on the type of intervention, as it may alter the treatment or require surgical approach to the fracture. There has been a substantial interobserver variability in treatment recommendations for fractures of the

upper extremity. [170,171] This can be explained by the variation from measuring or estimating radiographic deformity. Recently, it has been shown that CT image-based methods can obtain precise 3D measurements and their reliability is substantially higher. [172] De Muinck Keizer et al. found that using 3D measurements to plan corrective surgery resulted in improved radiographic and functional outcomes in patients with a malunited fracture of the distal radius. [173]

A previously developed CT-based imaging method for measuring in-vivo 3D kinematics of the carpal bones during motion can image and analyze dynamic 3D information of a moving joint *in vivo*. [174,175] This method calculates the joint space thickness using dynamic distance maps during different wrist motions instead of using a static CT scan. [176] In vivo carpal kinematics examines the 3D carpal movements during a step-wise motion of the wrist. [36] However, *in vivo* carpal kinematics are measured using static methods and only represent an approximation of the true *in vivo* kinematics of the carpal bones. [36] Therefore, the kinematics acquired in a step-wise motion can differ from kinematics during a continuous dynamic motion where tendon contractions and time-dependent soft tissue properties play a role in real-time motion. [36]

1.5.4   Four-Dimensional Computed Tomography

The wrist joint requires four-dimensional (4D) dynamic joint imaging because the wrist is a complex structure, consisting of a radius, ulna, eight carpals, and five metacarpals all engaged with each other. Each of these carpal bones exhibits multiplanar motion involving significant out-of-plane rotation of bone rows, which is prominent during radio-ulnar deviation. The kinematics of these carpal bones have not been adequately defined in the literature. [24]

Four-dimensional computed tomography (4DCT) is a dynamic CT technique similar to CT perfusion allows for evaluation of continuous wrist motion as opposed to sequential static 3DCT. Four-dimensional (4D) CT obtains three-dimensional computed tomography volume sequences of a moving structure imaged over time, creating a dynamic volume data set. [177] Four-dimensional CT has promising clinical potential for the visualization of dynamic musculoskeletal pathophysiology and is currently being used to depict normal and abnormal carpal kinematics. [177] Many studies have used this technique to examine the wrist, shoulder, knee, and hip. [178–180] Four-dimensional kinematic studies allow evaluation of bone impingement, dynamic instability conditions, intra-articular ligament injury, and vascular compression syndromes. [155,161] Moreover, 4DCT allows a kinematic assessment of active wrist motion with high temporal and spatial resolution. Dynamic instability methods need to be developed to capture carpal bone

trajectories during active motion or dynamic loading. [181] If physicians can diagnose dynamic instability early, interventions can be implemented to restore normal wrist function. [181]

In diseases related to carpal motion, such as dynamic carpal instability, diagnoses are made based on clinical history and signs because there are no accepted diagnostic imaging criteria. [182,183] Some joint disorders may not even show abnormalities in a static radiograph but will still have dormant abnormalities that are aggravated with joint movement that can only be visualized using dynamic wrist imaging. For example, diagnosis of ulnar impaction is also made based on clinical symptoms and ulnar positive variance on a plain radiograph. [184,185] Dynamic imaging can provide evidence of pathology that only occurs temporarily during motion, such as abnormal arrangement of carpal bones or impaction of the ulnar styloid process during motion. This technique has shown potential for the evaluation of carpal instability, particularly in cases of inconclusive initial assessment. [155] Currently, 4DCT is not in widespread clinical use due to the lack of data regarding normal baseline appearances and diagnostic thresholds for establishing a definitive diagnosis in clinically suspected wrist instabilities.

1.6   Rationale

Osteoarthritis is the narrowing of cartilage in the affected joint leading to pain and limitation of joint mobility. It has been theorized that joint mal-alignment after an undetected or improperly treated wrist fracture can increase the risk for early onset of cartilage degeneration and eventual development of osteoarthritis. Furthermore, one bone improperly aligned can affect the kinematics and load distributions of the surrounding joints potentially leading to restricted range of motion, pain, weakness, and stiffness. However, the evidence on the impact of degenerative changes in patients suffering from residual mal-alignment on functional outcomes is inconclusive. Additionally, the pathomechanics and clinical significance of this pathology is poorly understood and thus it is unclear whether anatomical restoration is a key component for the management of wrist injuries and limiting the progression of osteoarthritis.

There have been different approaches used to examine the relationship between joint mal-alignment and osteoarthritis in the biomechanical literature. Previous studies have investigated this relationship but were limited by 2D approaches (radioulnar line method, subluxation ratio method, epicenter method and the radioulnar ratio method) that do not take advantage of CT volumetric data. [186] This limitation resulted in researchers developing 3D techniques which were employed to examine joint congruency and joint mechanics of the wrist. However, these studies are also limited because of their small cohorts of patients, short follow-up times, and static wrist

positions. [30,187] At this time, recent advances in 4DCT (3D + time) imaging can examine subtle bony changes that cannot readily be seen in 2D radiographs and static 3DCT. Dynamic instabilities that only occur during motion can now be detected using 4DCT.

Our lab previously developed an image-based tool to non-invasively measure 3D implications of altered bony alignment on the surrounding wrist joints which may provide insight into the relationship between joint alignment and cartilage degeneration. This joint congruency technique has been previously employed in a cadaveric population examining the effect of distal radii dorsal angulation on joint surface area. [151] Recently, the joint congruency technique has been used to examine the long-term effects of distal radius fractures with follow-up times of 8-10 years. [30] This finding demonstrated the use of this image-based 3D measurement tool in a clinical population (*in vivo*) and therefore, it has the potential to be used in this work to characterize the effect of a scaphoid deformity on the joint mechanics as they are poorly understood. Additionally, studies using 3DCT images are limited to static wrist positions and this work employed a novel 4DCT (3D and time) approach that allows for the detection of subtle bony changes during wrist motion which cannot be seen in static 3DCT.

Therefore, the purpose of this thesis was to employ a previously developed joint congruency technique to determine if changes in 3D joint space can lead to the development of early osteoarthritis. These findings will further our understanding on the effect of joint alignment after a wrist fracture on joint congruency.

1.7   Objectives and hypothesis

1.7.1   Objectives

1. To employ CT imaging to determine the 3D implications (joint space area (JSA)) of altered bony alignment on the joint contact area of joints surrounding the scaphoid in patients with scaphoid malunions a minimum of four years post-fracture.
2. To employ 4DCT to examine the JSA of the distal-radial joint (DRUJ) and radio-carpal joints in cohort of patients with distal radius fractures a minimum of one year compared to a cohort of healthy patients.
3. To employ 4DCT to examine the JSA of DRUJ and radio-carpal joints at three wrist positions during extension/flexion motion in cohort of patients with distal radius fractures a minimum of one year compared to a cohort of healthy patients.

1.7.2   Hypotheses

1. a. Scaphoid malunion will alter JSA and load distributions at mid-term follow-up.

   b. The changes in JSA will lead to the development of degenerative changes in the wrist as early as four years post-fracture.

2. a. Distal radius fractures will alter JSA of DRUJ and radiocarpal joints compared to the age-matched healthy cohort.

   b. The changes in JSA will lead to the degeneration of DRUJ and radiocarpal joints.

3. Distal radius fractures will alter JSA in the radiocarpal joints across wrist extension/ flexion but not in the DRUJ which is largely responsible for pronation/supination.

1.8   Overview

Chapter 2 describes the use of a previously developed joint congruency technique to examine the effect of scaphoid malunion on 3D joint congruency of the joints surrounding the scaphoid.

Chapter 3 describes the use of the joint congruency technique and 4DCT images to examine the effect of distal radius fractures on dynamic joint congruency during extension/flexion

Chapter 4 provides a general discussion of the work in this thesis and describes ongoing and future studies.

Chapter 2 – The Effect of Scaphoid Malunion on Joint Congruency

2   Overview

There is little attention on scaphoid malunion in literature, and it is a potential complication of scaphoid non-union surgical treatment or in association to ligamentous injuries. Gaining a better understanding of the clinical impact of malunion will help define surgical interventions at restoring joint congruency and preventing the development of degenerative changes of the wrist. This in vivo study aims to employ a previously developed joint congruency technique to advance the biomechanical assessment of scaphoid malunion.

2.1   Introduction

Fracture characteristics including orientation, translation, and location are key considerations in the evaluation of scaphoid fractures as they contribute to the assessment of fracture stability and consequently, potential for fracture union. Clinical studies have found that the risk of non-union may be up to 20% with displaced fractures while biomechanical evaluation has found increased interfragmentary motion distal to the scaphoid apex may contribute to the risk of non-union. [188, 189] Unsurprisingly, the risk of non-union increases precipitously with greater displacement and instability of the fracture; however, occasionally, the fracture will heal in a malunited position despite unfavorable alignment.

As discussed in Chapter 1 section 1.2.2.2, the pathomechanics surrounding this deformity is less understood and the clinical consequences (pain, limited range of motion, development of degenerative changes in the wrist) are controversial. Additionally, as stated in Chapter 1 section 1.2.2.2, the carpal bones are closely inter-connected and the alignment of one can, in theory, affect the kinematics and joint loading of adjacent carpal bones. This is thought to potentially lead to pain, limited range of motion and abnormal cartilage wear. A previous study examined long-term outcomes of operative and non-operative management of scaphoid malunions and found similar outcomes between operative and non-operative treatment suggesting that mal-alignment may not play such a pivotal role in wrist function. [190] A corrective osteotomy to restore anatomical alignment in a healed scaphoid may expose patients to an unnecessary risk of non-union as the scaphoid has a tenuous blood supply. Because the consequences of malunion are not completely

understood, this surgical dilemma is further exacerbated when treating younger patients who have only minimal symptoms. [190] While this relationship has been investigated in the biomechanical literature, the literature describing the clinical impact of malunion is controversial. There is also no clear consensus regarding what degree of scaphoid deformity or carpal malalignment can be tolerated without clinically compromising wrist function.

Chapter 1 section 1.5 also explored several imaging techniques utilized to visualize carpal contact mechanics. Computed tomography (CT) is clinically employed when assessing scaphoid fractures to measure the height-to-length ratio (in the sagittal plane) to characterize the amount of deformity present. As previously described in Chapter 1 section 1.5.3, CT has shown to be superior to radiographs due to their higher sensitivity allowing for an accurate evaluation of displacement and deformity post-fracture but also has limitations including a higher dose and inferring motion from static positions. As stated in Chapter 1 section 1.2.2.2, the H/L ratio is shown to be a reliable measure of the humpback deformity. [74] Three-dimensional CT imaging was used to characterize the extent of scaphoid deformity on the joint mechanics and loading distributions of the surrounding carpals which may provide insight into the relationship between bone alignment and abnormal loading leading to the onset of cartilage degeneration.

As mentioned in Chapter 1 section 1.4.4, our lab has previously developed an image-based technique to accurately and non-invasively measure 3-dimensional joint space area (JSA). [152] This measure provides a clinical tool that can be used to characterize joint interaction and takes advantage of the volumetric dataset provided by the CT scan. Joint space narrowing is a key feature in radiographic degeneration. The JSA in this study is similar in that it measures joint space, but it does so in three dimensions and is quantified. It is unclear however, if altered JSA is in fact related to degenerative signs of arthritis or if altered JSA is a precursor to degenerative changes. Therefore, the purpose of this chapter was to examine the changes in JSA over time, and post-injury. This study employed CT imaging to determine the 3D implications of altered bony alignment on the JSA of joints surrounding the scaphoid in patients with scaphoid malunions, a minimum of four years (average 7±2.1 years) post-fracture (Objective 1).

The hypothesis of this study stated in Chapter 1 was that the characteristic humpback deformity would alter 3D joint space at the radiocarpal and midcarpal joints surrounding the scaphoid as early as four years post-fracture (Hypothesis 1a). As the bones of the wrist are highly congruent and interconnected, it was assumed that disruption of one bone (scaphoid) as a result of trauma/malalignment would significantly affect adjacent bones and surrounding joints.

Additionally, previous studies that suggest that the scaphoid is the most mobile in displacement under load, resulting in altered contact force and contact area. [191] The assumption is that altered alignment and JSA leads to initiation and progression of osteoarthritis (Hypothesis 1b), similar to the change in mechanics seen with scapholunate or scaphoid non-union advanced collapse. [192]

2.2   Materials and Methodology

Patients who had scaphoid fractures treated at the Roth|McFarlane Hand and Upper Limb Center between November 2005 and November 2013 and had scaphoid Computed Tomography (CT) scans conducted were included in a database of scaphoid fractures. These cases were reviewed and subjects meeting the eligibility criteria for malunion were contacted to participate in this follow-up study. The inclusion criteria were healed scaphoid fractures (minimum 50% union on CT scan) with a Height-to-Length (H/L) greater than 0.6 on the central CT image, and the ability to participate in a clinical follow-up. [74] Both operative and non-operative treatments were included with no preferences for fracture location and orientations. For this study, the exclusion criteria were age less than 16 years at the time of injury, concomitant injury to the ipsilateral upper extremity, a scaphoid non-union and any neurological disorder that affected hand function.

The H/L ratio was measured using a standard approach that has been described previously and has been shown to have high intra- and interobserver availability. [74] These measures were conducted by a single fellowship-trained hand surgeon on a central CT slice (verified by toggling between slices to find the slice that had the largest outer circumference). A line positioned along the volar aspect of the scaphoid was a measure of the proximal to distal length of the scaphoid. The maximal height was determined perpendicular to this line and the H/L ratio calculated. [193]

One hundred and two patients were eligible to participate in the study. Thirty-one patients declined, were unreachable, or unable to participate in this study (declined: n=4, unreachable: n=24, incarcerated: n=1, deceased: n=2). The remaining 71 patients agreed to complete questionnaires only. Thirty-seven patients agreed to undergo functional testing and follow-up CT imaging in addition to completing questionnaires. Of this group, 25 presented for clinical visits while 12 cancelled their appointments or failed to present. Twenty-four of those who presented for clinical testing and CT testing participated in all facets of assessment (one was not able to participate in the CT imaging due to scheduling conflicts). The average age of this group was 41±16 years (range: 16-64 years) and the average length of follow-up was 7 ±2.1 years (range: 4-

12 years) post-fracture. Fourteen of the 24 patients had baseline CT scans (at the time of fracture) and follow-up CT scans (minimum of 4 years post-fracture) and were included in this study. The final number of participants in this study was 14.

2.2.1 CT Scanning

Follow-up CT scans were acquired using a 64-slice CT scanner (GE Discovery CT750 HD, Waukesha, WI) with the wrist in radial deviation and positioned such that the long axis of the scaphoid was perpendicular to the axis of the scanner (slice thickness=0.625mm, pixel spacing approximately 0.4 x 0.4mm, 50mA, 120 kVp). [193] CT slices in this study were also used to detect radiographic signs of degeneration using the coronal and sagittal images. A single reviewer assessed the coronal and sagittal images for arthritic changes at the radioscaphoid (RS), scaphocapitate (SC) and scapho-trapezium-trapezoid (STT). The degree of arthritis was graded according to the Kellgren-Lawrence scale: grade 0: normal joint without evidence of arthritis; grade 1: minimal joint space narrowing (JSN) with some osteophytic lipping; grade 2: osteophytes and possible JSN; grade 3: osteophytes and JSN with possible bony deformity; and finally, a grade 4: large osteophytes, marked JSN and severe sclerosis. [194] The same analysis was carried out for the last CT obtained during the initial follow-up for all patients. These results were compared to those obtained from long-term follow-up images to detect any new changes.

2.2.2 Joint Congruency

Figure 2.1 shows an overview of the experimental protocol and data analysis. This analysis was conducted on the previously acquired baseline CT scans (acquired at time of fracture) and the follow-up CT scan. The DICOM data (Digital Imaging and Communications in Medicine) obtained from the CT scan were imported into Mimics 21.0 (Materialise, Leuven, Belgium). Three-dimensional reconstructions of the carpus, distal radius and ulna were created using a threshold-based semiautomatic segmentation that accurately represented the corresponding bone/soft tissue boundary. A previously developed inter-bone distance algorithm was used to measure relative 3D joint space reduction over time (between baseline and follow-up). [150] Briefly, the algorithm calculates minimum inter-bone distances between opposing bone surfaces using a point-to-point distance measurement. Inter-bone distances are displayed using a colored proximity contour map (0 mm=red, 2 mm=blue). A threshold value of 2.0 mm was selected because it approximately captured the entire articular surface of the joints surrounding the scaphoid and has been previously used to measure articular cartilage in the scaphoid and lunate fossae and along the

interfossal ridge. [195] In this study, high proximity was characterized as having an inter-bone distance less than 0.5 mm and corresponded to red-yellow on the color-bar, and low proximity was characterized as having an inter-bone distance between 1.0 mm and 2.0 mm, which corresponded to green-blue. Joint Space Area (JSA) was defined as the area on the surface of the scaphoid facet of the distal radius that is within 2.0 mm of the opposing surface for the radioscaphoid joint. Similarly, for the scaphocapitate joint, inter-bone distances were calculated between the scaphoid and capitate (scaphotrapezium joint: scaphoid and trapezium; scaphotrapeziodal joint: scaphoid and trapezoid). Note that for visualization the scapho-trapezium-trapezoid joint JSA is shown together. The JSA was reported for each joint, for baseline and follow-up CT scans and is a CT-derived measure of joint contact area.

2.2.3   Statistical Methods

A repeated-measures analysis of variance (ANOVA) test with a Bonferroni correction to detect statistical differences in the measured joint space area for inter-bone distance (less than 0 mm, 0.5 mm, 1.0 mm, 1.5 mm, and 2.0 mm) in the baseline and follow-up scenarios. Statistical significance was initially set at $p<0.05$ and then corrected by a Bonferroni correction factor which accounted for multiple comparisons.
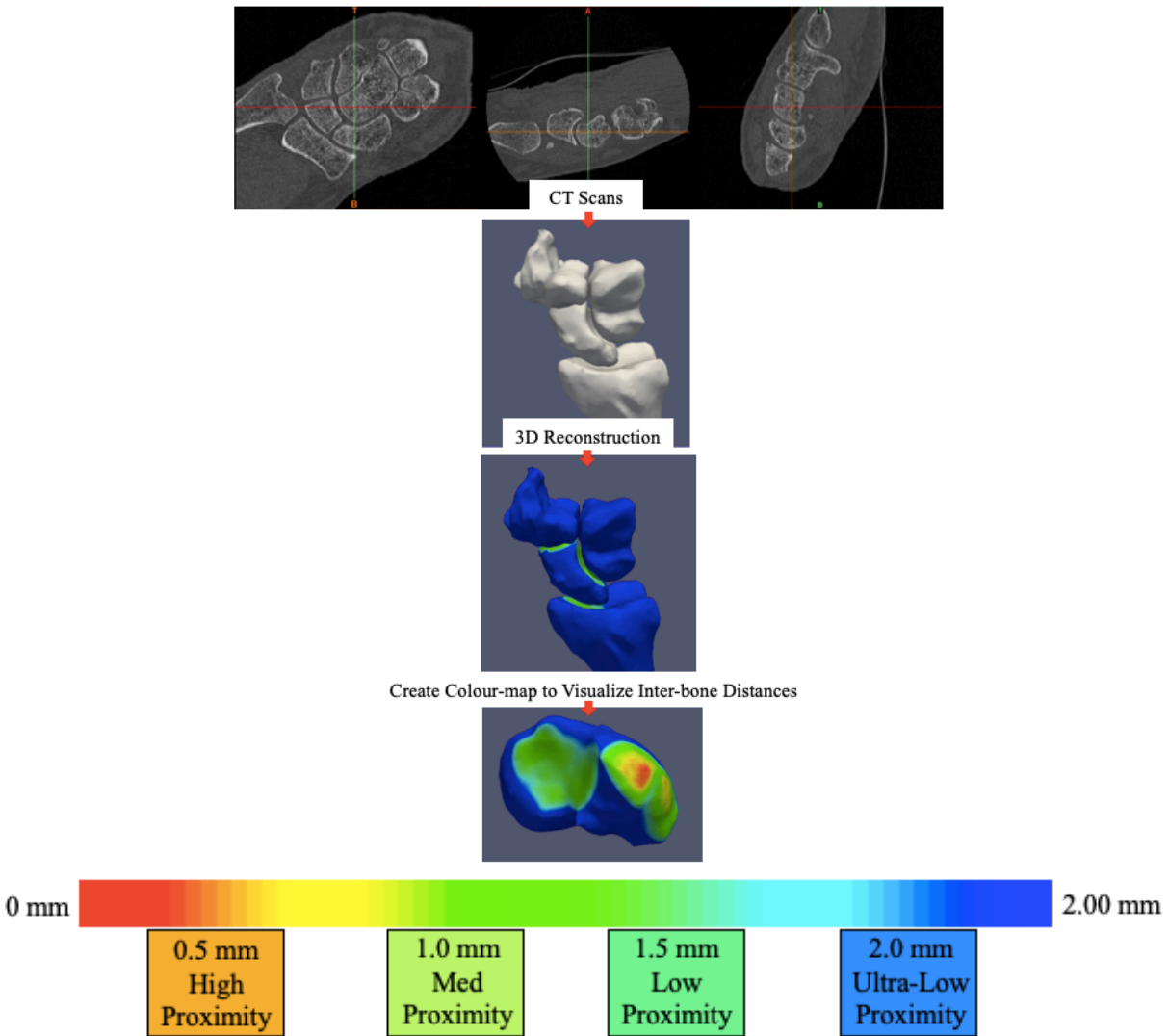
Figure 2.1. Flowchart showing Data Analysis for the Joint Surface Area.
A color-bar is shown (0-2 mm: red-blue) corresponds to high, medium, low and ultra-low proximity.

2.3   Results

The fracture characteristics and demographic data for all participants (n=14, mean age at injury:42 (range:16–64), mean age at long-term follow-up:49 (range:20–70), M:11 F:4) are shown in Table 2.1.

The proximity maps of each participant for each joint are shown in Figure 2.2 (A: Radioscahoid Joint, B: Scaphocapitate Joint, C: the Scapho-Trapezium-Trapezoid Joint). The Kellgren Lawrence (KL) osteoarthritis grades at baseline and follow-up for all participants (n=14) were listed in Figure 2.2 and indicates that there are "none" or "doubtful" degenerative changes in these wrists. The mean Joint Space Area (JSA) was compared between the baseline

and follow-up for each joint being examined and is shown in Figure 2.3 (A: Radioscahoid Joint, B: Scaphocapitate Joint, C: Scaphotrazepoid Joint, D: Scaphotrapezium Joint).
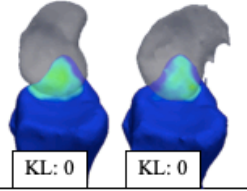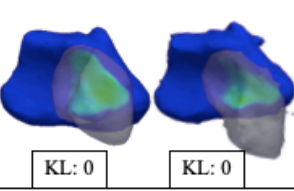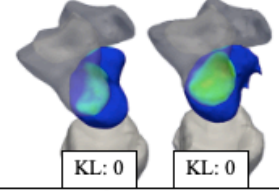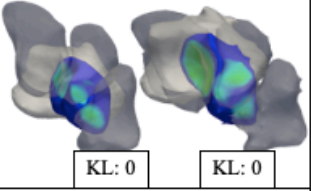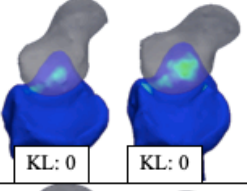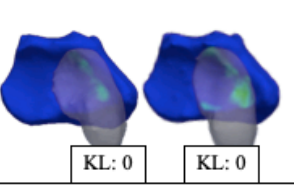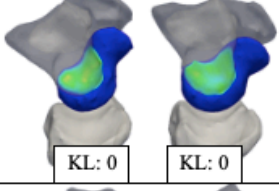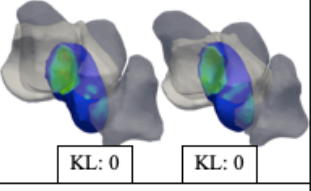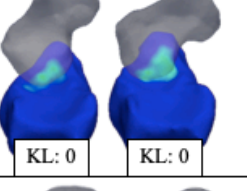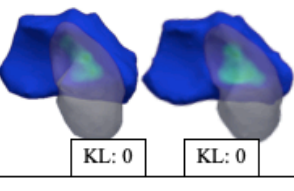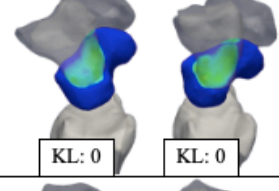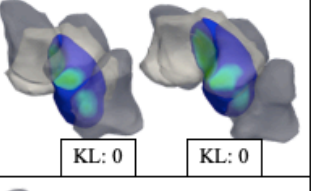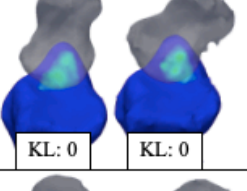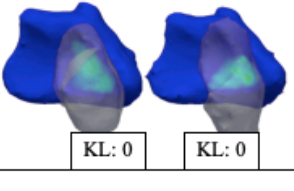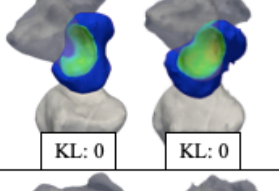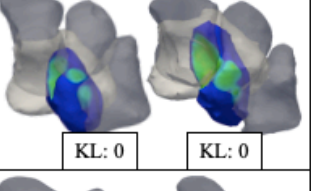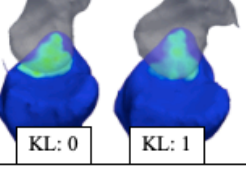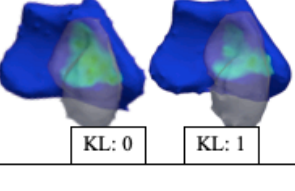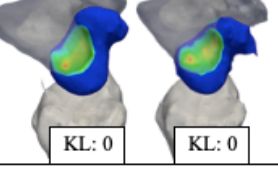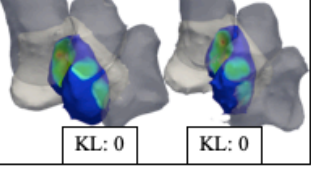
The results demonstrated a small increase in measured JSA at the radioscaphoid (Figure 2.3A) and scaphotrapezoid joints (Figure 2.3C) between baseline and follow-up scenarios (for all inter-bone distances examined) ($p > 0.05$). Figure 2.3B shows a significant increase in JSA four years after fracture at the scaphocapitate joint (inter-bone distances less than 1.5 mm and 2 mm) ($p < 0.05$). Joint space area also significantly increased four years post-fracture at the scaphotrapezium joint (Figure 2.3D) for inter-bone distance less than 2mm ($p < 0.05$).

Table 2.1. Demographic factors of participants with scaphoid malunions (n=14).
*Motor Vehicle Accident (MVA)
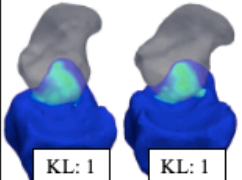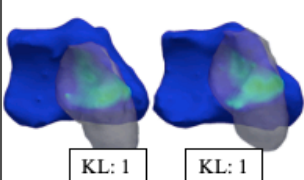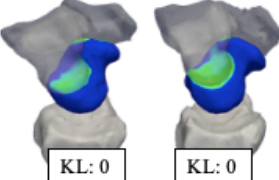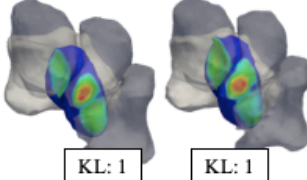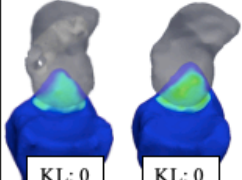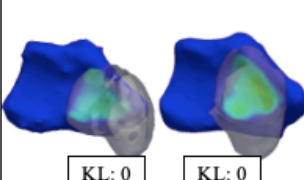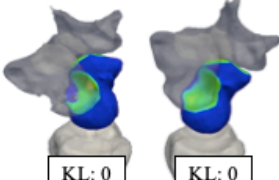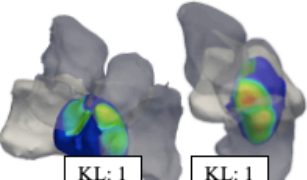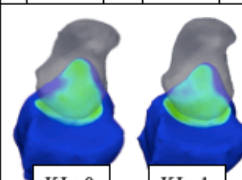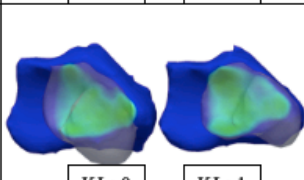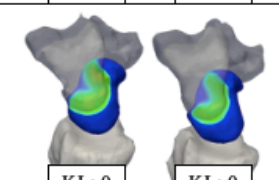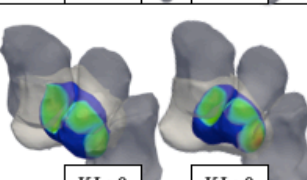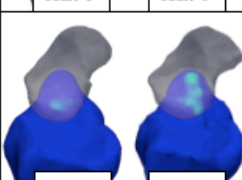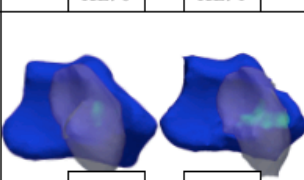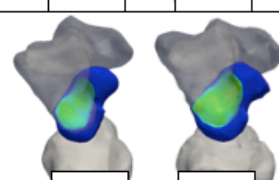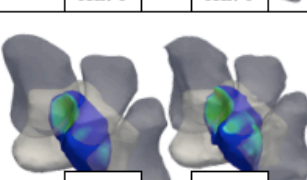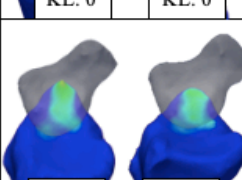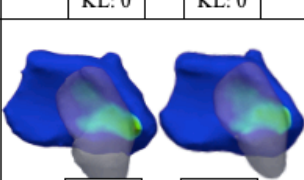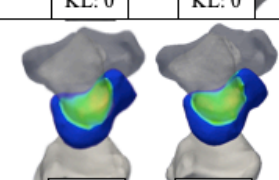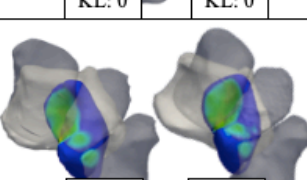
Patient	Gender	H/L ratio	Age at Injury	Age at Long-term follow-up	Follow up time (years)	Injured wrist	Dominant hand	Mechanism of Injury	DISI
106773-2	Male	0.622	16	20	4.35	Right	Yes	Punch	No
106773-3	Male	0.621	26	31	5.5	Right	Yes	Sports	No
106773-4	Male	0.604	60	66	5.5	Right	No	Sports	No
106773-8	Male	0.656	32	39	7.16	Left	No	Fall	No
106773-9	Male	0.671	53	64	11.17	Right	No	Fall	No
106773-12	Male	0.649	49	56	7.02	Right	Yes	Fall	No
106773-14	Female	0.650	60	66	5.31	Right	Yes	Fall	No
106773-15	Female	0.663	64	70	4.89	Left	No	Fall	No
106773-16	Male	0.610	17	23	6.35	Right	Yes	Sports	No
106773-19	Male	0.609	46	51	5.59	Left	No	MVA*	No
106773-20	Female	0.699	59	65	6.09	Right	Yes	Fall	No
106773-21	Male	0.660	33	46	6.29	Right	Yes	Sports	No
106773-22	Male	0.629	37	43	6.14	Left	No	Fall	No
106773-23	Male	0.618	34	42	8.07	Right	Yes	Sports	No
106773-24	Female	0.654	55	61	6.84	Right	Yes	Fall	No

Figure 2.2 (A)

Patient	Radioscaphoid (oblique view) (Baseline |Follow-Up)	Radioscaphoid (transverse view) (Baseline |Follow-Up)	Scaphocapitate (Baseline |Follow-Up)	Scaphotrapzium-trapezoid (Baseline |Follow-Up)
106773-2	KL: 0 KL: 0	KL: 0 KL: 0	KL: 0 KL: 0	KL: 0 KL: 0
106773-3	KL: 0 KL: 0	KL: 0 KL: 0	KL: 0 KL: 0	KL: 0 KL: 0
106773-4	KL: 0 KL: 0	KL: 0 KL: 0	KL: 0 KL: 0	KL: 0 KL: 0
106773-8	KL: 0 KL: 0	KL: 0 KL: 0	KL: 0 KL: 0	KL: 0 KL: 0
106773-9	KL: 0 KL: 1	KL: 0 KL: 1	KL: 0 KL: 0	KL: 0 KL: 0

Figure 2.2 (B)

Patient	Radioscaphoid (oblique view) (Baseline |Follow-Up)		Radioscaphoid (transverse view) (Baseline |Follow-Up)		Scaphocapitate (Baseline |Follow-Up)		Scaphotrapzium-trapezoid (Baseline |Follow-Up)	
106773-12	KL: 1	KL: 1	KL: 1	KL: 1	KL: 0	KL: 0	KL: 1	KL: 1
106773-14	KL: 0	KL: 0	KL: 0	KL: 0	KL: 0	KL: 0	KL: 1	KL: 1
106773-15	KL: 0	KL: 1	KL: 0	KL: 1	KL: 0	KL: 0	KL: 0	KL: 0
106773-16	KL: 0	KL: 0	KL: 0	KL: 0	KL: 0	KL: 0	KL: 0	KL: 0
106773-19	KL: 0	KL: 1	KL: 0	KL: 1	KL: 0	KL: 0	KL: 0	KL: 0

Figure 2.2 (C)
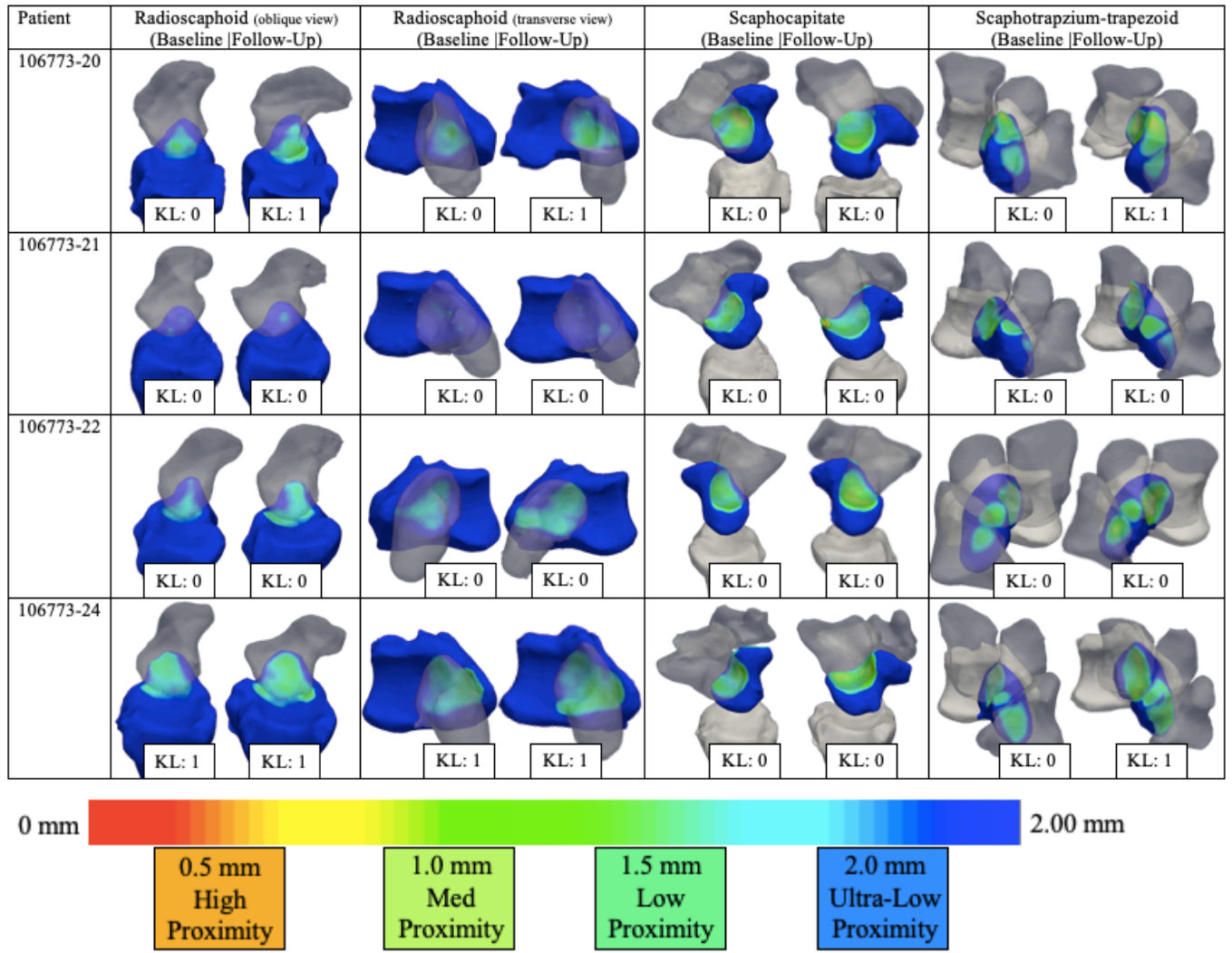
Figure 2.2 (A-C). Joint Congruency Maps for the Radioscaphoid, Scaphocapitate, and Scaphotrapezium-trapezoid (STT) Joints for all Specimens (n=14).
A color-bar is shown (0-2 mm: red-blue) corresponds to high, medium, low and ultra-low proximity. Kellgren Lawrence osteoarthritis grades are also shown for each participant at baseline and at long-term follow-up.

Figure 2.3 (A) Radioscaphoid Joint
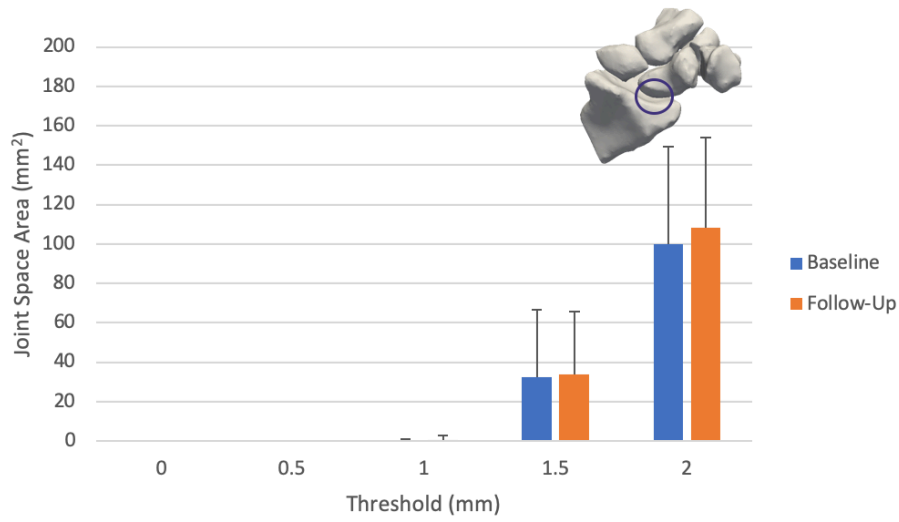
Figure 2.3 (B) Scaphocapitate Joint
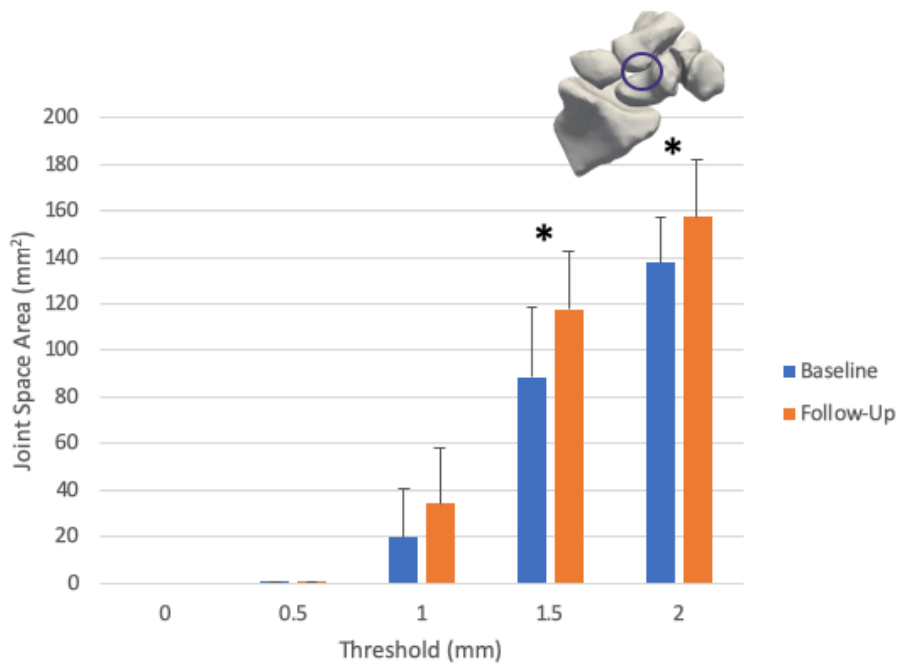
Figure 2.3 (C) Scaphotrapezoid Joint
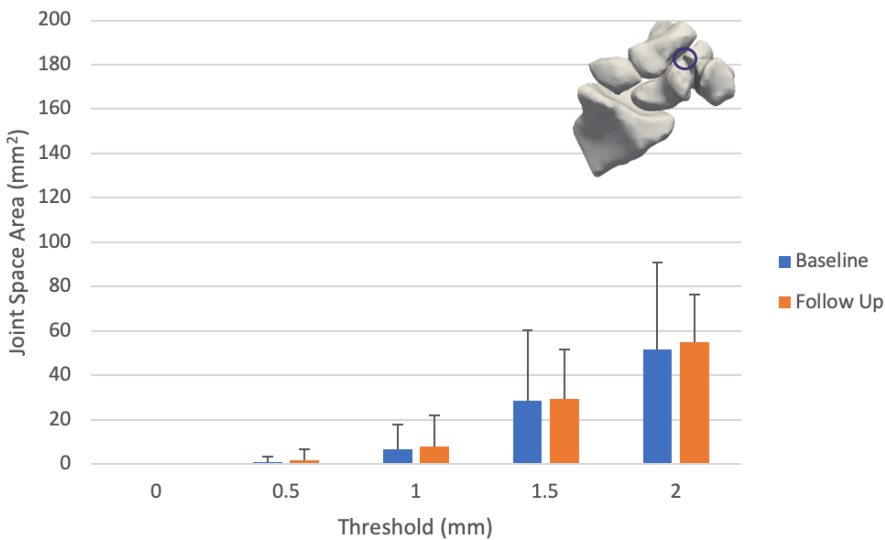
Figure 2.3 (D) Scaphotrapezium Joint
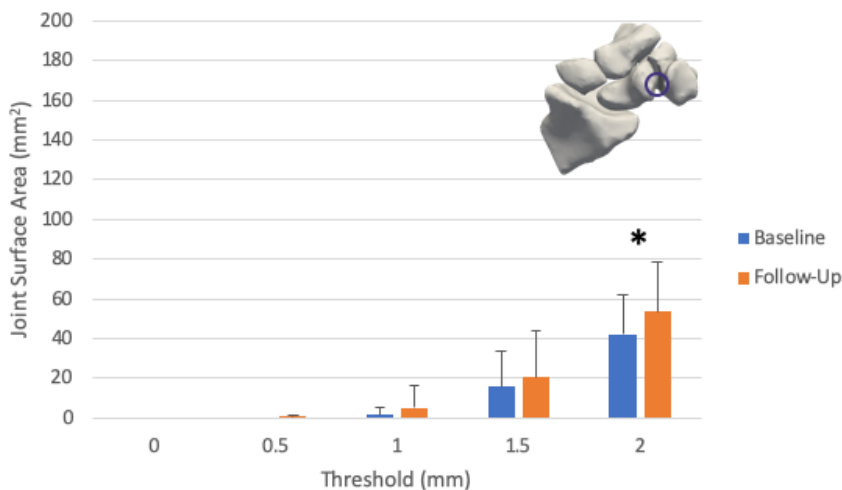
Figure 2.3 (A-D). Joint Surface Area for each Joint (inter-bone distances less than 2.0 mm) for all Specimens (n=14).
Bars represent mean, and error bars represent standard deviation of mean.

2.4   Discussion

With a scaphoid malunion, it is unclear how significantly the angulation or humpback within the scaphoid alters carpal mechanics. The important question is whether the malunion alters the joint mechanics enough to cause early osteoarthritis. The results of this study indicate that there is a significant difference in joint space area (JSA) with differences less than 2mm at

the scaphotrapezium and scaphocapitate joints when comparing the baseline and follow-up scans of the wrist as early as 4 years post-fracture. Additionally, there were no signs of degenerative changes (as measured using the KL grading) for any of the participants in this study at an average of 7 years post-fracture (minimum of 4 years). While commonly used, the KL grading may not be sensitive to early arthritis and it is therefore unclear whether or not these changes in JSA relate to degenerative changes (previous study suggested that the development of post-traumatic osteoarthritis occurs at a minimum of 5 years (average 7.1 years) [196] or if it is the case that these two measures are not associated.

Scapholunate Advanced Collapse (SLAC), as defined in Chapter 1 section 1.2.1.5, represents a characteristic degenerative pattern in the wrist after a chronic scapholunate (SL) injury and is well characterized by a progression of proximal migration of the capitate between the scaphoid and lunate. The pattern of degeneration that will appear is unclear; however, it is suspected that a similar progression of degeneration as seen after SL injury might also appear, however an important distinction must be made. With a scaphoid non-union, and scapholunate injury, the carpus 'collapses' because there is either a gap between the two halves of the scaphoid or between the scaphoid and lunate. With a scaphoid malunion, as defined in Chapter 1 section 1.2.2, the carpus might not necessarily 'collapse' or maybe not to the same extent as the radial column of the carpus remains solid. This proximal migration of scaphoid along with the trapezoid, trapezium, capitate bones could explain the increased JSA (within close proximity) or a reduced joint space narrowing.

This study did not find any signs of degenerative changes in these joints. Possible explanations for this discrepancy are primarily biomechanical. The capitate articulates with scaphoid and lunate and both midcarpal joints play a vital role in load transmission between the distal and proximal row. It is possible that the load is preferentially transferred through the lunocapitate joint rather than the scaphocapitate joint. Therefore, the lunocapitate might be subjected to higher contact under loading but this joint was not examined in this study. These variations in load distributions can explain changes in contact area, which is one of the primary mechanical factors associated with OA development. [197,198]

Current literature discussed in Chapter 1 section 1.2.2.2 does not clearly define whether the malunion alters the joint mechanics enough to cause early osteoarthritis. In addition to there being conflicting reports of the clinical significance of scaphoid malunions, there are also very few studies that focus on this pathology specifically in the context of an acute fracture healing in

a malunited position as previously described in Chapter 1 section 1.3.2. Much of the literature focuses on scaphoid non-unions that are treated surgically and then heal in a malunited position, making it unclear whether the changes seen are due to the malunion or because of the non-union. This study focused on a population of patients that had a primary scaphoid malunion to try to detect changes in joint loading as a result of the mal-aligned scaphoid. As well, we were able to compare baseline and follow-up CT image which reduces inter-subject variability and examines the same joint over time.

We employed H/L ratios as a measure of angular deformity because it is dependent on CT orientation (the longitudinal axis of the scaphoid), thickness of CT slices, and has intra- and inter-rater reliability. [70] However, this parameter is two-dimensional and limited in interpreting the multiplanar deformity of scaphoid and carpal instability, which is critical for assessing treatment options and planning surgical correction. [199] Also, the H/L ratio > 0.6 is an arbitrary number and has not demonstrated the ability to distinguish between different clinical results in previous studies. [84] Furthermore, there is no consistency in the H/L ratio value used to define scaphoid malunion which can make comparisons of findings across studies difficult. A previous study used a H/L ratio > 0.65 to define scaphoid malunion. [200]

A limitation of this study was that our small sample size did not allow us to examine the amount of deformity or severity of the malunion and amount of change in joint loading (JSA) by stratifying cases into mild, moderate and severe malunion. This study presented results using a small number of not severely malunited cases and we acknowledge that a larger sample size and severely malunited cases could have captured more information on altered joint contact mechanics. In addition, this study evaluated joint contact mechanics at the radial ulnar position and other positions such as the dart thrower's motion, extreme extension or extreme flexion could provide further useful data in the future.

2.5   Conclusion

This study provided carpal contact mechanics data that illustrate the effects of scaphoid malunion at a minimum of 4 years post-fracture. The results from this study demonstrated significant differences in joint congruency between baseline and a minimum of four years post-fracture at the scaphocapitate and STT joints. However, radiographic evidence of degeneration was not found at a mid-term follow-up. This study provides a first step in determining the three-dimensional consequences of scaphoid malunion on surrounding joint mechanics. These findings are of importance to furthering knowledge on the clinical significance of scaphoid malunion. The

relationship between measurable deformity and clinical symptoms and long-term sequelae is not clearly defined in the literature and in this study, therefore, it is not possible to, at this point, create operative guidelines of when and how to intervene surgically. The study presented in the next chapter will extend the use of the joint congruency technique and employ a 4DCT approach to examine another common upper extremity injury, distal radius fractures at wrist positions during motion.

Chapter 3 Four-Dimensional Computed Tomography to Measure Distal Radial-Ulnar and Radio-Carpal Joint Congruency After Distal Radius Fractures

3   Overview

Previous studies investigating the effect of distal radius fracture mal-alignment have focused solely on the distal radioulnar joint and forearm rotation using static imaging. The wrist is extremely interconnected and experiences different joint positions during tasks of daily living. Therefore, the impact of distal radius fracture on the surrounding joint mechanics during wrist extension/flexion motion needs to be considered. This in vivo study employs a 4DCT approach to better visualize the mechanical abnormalities of individuals with distal radius fractures compared to healthy individuals.

3.1   Introduction

Distal radius fractures (DRF) are common orthopedic injuries accounting for 75% of all forearm fractures and subject to a high rate of misdiagnosis [201,202]. Complications arising from DRF occur in nearly 30% of patients and are a consequence of either the initial injury or subsequent treatment. [89] As highlighted in Chapter 1 section 1.2.3.5, one of the major complications after a DRF is the radius healing in mal-aligned positions, called malunion, which is seen in up to 33% of cases. [203] Chapter 1 section 1.2.4.1 also described the distal radial deformities used to confirm a suspected malunion and these measurements included radial shortening, dorsal tilt, and loss of radial inclination. The residual incongruity during fracture healing may lead to joint stiffness and long-term morbidity; therefore, the restoration of articular congruity is a key component for the management of these injuries. [204]   Additionally, abnormal carpal mechanics resulting from articular surface incongruity and joint instability may cause irreversible cartilage degeneration. [89] Current literature discussed in Chapter 1 section 1.2.4.2, is controversial regarding the relationship between residual deformity and long-term clinical and radiographic outcomes including post-traumatic osteoarthritis development. It is unclear whether altered joint congruency and mechanics is an important contributor to patient outcomes post-fracture.

As stated in Chapter 1 section 1.2.3.3, radiographs are commonly used by clinicians to evaluate anatomical restoration and to monitor the development of osteoarthritis after a DRF. Radiographic degenerative changes are frequently reported in patients who have suffered a DRF,

but the long-term clinical impact of these changes has not been clearly defined. Current literature, discussed in Chapter 1 section 1.2.4.2 has shown conflicting reports on the correlation between well reduced fracture (according to standard radiographic measures on the radial height, radial inclination, volar tilt, etc.) and functional outcomes or patient satisfaction. Therefore, the clinical evidence linking incongruity to post-traumatic arthritis is inconclusive. However, the validity of these findings is questionable as radiographs are limited by the anatomical complexity of the wrist. [205] Chapter 1 section 1.5 explored the advantages as well as the challenges of several imaging techniques. As stated in Chapter 1 section 1.5.1, the challenge is that the wrist is very complex and relying on two-dimensional (2D) projection-based images limits the clinician in assessing the extent of the mal-alignment and the consequences of mal-alignment on the surrounding joints in the wrist. Additionally, symptoms arising from malalignment may only occur when a patient is performing a functional task with their wrist. [206] Since, radiographs are static in nature, they are do not present dynamic instabilities and these patients continue to have debilitating wrist pain. [207]

Studies have reported better measurement accuracy of articular surface displacements when using three-dimensional (3D) measurements (CT) compared to the standard 2D radiographs. [208] Even though volumetric images can be used to create 3D models, many studies have continued to examine joint alignment from 2D slices obtained from 3DCT, using the radioulnar line method, subluxation ratio method, epicenter method and the radioulnar ratio method. [186] Conversely, previous studies have examined the consequence of the wrist fracture in 3D as discussed in Chapter 1 section 1.3.3. But these studies are limited to a small case series (Crisco et al.: n=9, Kihara et al.: n=6 cadaveric wrists) and short follow-up times of 1 year or less (Crisco et al.: 10-month follow-up), which may not capture the 3D degenerative changes that occur over time. [29,209]

Previous studies also focused solely on DRUJ and did not investigate the impact of the fracture on the surrounding joint mechanics. Radiocarpal joint mechanics can play an important role in the functional dysfunction associated with distal radius malunions and radiocarpal post-traumatic arthritis is common after a wrist fracture. [210] Therefore, the effect of distal radius malunion on the *in vivo* contact patterns of the radiocarpal joints needs to be further examined in a larger cohort.

Studies have demonstrated deviations from normal wrist kinematics at the extreme positions of motion post-injury using 3D measurements. As discussed in Chapter 1 section 1.3.3, several studies have investigated the *in vitro* effect of distal radius malunion on contact patterns

(contact area and centroid location) of the DRUJ during forearm rotation. [151,209] These studies were limited to cadaveric wrist simulators and focused on one of the distal radial deformities (dorsal angulation). Other studies have inferred the *in vivo* effect of motion on joint contact mechanics from static positions. However, static testing cannot detect the mechanical abnormalities throughout the full range of motion, and thus the contact patterns at intermediate positions of the motion are not examined.

Four-dimensional Computed Tomography (4DCT) allows for a kinematic assessment of active wrist motion capturing subtle positional bone changes with high temporal and spatial resolution. [211,212] Four-dimensional CT, previously described in Chapter 1 section 1.5.4, is an imaging technique where joint motion is acquired using a dynamic sequential scanning technique. The images are acquired while the joint is moving allowing for a dynamic assessment of the joint mechanics, such as identify areas with focal loading and potential for pain with load bearing movement. The 4DCT approach enables 3D volume sequences to be obtained over time while the wrist is in motion. [213] Zhao et al. validated the 4DCT technique using the bead-based and bone-based registrations and found the accuracy to be consistent with other static and dynamic image-based kinematic techniques. [201] However, this study was limited by two cadaveric specimens, and segmentation and registration inaccuracy (0.943 and 0.376 mm respectively). [201]

Recent advances in 4DCT imaging (3D and time) can examine subtle bony changes that cannot readily be seen in 2D radiographs and static 3DCT. Using 4DCT, we are now able to detect dynamic instabilities that only occur during motion. Therefore, the purpose of this chapter was to extend the findings from our previous studies to now examine the effect of DRF on dynamic joint congruency in a cohort of patients who have previously suffered a DRF and compare those results with an age-matched healthy cohort (Objective 2). This chapter also examines the differences in the joint surface area (JSA) due to differences in wrist position (extension/flexion) in the healthy population and determine if these trends were also reflected in the fractured population (Objective 3). A previous study has employed clinical 3DCT to examine one static position of the wrist (full pronation) and found that at an average of 8 years post-fracture, JSA was reduced in the radiolunate joint when comparing the injured and uninjured wrists. [30] While this finding was novel and demonstrated the use of this image-based 3D measurement tool in a clinical population (*in vivo*), the study was limited to a small cohort of patients and only one static position. Using 4DCT, these changes in JSA can be shown dynamically during wrist motion.

One hypothesis of this study stated in Chapter 1 was that patients with healed distal radius fracture will demonstrate altered joint contact mechanics so that either the JSA will decrease indicating areas of point loading and potential pain (Hypothesis 2a). This may predispose the wrist joint to the development of early osteoarthritis that ultimately changes the kinematic behavior of the interconnected wrist bones during *in vivo* extension/flexion (Hypothesis 2b). The other hypothesis of this study stated in Chapter 1 was that patients with a healed DRF will demonstrate altered joint contact mechanics in the radiocarpal joints across extension/flexion such that the JSA will decrease (Hypothesis 3).

3.2   Materials and Methodology

3.2.1   Participants

This is a Level 3 Case Control Study. Patients who had previous DRFs treated at the Roth|McFarlane Hand & Upper Limb Centre were identified and included in the injured cohort. These cases were reviewed and subjects meeting the eligibility criteria were contacted to participate in the study. The inclusion criteria were healed DRFs, minimum of one-year post-fracture, and ability to participate in a clinical follow-up.   For this study, the exclusion criteria were less than 18 years old at the time of injury, a concomitant injury to the ipsilateral hand or wrist, presence of metal pins/plates and any neurological disorder that affected hand function. Seventeen patients had consented to undergo functional testing and 4DCT imaging in addition to completing questionnaires. Of this group, 14 presented for clinical testing and CT testing, while three cancelled their appointments or failed to present. Healthy individuals with no previous wrist fractures were also recruited to participate in the study. These cases were reviewed, and subjects were age-matched to the 11 individuals with DRF (age matching range is age ± 5). Twenty-two participants (11 individuals with distal radius fractures and 11 healthy controls) were included in this study. Prior to study participation, each participant signed a consent to participate. Participants were seen for a follow-up assessment by a fellowship-trained hand surgeon (N.S) at our institution. The study protocol was approved by the ethics review board of our institute and hospital and complied with the Declaration of Helsinki of 1975, revised 2000.

3.2.2   4D CT Imaging

A CT scanner (Revolution CT Scanner, GE Healthcare, Waukesha, Wisconsin, USA) was used to acquire kinematic scans of the distal forearm and hand using a routine wrist scan protocol

(80 kV, 125 effective mA, 0.35 s rotation time, axial). The CT scanner imaged a 16 cm volume, configured as 128, 1.25 mm thick slices, repeatedly at 0.35 s intervals over a duration of 24.5 s for a total of 70 volumes at 2.86 Hz. The voxel size was $0.625 \times 0.625 \times 1.25$ mm. For the purposes of this study, three passes of flexion-extension were performed (extreme extension to extreme flexion was the first pass (25 volumes, 8.75 s), extreme flexion to extreme extension was the second pass (25 volumes, 8.75 s), and extreme extension to extreme flexion was the third pass (20 volumes, 7.0 s), resulting in a total time of 24.5 s per motion and 25 frames of motion per pass. Three passes of motion were obtained to ensure the total range of motion was captured if the participant moved too slowly or if they missed the trigger to begin motion at the start of the scan. The first instance of extreme extension/flexion was analyzed in this study. In addition to these kinematic scans, a static scan with the wrist in 30 degrees of supination was acquired ($0.35 \times 0.35 \times 0.625$ mm for the scan, 125 mA, 120 kVp). The total exposure time for three passes per motion was 24.5 s, resulting in a dose length product (DLP) of 713.64 [mGy-cm]. Alternatively, the total skin dose was 0.067 Gy from the hand scans and the threshold for skin erythema from radiation exposure is 2 Gy. Thus, the skin dose from the research study was ten times lower than the threshold. The speed of the scan was approximately 22°/s for extension/flexion. During imaging, the individuals were lying in prone with their arm outstretched inside of the scanner. The participants also wore protective gear (lead apron, neck band and protective eyeglasses). The scatter radiation dose measured under lead apron, 0.013 mSv, was representative of what the participants received from the research study. The average person receives a higher annual dose of 3 mSv from natural background radiation and cosmic radiation from outer space. This value is 231 times higher than the dose in our research study, therefore, the effects from this scatter dose were negligible.

3.2.3   Radiographic Evaluation

Follow-up radiographs (posteroanterior and lateral views) were obtained from each participant (follow-up mean: 5 months, range: 3-10 months). Plain radiographs were used to measure the Radial Inclination (RI), Dorsal Angulation (DA) and Ulnar Variance (volar +, dorsal -) (UV). All measurements were performed by a fellowship-trained hand surgeon (M. M). Overall, distal radius alignment was determined to be unacceptable if RI <15°, if DA >10°, or if there was ≥3 mm of UV positive using the guidelines written by the American Society for Surgery of the Hand (ASSH). The follow-up radiographs were also classified according to the

Müller AO system [214], which is a widely used classification system for DRFs in clinical research [215]. This system classifies fractures into 3 types: A (extra-articular), B (partial articular), and C (complete articular) which describes the joints involved [214].

Evidence of osteoarthritis in the radioscaphoid (RS), radiolunate (RL) and distal radioulnar joint (DRUJ) were assessed by grading the follow-up CT images using the Kellgren and Lawrence (KL) Grading system: 0- None, 1- Doubtful, 2- Minimal, 3- Moderate, 4- Severe [194]. Grades were based on the presence of joint space narrowing, osteophytes, sclerosis, and deformity of bone ends [194]. The follow-up CT images (coronal views) obtained from each participant were used to assign KL grades to the injured and uninjured cohorts. Kellgren Lawrence Osteoarthritis (KL OA) scores were used to predict long-term degenerative changes (as defined by a grade of greater than 2 on the KL OA scale).

3.2.4 Image Analysis

In this current study, three static phases of the extension/flexion motion were of interest. The 3DSlicer software (version 4.11.0) was used to visualize 25 frames of data. Three static phases of the extension/flexion motion of interest were maximum extension, neutral and maximum flexion. The joint angles at each position of interest were recorded using a standardized approach employing a digital goniometer in 3DSlicer. The static phases were chosen as they show the joint contact mechanics at the extreme positions of the range of motion. This is important because carpal ligaments are more prone to strain and injuries in these positions [216,217].

3.2.5 Joint Congruency

The data analysis process was similar to the analysis described in Chapter 2 section 2.2.2. The DICOM images (Digital Imaging and Communications in Medicine) obtained from the CT scan were imported into Mimics 21.0 (Materialise, Leuven, Belgium). Three-dimensional reconstructions of the carpus, ulna, and radius were created using a semi-automatic threshold-based segmentation technique to reconstruct the outer most bony surface. A previously developed inter-bone distance algorithm was used to measure relative 3D joint space area (mm^2) [218]. In this current study, Joint surface area (JSA) was defined as the area on the surface of the scaphoid facet on the distal radius that is within 2.0 mm of the opposing surface for the radioscaphoid, radiolunate and distal radioulnar joints. The JSA was normalized to the individual's total static JSA of the scaphoid fossa, lunate fossa, and sigmoid notch of the distal

radius. The mean JSA % for the healthy and injured cohorts were reported. The effect of the range of motion and the effect of fracture on measured JSA % (inter-bone distances less than 2.0 mm) was examined.

3.2.6   Functional and Pain Assessment

After CT scanning, individuals underwent functional tests to examine their grip strength and range of motion. The data was collected from each individual in the healthy and injured cohort and inputted into IMB SPSS Statistics software version 25. The clinical outcome measurements were grip strength recorded using a hand dynamometer (Alyatus), static joint angles at extreme flexion, neutral and extreme extension positions recorded using the goniometer.

3.2.7   Statistical Analysis

To detect differences in JSA % between health status and joint position, a Univariate ANOVA (Analysis of Variance) was conducted (IMB SPSS Statistics software version 25) for each joint of interest; p-value=0.05 was considered significant. This test examined the interaction between the independent variables of health status (uninjured and injured) and joint position (extreme flexion, neutral and extreme extension) to the dependent variable of JSA % at each inter-bone distances, 0 mm, 0.5mm, 1.0mm, 1.5mm, 2.0mm. To compare clinical outcomes between the healthy and fracture cohorts, a Paired T-Test analysis was conducted for grip strength, range of motion (static and dynamic extension and flexion angles) and pain.

3.3   Results

Table 3.1 shows the demographic data for all participants in the injured and the healthy (control) cohorts, as well as the age at time of injury (n=22, mean age of distal radius fracture cohort: 71± 16 years (range:60-84 years), mean length of follow-up was 12 years±13 (range:1-47 years) post-fracture, mean age of the healthy control cohort: 68± 9 years (range:60-84 years)). The injured cohort consisted of five extra-articular, four intra-articular and one partial DRF (one fracture was not classified; no injury films).

The KL scores for the injured and uninjured cohorts are listed in Table 3.3. Overall, seven out of the 11 injured participants were considered to have unacceptable radiographic distal radius alignment according to the ASSH guidelines (Table 3.2). The injured cohort demonstrated

degenerative changes in the DRUJ (n=6) and radiocarpal joints (n=10). The uninjured cohort also demonstrated degenerative changes in DRUJ (n=5) and radiocarpal joints (n=10).

The individual's grip strength, static and dynamic extension and flexion angles, and patient rated wrist evaluation (PRWE) scores for the age-matched injured and healthy cohorts are listed in Table 3.4. There was a significant difference in grip strength between the injured cohort (mean: 23 Kg) and healthy cohort (mean: 32 Kg) ($p<0.05$). The mean joint angles for the injured cohort was F 45° (range: 20°-68°) to E 65° (range: 41°-71°) and for the healthy control cohort was F 48° (range: 32°-68°) to E 62° (range: 45°-74°); no significant differences were found at extreme flexion ($p>0.05$) and at extreme extension ($p>0.05$).

Figure 3.1 shows the changes in percent mean JSA % (inter-bone distances less than 2.0 mm) in each joint for injured (n=11) and healthy (n=11) participants at the A) distal radioulnar joint, B) radioscaphoid joint and C) radiolunate joint. There was a significant difference between the healthy and injured participants for the mean JSA (%) across wrist extension/flexion motion in only the DRUJ at inter-bone ($p<0.05$) whereas there were no statistical differences found between joint space area during extension, neutral, and flexion at the radiolunate ($p>0.05$) or radioscaphoid joint ($p>0.05$) The largest difference between the healthy and fracture patients observed for the DRUJ was at maximum flexion showing a difference of approximately 20% (19.6 mm^2). When examining differences JSA % between extension, neutral and flexion, there was a difference in JSA at the radiolunate joint ($p<0.05$) but not at the radioscaphoid joint($p>0.05$) and DRUJ ($p>0.05$) in the healthy cohort, but after fracture, this finding was only true for the radioscaphoid joint ($p<0.05$).

Table 3.1. Demographic factors and injury characteristics of participants in the injured cohort (n=11) and the age-matched healthy (control) cohort (n=11).

Injured Participants						Healthy Participants		
Participant ID	Gender	Age at Injury	Age at Follow-up	Follow-up time (years)	AO Classification	Participant ID	Gender	Age
1A	Female	65	66	1	2R3A3	1B	Female	61
2A	Female	59	73	2	2R3A2	2B	Male	73
3A	Female	58	61	10	2R3C2	3B	Male	57
4A	Female	76	68	8	2R3A3	4B	Male	71
5A	Female	58	84	2	2R3C2	5B	Female	80
6A	Female	63	60	12	2R3C3	6B	Female	56
7A	Female	64	75	13	2R3C2	7B	Female	73
8A	Female	65	77	15	2R3B1	8B	Male	72
9A	Male	15	80	47	No injury films	9B	Female	76
10A	Female	67	62	10	2R3A2	10B	Female	57
11A	Female	66	77	7	2R3A2	11B	Male	75

Table 3.2. Radiographic measurements taken at long-term follow-up (mean: 5 months, range: 3-10 months).

Radiographic alignment measurements included Radial Inclination (RI), Dorsal Angulation (DA), Ulnar Variance (mm)- measured from the line tangential to the lunate fossa and perpendicular to the radial shaft compared to the line tangential to the distal articular surface of the ulna. positive variance (+) is when the ulna is longer than the tangential line from the lunate fossa while negative variance (-) is when the ulna is shorter than the tangent (UV). The radiographic measurements highlighted in red are classified as unacceptable according to previous studies (RI <15°, DA >10° and UV ≥3 mm)

Injured Participant	RI	DA	UV
1A	12	8.5	1mm+
2B	21.9	11.2	2mm+
3A	20.6	30.2	4mm+
4A	19.5	2.9 volar	1mm+
5A	23.5	14.2 volar	0
6A	26.7	5.4 volar	3mm +
7A	27.6	25	3mm +
8A	18	4.1	0
9A	21.3	6.3	1mm+
10A	17.3	25.9	6mm+
11A	25	3.1 volar	1mm+

Table 3.3. Joint Congruency Maps for the Distal Radioulnar, Radioscaphoid and Radiolunate Joints at the Extremes of Wrist Extension-Flexion for Age-Matched Injured (n=11) and Healthy Participants (n=11).

A color-bar is shown (0-2 mm: red-blue) corresponds to high, medium, low and ultra-low proximity.

0 mm		2.00 mm

0.5 mm High Proximity	1.0 mm Med Proximity	1.5 mm Low Proximity	2.0 mm Ultra-Low Proximity
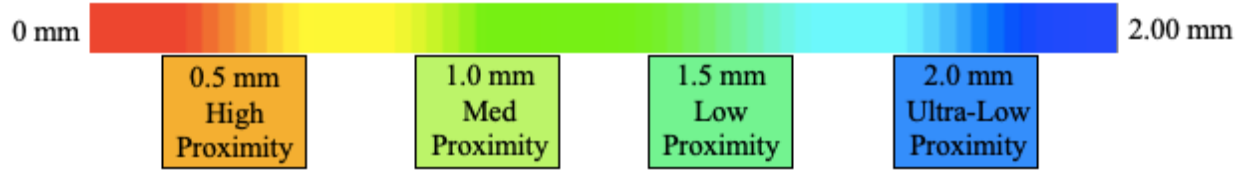
Health status	Injured			Healthy		
ID	1A (mal-union)			1B		
Joint	Distal radio-ulnar	Radio-scaphoid	Radio-lunate	Distal radio-ulnar	Radio-scaphoid	Radiolunate
Maximum Extension	KL: 1	KL: 1		KL: 1	KL: 1	
Neutral						
Maximum Flexion						
ID	2A (mal-union)			2B		
Joint	Distal radio-ulnar	Radio-scaphoid	Radio-lunate	Distal radio-ulnar	Radio-scaphoid	Radiolunate
Maximum Extension	KL: 2	KL: 1		KL: 2	KL: 1	
Neutral						
Maximum Flexion						
ID	3A (mal-union)			3B		
Joint	Distal radio-ulnar	Radio-scaphoid	Radio-lunate	Distal radio-ulnar	Radio-scaphoid	Radiolunate

Maximum Extension	KL: 3		KL: 2	KL: 2		KL: 2
Neutral						
Maximum Flexion						
ID	4A			4B		
Joint	Distal radio-ulnar	Radio-scaphoid	Radio-lunate	Distal radio-ulnar	Radio-scaphoid	Radiolunate
Maximum Extension	KL: 2	KL: 2		KL: 2	KL: 3	
Neutral						
Maximum Flexion						
ID	5A (mal-union)			5B		
Joint	Distal radio-ulnar	Radio-scaphoid	Radio-lunate	Distal radio-ulnar	Radio-scaphoid	Radiolunate
Maximum Extension	KL: 2	KL: 2		KL: 2	KL: 1	
Neutral						
Maximum Flexion						
ID	6A (mal-union)			6B		
Joint	Distal radio-ulnar	Radio-scaphoid	Radio-lunate	Distal radio-ulnar	Radio-scaphoid	Radiolunate

Maximum Extension		KL: 3		KL: 1	KL: 2	KL: 1
Neutral						
Maximum Flexion						
ID	7A (mal-union)			7B		
Joint	Distal radio-ulnar	Radio-scaphoid	Radio-lunate	Distal radio-ulnar	Radio-scaphoid	Radiolunate
Maximum Extension		KL: 3		KL: 2	KL: 2	KL: 2
Neutral						
Maximum Flexion						
ID	8A			8B		
Joint	Distal radio-ulnar	Radio-scaphoid	Radio-lunate	Distal radio-ulnar	Radio-scaphoid	Radiolunate
Maximum Extension		KL: 4		KL: 1	KL: 2	KL: 1
Neutral						
Maximum Flexion						
ID	9A			9B		
Joint	Distal radio-ulnar	Radio-scaphoid	Radio-lunate	Distal radio-ulnar	Radio-scaphoid	Radiolunate

Maximum Extension	KL: 4	KL: 2		KL: 3	KL: 2
Neutral					
Maximum Flexion					
ID	10A (mal-union)			10B		
Joint	Distal radio-ulnar	Radio-scaphoid	Radio-lunate	Distal radio-ulnar	Radio-scaphoid	Radiolunate
Maximum Extension	KL: 4	KL: 3		KL: 2	KL: 1	
Neutral						
Maximum Flexion						
ID	11A			11B		
Joint	Distal radio-ulnar	Radio-scaphoid	Radio-lunate	Distal radio-ulnar	Radio-scaphoid	Radiolunate
Maximum Extension	KL: 3	KL: 1		KL: 2	KL: 3	
Neutral						
Maximum Flexion						

Table 3.4. Functional and pain assessment of participants in the injured cohort (n=11) and the age-matched healthy (control) cohort (n=11).

Range of motion measures were taken on the injured wrist and were compared to the same side wrist in the healthy cohort.

Injured Participant							Healthy Participant						
ID	Static Extension (°)	Static Flexion (°)	Dynamic Extension (°)	Dynamic Flexion (°)	Grip Strength (Kg)	PRWE	ID	Static Extension (°)	Static Flexion (°)	Dynamic Extension (°)	Dynamic Flexion (°)	Grip Strength (Kg)	PRWE
1A	60	25	62.5	32.6	14	36.5	1B	65	80	74	42.1	26	0
2A	50	65	71.1	38.5	23	10	2B	60	70	64.7	49.9	42	18
3A	50	75	65	47.2	20	5	3B	60	70	68.7	31.9	40	0
4A	70	60	57.7	37.2	26	26.5	4B	70	70	69.2	35.5	43	0
5A	77	55	66.9	46.3	24	3	5B	70	50	55.5	57.9	19	54
6A	86	66	62.3	68.1	23	3.5	6B	75	65	71.6	61.9	40	0
7A	50	55	53.9	43.6	28	12	7B	55	85	57	59	28	0
8A	55	60	40.5	42.6	30	2.5	8B	65	75	66.6	42	34	0
9A	55	87	71.3	52.5	20	0	9B	70	70	51.5	68.1	24	0
10A	60	30	55.6	20	20	0	10B	60	50	57	46.8	18	65
11A	75	55	57.7	61.7	23	41	11B	66	32	45.3	37.3	40	1
Average	63	58	60	45	23	13	Average	65	65	62	48	32	13

Figure 3.1. (A)
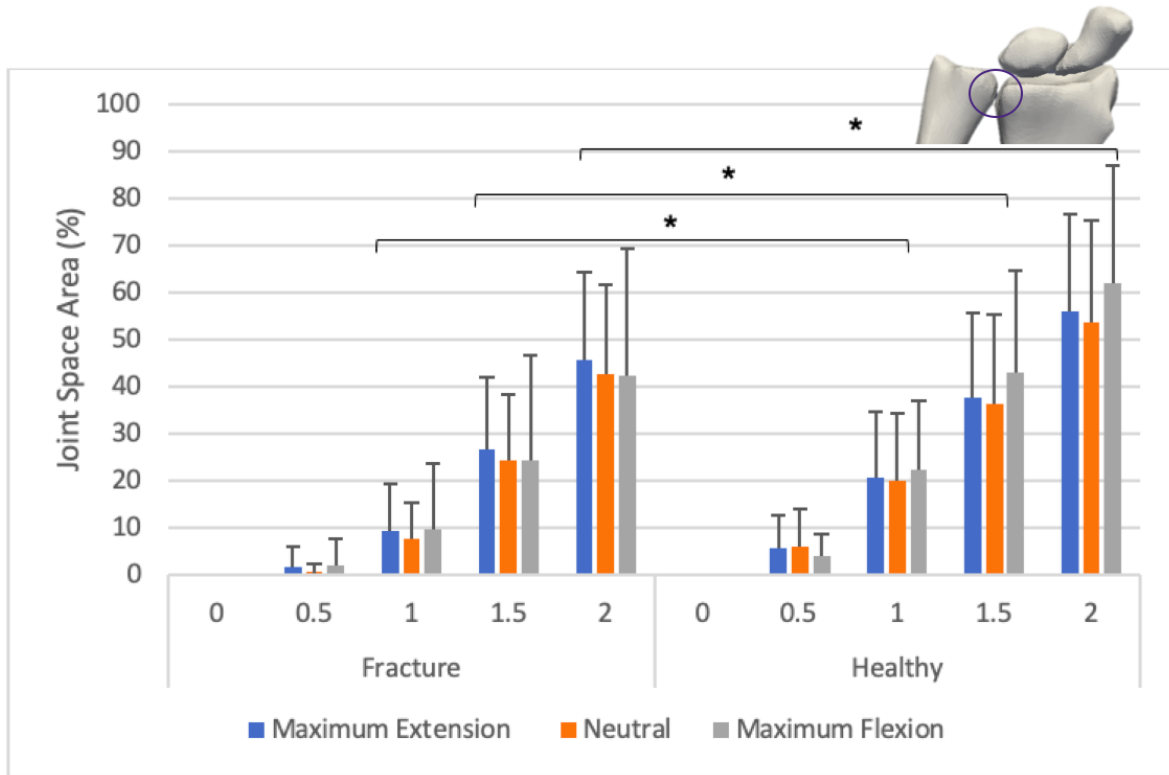
Figure 3.1. (B)
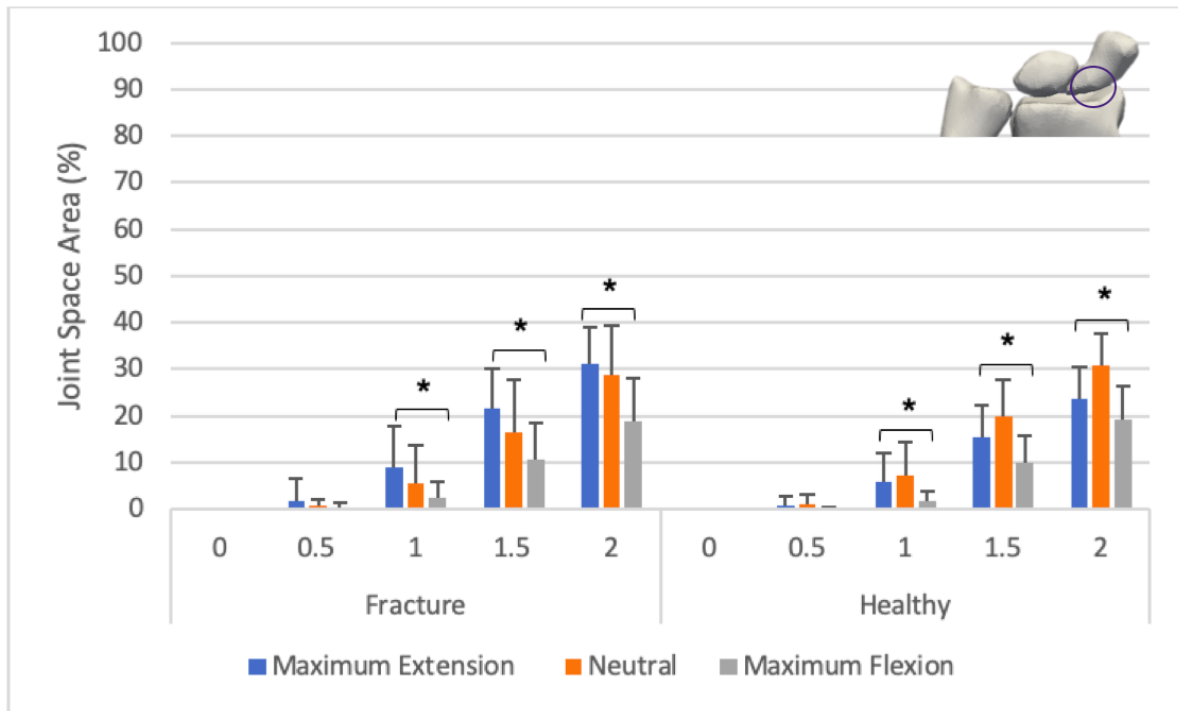
Figure 3.1. (C)
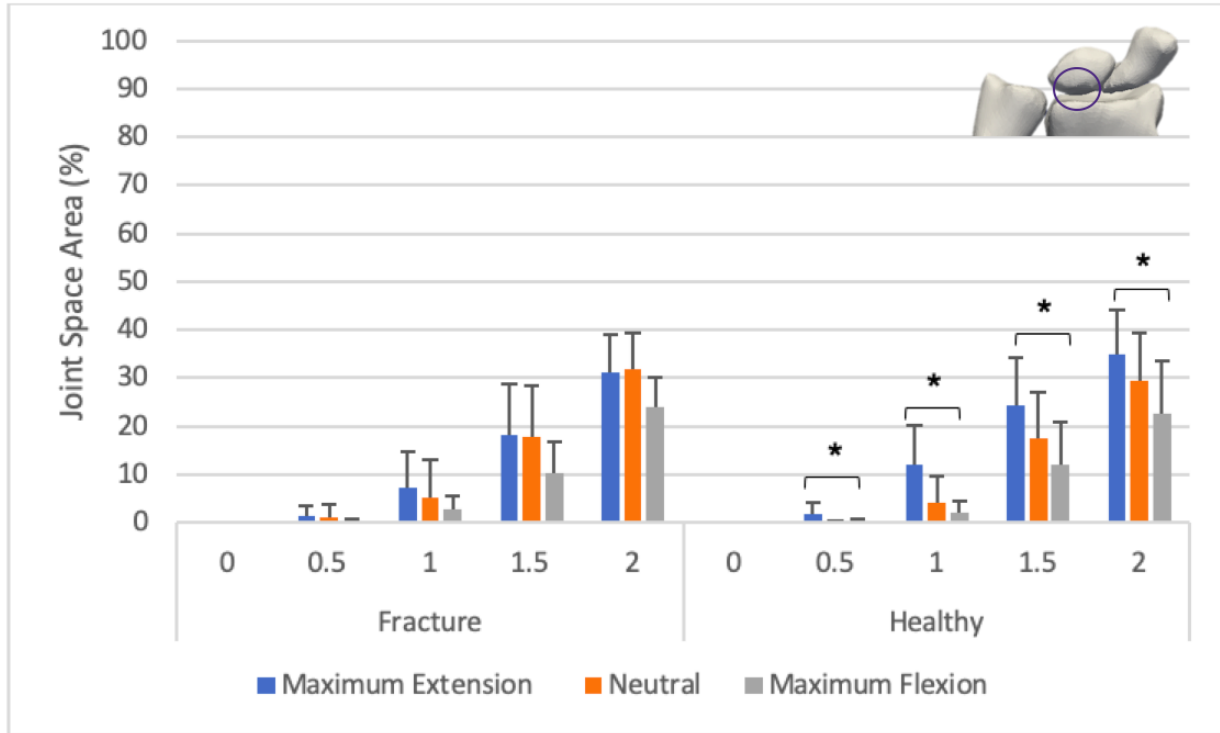
Figure 3.1 (A-C). Changes in percent mean joint surface areas (inter-bone distances less than 2.0 mm) in each joint for injured (n=11) and healthy (n=11) participants.
Bars represent mean and error bars represent standard deviation of the sample.
A) Average Contact Area Percentage For the Distal Radioulnar Joint in Healthy and Fracture Patients
B) Average Contact Area Percentage For the Radioscaphoid Joint in Healthy and Fracture Patients
C) Average Contact Area Percentage for the Radiolunate Joint in Healthy Patients and Fracture Patients

3.4   Discussion

This study investigated the use of 4DCT to measure the effect of DRF and joint mal-alignment on the dynamic joint congruency for the following joints of interest: DRUJ, radioscaphoid, and radiolunate joints. This study evaluated the dynamic signs of injury by visualizing the JSA during *in vivo* wrist extension/flexion motion. The results demonstrated that the joint congruency at the DRUJ was affected by the health status such that the JSA at the DRUJ significantly decreased in individuals with DRFs. This study demonstrated no effect of joint position on JSA percentage at the DRUJ supporting the notion that extension/flexion is a

radiocarpal driven motion. The results also demonstrated joint position (extreme flexion, neutral and extreme extension) affected JSA % at the radioscaphoid joint for both the healthy and injured cohorts. This, however, was not the case at the radiolunate where only differences in JSA % throughout wrist flexion were found in the healthy cohort and only observed a trend of decreased JSA % from extension to flexion in the fracture cohort. Individuals with DRF also demonstrated decreased grip strength but no differences were found in range of motion, pain, and degenerative changes in the wrists when compared to the healthy cohort.

Previous studies, described in Chapter 1 section 1.3.3, have investigated the effect of health status on joint congruency after DRFs. Crisco and colleagues found that the JSA at the DRUJ during forearm rotation significantly decreased by approximately 25% or 56 mm^2 in the malunited forearm compared to the contralateral uninjured arm. [187] This study only recruited patients with mal-aligned DRFs, examined forearm rotation, and had contralateral wrists as their control group which can explain the larger difference found between the injured and uninjured wrists in their study. [187] Our data did follow a similar trend, where JSA at the DRUJ significantly decreased by approximately 20% and 10% at extreme flexion and at extreme extension, respectively, in the injured cohort compared to the healthy cohort. Recently, a study from our group employed 3DCT using static, fully pronated images and found a smaller reduction (approximate 3%) in JSA at the DRUJ when comparing injured and uninjured wrists. This previous study included patients with mild mal-alignment, which is similar to the injured cohort in this study. [30]

This previous study examined the overall joint congruency at the radiocarpal joints and found similar locations for the high contacting regions but asymmetric amounts (surface area) of the high contacting regions when comparing the injured and non-injured wrists. [30] The purpose of this previous study was to test the feasibility of applying the inter-bone distance technique to the radiocarpal joints and thus was limited to a small case series and a single static position. [30] While there were no significant differences in JSA at the radiocarpal joints between the injured and healthy cohorts in our current study, there were asymmetric differences in joint congruency post-fracture.

Radiocarpal joint mechanics can play an important role in the dysfunction associated with distal radius malunions. It has been suggested that residual deformity of the joint may affect loading mechanics and potentially cause pain, loss of motion, diminished grip strength, and an

increase in the risk for post traumatic arthritis which commonly occurs at the radiocarpal joint. [210] This is consistent with our findings of increased incidence of arthritis at the radiocarpal joints in the injured cohort (n=10). Our study also demonstrated a decrease in grip strength in the injured cohort, but no differences in symptoms of pain, range of motion and arthritis at the DRUJ and radiocarpal joints. This may be due to the age of the patient population and the long follow-up period (mean= 12 years). The age of the patient population is a limitation of this study. [219]

Several studies have measured JSA across multiple static positions for wrist motions. Rainbow et al. demonstrated that the contact areas of the lunate and scaphoid on the radius significantly decreased 39% ± 22% and 66% ± 13%, respectively, when the wrist was in extreme flexion from neutral grip in healthy patients (n=12). [216] Additionally, the contact areas of the lunate and scaphoid significantly increased 45% ± 22% and 13% ± 16%, respectively, in extreme extension from neutral grip. [216] Our data followed a similar trend and found significant differences in the JSA % at the radiolunate joint across the joint positions in healthy wrists but not in injured wrists. These findings indicate that the radiocarpal joint is largely responsible for extension/flexion. Furthermore, changes in the joint congruency post-fracture demonstrate the effect of the altered anatomy of the distal radius and joint mal-alignment on wrist mechanics.

Additionally, the scaphoid and lunate do not contribute equally to wrist extension/flexion and these bones do not function as a unit. Evidence supporting this notion does exists, but studies are limited to invasive techniques, in vitro models, and static positions. [36,131] These studies also investigated the kinematic patterns rather than assessing the joint congruency and its differences in healthy participants and post-fracture. [36,131] This study demonstrated the interactions between these articulating bone surfaces *in vivo*. The radiolunate joint also demonstrated greater congruence at extension compared to the radioscaphoid in our healthy cohort. This may be the result of its hemi-moon shape.

Limitations of the study are the small series of patients included, use of a convenience sample (no preference for mild or severe mal-alignment). The mal-alignment in this cohort of patients was mild which may explain no significant degenerative changes when comparing the injured cohort with the uninjured cohort. JSA is not a direct measure of cartilage contact. The JSA are inferred contact region because it does not consider cartilage thickness. This study did not consider the loading conditions that are reflective of functional loads experienced during

activities of daily living. Since patients experience symptoms under loading, it is important to determine what the effect of weight-bearing is on the joint mechanics of the wrist.

3.5   Conclusion

This study gives insight into a dynamic assessment of wrist biomechanics post-fracture across extension/flexion motion using 4DCT. The results from this study demonstrate that post-fracture, joint congruency decreased at the distal radioulnar joint when compared to the healthy control population. Additionally, wrist position was found to have a significant effect on radioscaphoid JSA in both the injured and uninjured cohorts but only in the uninjured participants in the radiolunate joint. This study demonstrates the use of a non-invasive tool that can be used to examine the effect of wrist fracture on surrounding joint contact mechanics. This is an important step in the quest to determine causal relationship between joint structure and patient function.

Chapter 4 – General Discussion and Conclusion

4   *Overview*

This chapter will outline the objectives and hypotheses stated in Chapter 1 of this thesis. The major conclusions of each study as well as their strengths, weaknesses and future directions are summarized.

4.1   Summary

The purpose of this work was to expand the current knowledge of the impact of joint mal-alignment after wrist fractures on joint congruency and mechanics, and to examine if changes in joint congruency and mechanics relate to the development of osteoarthritis. Presented in this thesis are the results of two *in vivo* studies: the first examines 3D implications of a scaphoid malunion on joint congruency and mechanics, four years post-fracture; and the second examines joint congruency and mechanics across wrist extension/flexion in patients with and without a previous distal radius fracture. The specific objectives previously stated in Chapter 1 have been achieved.

The following is a list of the thesis objectives:

1. To employ CT imaging to determine the 3D implications (joint space area (JSA)) of altered bony alignment on the joint contact area of joints surrounding the scaphoid in patients with scaphoid malunions a minimum of four years post-fracture.

2. To employ 4DCT to examine the JSA of the distal-radial joint (DRUJ) and radio-carpal joints in cohort of patients with distal radius fractures a minimum of one year compared to a cohort of healthy patients.

3. To employ 4DCT to examine the JSA of DRUJ and radio-carpal joints at three wrist positions during extension/flexion motion in cohort of patients with distal radius fractures a minimum of one year compared to a cohort of healthy patients.

4.2 Chapter 2: The Effect of Scaphoid Malunion on Joint Congruency

The first objective of this thesis was to employ CT imaging to determine the 3D implications (JSA) of altered bony alignment on the joint contact area of joints surrounding the scaphoid in patients with scaphoid malunions a minimum of four years post-fracture. This objective was achieved using an *in vivo* study that included fourteen subjects with previous unilateral malunited scaphoid fractures. Three-dimensional inter-bone distance (joint space), a measure of joint congruency and 3D alignment, was quantified from reconstructed computed tomography bone models of the carpus.

The results presented in Chapter 2 demonstrate a significant difference in measured joint space area (and therefore corresponding reduced 3D joint space) at the scaphotrapezoid, scaphotrapezial and scaphocapitate joints when comparing the baseline and follow-up scans of the wrist. In addition, the results demonstrate no changes in degeneration of the wrist joints at an average of 7 years post-fracture (minimum of 4 years). These results confirm the thesis hypothesis scaphoid malunion will alter JSA and load distributions at mid-term follow-up (Hypothesis 1a). The results reject the hypothesis, however, that the changes in JSA will lead to the development of degenerative changes in the wrist as early as four years post-fracture (Hypothesis 1b).

4.3   Chapter 3: Four-Dimensional Computed Tomography to Measure Distal Radial-Ulnar and Radio-Carpal Joint Congruency After Distal Radius Fractures

The second objective of this thesis was to employ 4DCT to examine the JSA of the distal-radial joint (DRUJ) and radio-carpal joints in a cohort of patients with previous distal radius fractures a minimum of one year, compared to a cohort of healthy patients. This objective was achieved using an *in vivo* study that included patients with and without a previous distal radius fracture (11 fractures: 11 healthy controls). Unilateral 4DCT images were acquired while participants actively moved their wrist from full extension to flexion. Three-dimensional reconstructions were created and used with a previously developed inter-bone distance algorithm to measure 3D joint space.

The results presented in Chapter 3 indicate that, post-fracture, there was a decrease in the joint congruency at the distal radioulnar joint when compared to the healthy control population. This finding rejects the hypothesis that distal radius fractures will alter JSA of DRUJ and radiocarpal joints compared to the age-matched healthy cohort (Hypothesis 2a); although it was significantly proven for JSA in the DRUJ, JSA in radiocarpal joints did not demonstrate a significant difference. The results also demonstrated a significant decrease in grip strength, but no difference in the range of motion, pain, and degenerative changes. This finding also rejects the hypothesis that the changes in JSA will lead to the degeneration of DRUJ and radiocarpal joints (Hypothesis 2b). In addition, this study found that wrist position had a significant effect on radioscaphoid JSA in both the injured and uninjured cohorts but only in the uninjured participants in the radiolunate joint. This is suggestive of the hypothesis that distal radius fractures will alter JSA in the radiocarpal joints across wrist extension/ flexion, but not in the DRUJ, which is largely responsible for pronation/supination (Hypothesis 3).

4.4   Strengths and Limitations

The studies conducted in Chapter 2 and Chapter 3 had several strengths, including the analysis of joint mechanics *in vivo,* the avoidance of potential alterations of tissue properties when using cadaver material, the incorporation of actual muscular forces, and the ability to evaluate the long-term effects of healing and surgical intervention. Both studies implemented the scanning protocol in a large cohort of patients. Studies measured 3D joint space using volumetric data obtained from CT imaging and thus did not rely on 2D radiographs that are limited by the anatomical complexity of the wrist. Furthermore, these studies applied a previously developed inter-bone distance (3D joint space) technique to the radiocarpal and midcarpal joints to determine the impact of the fracture on the highly integrated joints surrounding the fractured bone within the wrist. This CT-based technique allows for a non-invasive characterization of wrist injuries to visually examine 3D joint mechanics.

These studies are not without limitations. First, static positions were used from 3DCT and 4DCT acquisitions. The study did lay the groundwork of the feasibility of using dynamic 4DCT to acquire images and create 3D reconstructions of the wrist bones, but these static positions cannot address the altered joint mechanics at intermediate positions. Second, the JSA metric, which indicates joint space narrowing used to monitor the development of osteoarthritis, is not a direct measure of joint contact area because cartilage is poorly imaged with CT. Third, CT, often used by clinicians to evaluate complex fractures and confirm suspected malunions, expose participants to extra radiation dose; furthermore, CT scans can be time-consuming and uncomfortable for participants who are typically asked to undergo multiple scans. Fourth, these studies present no data regarding joint mechanics under physiological loading conditions; however, this area of research is important because patients suffering from wrist fractures usually experience pain when they load their wrist during activities of daily living.

4.5   Current and Future Directions

This thesis provides insight into the effect of joint alignment on joint contact mechanics using static (3DCT) and dynamic (4DCT) CT imaging. The two studies have extended the use of a previously developed joint congruency technique (joint space mapping) *in vivo* in a cohort of patients. These studies discussed in Chapter 2 and Chapter 3 were able to successfully reconstruct and analyze volumetric data from 3DCT and 4DCT images of the wrist, respectively. These image-based measures provided valuable information on the changes in joint mechanics as a result of a wrist fracture and associated patient outcomes such as wrist pain, function and degenerative changes in the wrist. However, the 3D reconstructions were created using semiautomatic segmentation and manual registration techniques; this process was time-consuming, and the accuracy was user-dependent.

Current directions of ongoing studies focus on overcoming the limitations of the studies in Chapters 2 and 3. First, some studies are focusing on using machine learning and AI algorithms to develop a technique for automatic segmentation and semi-automatic registration in order to implement a more efficient data analysis strategy. These studies will not only increase the accuracy and quality of the 3D reconstructions but also allow researchers to create these reconstructions at a faster rate.

Second, studies examining the role of acquisition time and wrist speed are important to reduce dose exposure and avoid image blurring. Chapter 3 used speeds that were comfortable to the participants who have recently took off their cast and may be in pain. Current ongoing studies using i*n vitro* cadaveric testing focusing on different wrist speeds is beneficial in determining which speeds do not produce blurry images. These studies will optimize the scanning speed to realistically represent physiological wrist motion and allow for conclusions to be generalized to typical wrist motions during activities of daily living.

Third, standardizing the data collection will lead to more accurate and repeatable results. Chapter 3 was a feasibility study to determine if previously developed segmentation and registration algorithms can be applied to 4DCT acquisitions and produce results. The participants in this study either moved too fast creating blurry images or too slow so not capturing the entire range of motion during the short acquisition time. Current ongoing studies are focusing on standardizing the data by determining the angular velocity using degree intervals or second intervals throughout the range motion which can be used to compare data between participants.

71

Future directions will aim to evaluate the effectiveness of the surgical outcomes according to the H/L ratio; since the study in Chapter 2 did not distinguish between types of surgical procedure performed on each subject. Additionally, future work would need to distinguish between the severity of malunion (mild, moderate and severe) and the observed changes in joint mechanics and patient outcomes such as range of motion and degenerative changes. The Chapter 2 study also did not examine clinical outcome measures related to hand function and patient rating of wrist pain and disability. Future work will be needed to investigate how these joint contact changes relate to wrist function.

Wrist movements are rarely planar during activities of daily living and considered to be essential for rehabilitation after wrist injury. The studies in Chapters 2 and 3 do not adequately represent joint positions of the wrist that patients experience in their daily lives. However, Chapter 2 focused on one static position and Chapter 3 focused on one wrist motion. More specifically, Chapter 3 focused on the flexion and extension motion which occurs in one plane. Future studies need to consider obtaining functional range of motion scans of more complex movements that involve multiple planes, which would provide valuable information on joint mechanics. Future work also needs to consider loading the wrist with typical loads experienced in their daily lives.

Finally, our lab in the past years mainly focused on creating 3D reconstructions of the wrist and efforts should be made to develop a 4DCT grading system which can be used as a clinical tool for surgeons to see the instability in real time in wrist injury population. In addition, there are many theories in the literature about the movement of the individual wrist bones, but no conclusive theory has been accepted. However, more accurate kinematic data from 4DCT imaging can examine subtle bony movements and refine mechanisms.

4.6   Conclusion

There have been high rates of arthritis after an orthopaedic injury and thus a greater understanding of what causes the development of arthritis and how it progresses is needed. It has been assumed that mal-alignment after wrist fractures leads to the development of post-traumatic osteoarthritis and poor functional outcomes. However, the mechanistic pathways between mal-alignment and development of post-traumatic osteoarthritis are not clearly understood due to limitations in current techniques. The present work in this thesis is an essential first step in generating image and functional data of patients suffering a wrist fracture. The studies used image-based measures to further our understanding of the relationship between joint structure (and mal-alignment) and joint contact mechanics after a wrist fracture to limit the progression of osteoarthritis and restore joint function at the wrist. Eventually, this research will be used to inform clinical guidelines relating to fracture mal-alignment that can guide treatments and ensure better patient outcomes.

References

1. Hand and Wrist Anatomy and Biomechanics: A Comprehensive Guide - Bernhard Hirt, Harun Seyhan, Michael Wagner - Google Books. https://books.google.ca/books?id=3H5FDQAAQBAJ&pg=PT21&source=gbs_selected_pages&cad=3#v=onepage&q&f=false. Accessed September 30, 2020.
2. Carlsen BT, Shin Y, Shin AY. *Wrist Instability*. Vol 97.; 2008.
3. Mansfield PJ, Neumann DA. Structure and Function of the Wrist. In: *Essentials of Kinesiology for the Physical Therapist Assistant*. Elsevier; 2019:120-140. doi:10.1016/b978-0-323-54498-6.00006-0
4. The Wrist: Diagnosis and Operative Treatment - William P. Cooney - Google Books. https://books.google.ca/books?id=qva8f16BewEC&pg=PA37&lpg=PA37&dq=fossae+are+separated+by+a+fibrocartilage+ridge+known+as+the+interfacet+prominence.&source=bl&ots=atLCUXglxf&sig=ACfU3U1iaWPtUrKzfV6Om6YK9Ya_BPqpvQ&hl=en&sa=X&ved=2ahUKEwjvxpLFg5HsAhUBHs0KHeJWDGEQ6AEwBHoECAIQAQ#v=onepage&q&f=false. Accessed September 30, 2020.
5. Vezeridis PS, Yoshioka H, Han R, Blazar P. Ulnar-sided wrist pain. Part I: Anatomy and physical examination. *Skeletal Radiol*. 2010;39(8):733-745. doi:10.1007/s00256-009-0775-x
6. Tang A, Varacallo M. *Anatomy, Shoulder and Upper Limb, Hand Carpal Bones*. StatPearls Publishing; 2019. http://www.ncbi.nlm.nih.gov/pubmed/30571003. Accessed September 30, 2020.
7. Wadsworth CT. *Journal of Orthopaedic & Sports Physical Therapy® Downloaded from Www.Jospt.Org at On.*; 2020. www.jospt.org.
8. The Wrist: Diagnosis and Operative Treatment - William P. Cooney - Google Books. https://books.google.ca/books?id=qva8f16BewEC&pg=PA25&dq=anatomy+of+the+wrist&hl=en&sa=X&ved=0ahUKEwjru4il7szoAhUoTd8KHX8WAqAQ6AEIWDAG#v=onepage&q=anatomy of the wrist&f=false. Accessed April 3, 2020.
9. Viegas SF. The lunatohamate articulation of the midcarpal joint. *Arthrosc J Arthrosc Relat Surg*. 1990;6(1):5-10. doi:10.1016/0749-8063(90)90089-V
10. II. Osteology. 6b. The Hand. 1. The Carpus. Gray, Henry. 1918. Anatomy of the Human Body. https://www.bartleby.com/107/54.html. Accessed October 1, 2020.
11. Fundamentals of Hand Therapy - E-Book: Clinical Reasoning and Treatment ... - Cynthia Cooper - Google Books. https://books.google.ca/books?id=UcrsAwAAQBAJ&pg=PA342&lpg=PA342&dq=The+process+of+maintaining+joint+control+and+stability+is+accomplished+through+the+relationship+between+the+static+and+dynamic+joint+stabilizers.&source=bl&ots=YcqOHPVjqR&sig=ACfU3U0xzht_X7f5g-hPjeYPoVSdd3cwew&hl=en&sa=X&ved=2ahUKEwidnq-fgJTsAhWKaM0KHUCLD8EQ6AEwCnoECAwQAg#v=onepage&q&f=false. Accessed October 1, 2020.
12. Helms JTH, Burns B. *Anatomy, Shoulder and Upper Limb, Hand Radiocarpal Joint*. StatPearls Publishing; 2019. http://www.ncbi.nlm.nih.gov/pubmed/30969566. Accessed March 21, 2020.
13. Taljanovic MS, Goldberg MR, Sheppard JE, Rogers LF. US of the Intrinsic and Extrinsic Wrist Ligaments and Triangular Fibrocartilage Complex—Normal Anatomy and Imaging Technique. *RadioGraphics*. 2011;31(1):79-80. doi:10.1148/rg.e44

14. Brown RR, Fliszar E, Cotten A, Trudell D, Resnick D. *Extrinsic and Intrinsic Ligaments of the Wrist: Normal and Pathologic Anatomy at MR Arthrog-Raphy with Three-Com-Partment Enhancement.*

15. Berger RA. The anatomy of the ligaments of the wrist and distal radioulnar joints. In: *Clinical Orthopaedics and Related Research*. Lippincott Williams and Wilkins; 2001:32-40. doi:10.1097/00003086-200102000-00006

16. Viegas SF, Yamaguchi S, Boyd NL, Patterson RM. The dorsal ligaments of the wrist: Anatomy, mechanical properties, and function. *J Hand Surg Am*. 1999;24(3):456-468. doi:10.1053/jhsu.1999.0456

17. Henderson A, Pehoski C. *Hand Function in the Child: Foundations for Remediation*. Mosby Inc.; 2006. doi:10.1016/B978-0-323-03186-8.X5001-1

18. Ralphs JR, Benjamin M. The joint capsule: structure, composition, ageing and disease. *J Anat*. 1994;184 (Pt 3)(Pt 3):503-509. http://www.ncbi.nlm.nih.gov/pubmed/7928639. Accessed October 1, 2020.

19. Berger RA. The anatomy and basic biomechanics of the wrist joint. *J Hand Ther*. 1996;9(2):84-93. doi:10.1016/S0894-1130(96)80066-4

20. Short WH, Palmer AK, Werner FW, Murphy DJ. A biomechanical study of distal radial fractures. *J Hand Surg Am*. 1987;12(4):529-534. doi:10.1016/S0363-5023(87)80202-2

21. Schuind F, Cooney WP, Linscheid RL, An KN, Chao EYS. Force and pressure transmission through the normal wrist. A theoretical two-dimensional study in the posteroanterior plane. *J Biomech*. 1995;28(5). doi:10.1016/0021-9290(94)00093-J

22. Viegas SF, Patterson RM, Todd PD, McCarty P. Load mechanics of the midcarpal joint. *J Hand Surg Am*. 1993;18(1):14-18. doi:10.1016/0363-5023(93)90238-X

23. Kaufmann RA, Pfaeffle HJ, Blankenhorn BD, Stabile K, Robertson D, Goitz R. Kinematics of the Midcarpal and Radiocarpal Joint in Flexion and Extension: An In Vitro Study. *J Hand Surg Am*. 2006;31(7):1142-1148. doi:10.1016/j.jhsa.2006.05.002

24. Stoesser H, Padmore C, Nishiwaki M, Gammon B, Langohr G, Johnson J. Biomechanical Evaluation of Carpal Kinematics during Simulated Wrist Motion. *J Wrist Surg*. 2016;06(02):113-119. doi:10.1055/s-0036-1588025

25. Essentials of Kinesiology for the Physical Therapist Assistant E-Book - Paul Jackson Mansfield, Donald A. Neumann - Google Books. https://books.google.ca/books?id=H2N0DwAAQBAJ&pg=PA126&lpg=PA126&dq=On+average,+from+a+neutral+(0-degree)+position,+the+wrist+flexes+approximately+70+to+80+degrees+and+extends+approximately+60+to+75+degrees,+for+a+total+of+approximately+130+to+155+degrees.+Total+flexion+normally+exceeds+extension+by+approximately+15+degrees&source=bl&ots=O7pDbWCrec&sig=ACfU3U0Mmm_4otYQIyDRglEE7Pgs29lOUw&hl=en&sa=X&ved=2ahUKEwjZqqvT85TsAhXUgnIEHQLHDf8Q6AEwAHoECAEQAg#v=onepage&q=On average%2C from a neutral (0-degree) position%2C the wrist flexes approximately 70 to 80 degrees and extends approximately 60 to 75 degrees%2C for a total of approximately 130 to 155 degrees. Total flexion normally exceeds extension by approximately 15 degrees&f=false. Accessed October 1, 2020.

26. O'Driscoll SW, Horii E, Ness R, Cahalan TD, Richards RR, An KN. The relationship between wrist position, grasp size, and grip strength. *J Hand Surg Am*. 1992;17(1):169-177. doi:10.1016/0363-5023(92)90136-D

27. Spilman HW, Pinkston D. Relation of test positions to radial and ulnar deviation. *Phys Ther*. 1969;49(8):837-844. doi:10.1093/ptj/49.8.837

28. Sauerbier M, Unglaub F. Anatomy and biomechanics of forearm rotation. In: *Fractures

and Injuries of the Distal Radius and Carpus. Elsevier Inc.; 2009:285-296. doi:10.1016/B978-1-4160-4083-5.00029-9

29.   Crisco JJ, Moore DC, Marai GE, et al. Effects of distal radius malunion on distal radioulnar joint mechanics—an in vivo study. J Orthop Res. 2007;25(4):547-555. doi:10.1002/jor.20322

30.   Lalone EA, MacDermid J, King G, Grewal R. The Effect of Distal Radius Fractures on 3-Dimensional Joint Congruency. J Hand Surg Am. 2020;0(0). doi:10.1016/j.jhsa.2020.05.027

31.   King GJ, McMurtry RY, Rubenstein JD, Gertzbein SD. Kinematics of the distal radioulnar joint. J Hand Surg Am. 1986;11(6):798-804. doi:10.1016/S0363-5023(86)80225-8

32.   Ekenstam FA, Hagert CG. Anatomical studies on the geometry and stability of the distal radio ulnar joint. Scand J Plast Reconstr Surg Hand Surg. 1985;19(1):17-25. doi:10.3109/02844318509052861

33.   Moritomo H, Apergis EP, Herzberg G, Werner FW, Wolfe SW, Garcia-Elias M. REVIEW ARTICLE 2007 IFSSH Committee Report of Wrist Biomechanics Committee: Biomechanics of the So-Called Dart-Throwing Motion of the Wrist.; 2007.

34.   Palmer AK, Werner FW, Murphy D, Glisson R. Functional wrist motion: A biomechanical study. J Hand Surg Am. 1985;10(1):39-46. doi:10.1016/S0363-5023(85)80246-X

35.   Mitsukane M, Sekiya N, Kamono A, Nakabo T. Motion-plane dependency of the range of dart throw motion and the effects of tendon action due to finger extrinsic muscles during the motion. J Phys Ther Sci. 2018;30(3):355-360. doi:10.1589/jpts.30.355

36.   Wolfe SW, Neu C, Crisco JJ. In vivo scaphoid, lunate, and capitate kinematics in flexion and in extension. J Hand Surg Am. 2000;25(5):860-869. doi:10.1053/jhsu.2000.9423

37.   Kaufmann R, Pfaeffle J, Blankenhorn B, Stabile K, Robertson D, Goitz R. Kinematics of the midcarpal and radiocarpal joints in radioulnar deviation: An in vitro study. J Hand Surg Am. 2005;30(5):937-942. doi:10.1016/j.jhsa.2005.05.016

38.   Krasin E, Goldwirth M, Gold A, Goodwin DR. Review of the current methods in the diagnosis and treatment of scaphoid fractures. Postgrad Med J. 2001;77(906):235-237. doi:10.1136/PMJ.77.906.235

39.   Hove LM. Epidemiology of scaphoid fractures in Bergen, Norway. Scand J Plast Reconstr Surg Hand Surg. 1999;33(4):423-426. doi:10.1080/02844319950159145

40.   Kawamura K, Chung KC. Treatment of scaphoid fractures and nonunions. J Hand Surg Am. 2008;33(6):988-997. doi:10.1016/j.jhsa.2008.04.026

41.   Hayat Z, Varacallo M. Scaphoid Wrist Fracture. StatPearls Publishing; 2019. http://www.ncbi.nlm.nih.gov/pubmed/30725592. Accessed March 22, 2020.

42.   Wang R, Reed J, Leone J, Bhandari M, Moro JK. A Systematic Approach To A Painful Wrist.; 2001. www.scar.rad.washington.edu/RadAnat/WristPA-Labelled.html. Accessed September 26, 2020.

43.   Dias J, Brealey S, Choudhary S, et al. Scaphoid Waist Internal Fixation for Fractures Trial (SWIFFT) protocol: A pragmatic multi-centre randomised controlled trial of cast treatment versus surgical fixation for the treatment of bi-cortical, minimally displaced fractures of the scaphoid waist in adults. BMC Musculoskelet Disord. 2016;17(1):248. doi:10.1186/s12891-016-1107-7

44.   Garala K, Taub NA, Dias JJ. The epidemiology of fractures of the scaphoid. Bone Jt J. 2016;98(5):654-659. doi:10.1302/0301-620X.98B5.36938

45.   Ahmed I, Ashton F, Tay WK, Porter D. The pediatric fracture of the scaphoid in patients

aged 13 years and under: An epidemiological study. *J Pediatr Orthop*. 2014;34(2):150-154. doi:10.1097/BPO.0000000000000102

46. Ghane MR, Rezaee-Zavareh MS, Emami-Meibodi MK, Dehghani V. How trustworthy are clinical examinations and plain radiographs for diagnosis of scaphoid fractures? *Trauma Mon*. 2016;21(5):23345. doi:10.5812/traumamon.23345

47. Johnson MR, Fogarty BT, Alitz C, Gerber JP. Non-FOOSH Scaphoid Fractures in Young Athletes: A Case Series and Short Clinical Review. *Sports Health*. 2013;5(2):183-185. doi:10.1177/1941738112464762

48. Bhat M, McCarthy M, Davis TRC, Oni JA, Dawson S. MRI and plain radiography in the assessment of displaced fractures of the waist of the carpal scaphoid. *J Bone Joint Surg Br*. 2004;86(5):705-713. doi:10.1302/0301-620x.86b5.14374

49. Breederveld RS, Tuinebreijer WE. Investigation of computed tomographic scan concurrent criterion validity in doubtful scaphoid fracture of the wrist. *J Trauma - Inj Infect Crit Care*. 2004;57(4):851-854. doi:10.1097/01.TA.0000124278.29127.42

50. Tiel-Van Buul MMC, Van Beek EJR, Borm JJJ, Gubler FM, Broekhuizen AH, Van Royen EA. The value of radiographs and bone scintigraphy in suspected scaphoid fracture: A statistical analysis. *J Hand Surg (British Eur Vol*. 1993;18(3):403-406. doi:10.1016/0266-7681(93)90074-P

51. Herneth AM, Siegmeth A, Bader TR, et al. Scaphoid fractures: Evaluation with high-spatial-resolution US - Initial results. *Radiology*. 2001;220(1):231-235. doi:10.1148/radiology.220.1.r01jl15231

52. Toth F, Mester S, Cseh G, Bener A, Nyarady J, Lovasz G. Modified carpal box technique in the diagnosis of suspected scaphoid fractures. *Acta radiol*. 2003;44(3):319-325. doi:10.1034/j.1600-0455.2003.00064.x

53. Rhemrev SJ, Ootes D, Beeres FJP, Meylaerts SAG, Schipper IB. Current methods of diagnosis and treatment of scaphoid fractures. *Int J Emerg Med*. 2011;4(1):4. doi:10.1186/1865-1380-4-4

54. Fundamentals of Hand and Wrist Imaging - Giuseppe Guglielmi, Cornelis Van Kuijk - Google Books. https://books.google.ca/books?id=qTCbB2N2UFcC&pg=PA406&lpg=PA406&dq=The+majority+of+these+fractures+occur+at+the+waist+of+the+scaphoid+(65%25-75%25).&source=bl&ots=ju-1kwNV9k&sig=ACfU3U21AkpQFVxylIDgW8FEk7Bh0g9tug&hl=en&sa=X&ved=2ahUKEwi0oM-fr6_oAhUNK80KHXUoBKUQ6AEwCXoECAkQAQ#v=onepage&q=The majority of these fractures occur at the waist of the scaphoid (65%25-75%25).&f=false. Accessed March 22, 2020.

55. Watson HK, Ryu J. Evolution of arthritis of the wrist. *Clin Orthop Relat Res*. 1986;(202):57-67. http://www.ncbi.nlm.nih.gov/pubmed/3955970. Accessed September 16, 2019.

56. Watson HK, Ballet FL. The SLAC wrist: scapholunate advanced collapse pattern of degenerative arthritis. *J Hand Surg Am*. 1984;9(3):358-365. http://www.ncbi.nlm.nih.gov/pubmed/6725894. Accessed August 10, 2019.

57. Traverso P, Wong A, Wollstein R, Carlson L, Ashmead D, Watson HK. Ten-Year Minimum Follow-Up of 4-Corner Fusion for SLAC and SNAC Wrist. *Hand*. 2017;12(6):568-572. doi:10.1177/1558944716681949

58. Mack GR, Bosse MJ, Gelberman RH, Yu E. The natural history of scaphoid non-union. *J Bone Joint Surg Am*. 1984;66(4):504-509. http://www.ncbi.nlm.nih.gov/pubmed/6707028. Accessed May 3, 2019.

59. Moritomo H, Tada K, Yoshida T, Masatomi T. The relationship between the site of nonunion of the scaphoid and scaphoid nonunion advanced collapse (SNAC). *J Bone Jt Surg - Ser B*. 1999;81(5):871-876. doi:10.1302/0301-620X.81B5.9333

60. Vender MI, Watson HK, Wiener BD, Black DM. Degenerative change in symptomatic scaphoid nonunion. *J Hand Surg Am*. 1987;12(4):514-519. doi:10.1016/S0363-5023(87)80198-3

61. Weiss KE, Rodner CM. Osteoarthritis of the Wrist. *J Hand Surg Am*. 2007;32(5):725-746. doi:10.1016/j.jhsa.2007.02.003

62. Burgess RC. The effect of a simulated scaphoid malunion on wrist motion. *J Hand Surg Am*. 1987;12(5):774-776. doi:10.1016/S0363-5023(87)80067-9

63. Gillette BP, Amadio PC, Kakar S. Long-Term Outcomes of Scaphoid Malunion. *Hand (N Y)*. 2017;12(1):26-30. doi:10.1177/1558944716643295

64. Kawamura K, Chung KC. Treatment of Scaphoid Fractures and Nonunions. *J Hand Surg Am*. 2008;33(6):988-997. doi:10.1016/j.jhsa.2008.04.026

65. Burgess RC. The effect of a simulated scaphoid malunion on wrist motion. *J Hand Surg Am*. 1987;12(5):774-776. doi:10.1016/S0363-5023(87)80067-9

66. Smith DK, Cooney WP, An KN, Linscheid RL, Chao EYS. The effects of simulated unstable scaphoid fractures on carpal motion. *J Hand Surg Am*. 1989;14(2 PART 1):283-291. doi:10.1016/0363-5023(89)90022-1

67. Berdia S, Wolfe SW. Effects of scaphoid fractures on the biomechanics of the wrist. *Hand Clin*. 2001;17(4):533-540, vii-viii. http://www.ncbi.nlm.nih.gov/pubmed/11775466. Accessed March 22, 2020.

68. Larsen CF, Stigsby B, Lindequist S, Bellstrøm T, Mathiesen FK, Ipsen T. Observer variability in measurements of carpal bone angles on lateral wrist radiographs. *J Hand Surg Am*. 1991;16(5):893-898. doi:10.1016/S0363-5023(10)80157-1

69. Tiel-van Buul MMC, van Beek EJR, Broekhuizen AH, Nooitgedacht EA, Davids PHP, Bakker AJ. Diagnosing scaphoid fractures: radiographs cannot be used as a gold standard! *Injury*. 1992;23(2):77-79. doi:10.1016/0020-1383(92)90035-Q

70. Bain GI, Bennett JD, MacDermid JC, Slethaug GP, Richards RS, Roth JH. Measurement of the scaphoid humpback deformity using longitudinal computed tomography: Intra- and interobserver variability using various measurement techniques. *J Hand Surg Am*. 1998;23(1):76-81. doi:10.1016/S0363-5023(98)80093-2

71. Seltser A, Suh N, MacDermid JC, Grewal R. The Natural History of Scaphoid Fracture Malunion: A Scoping Review. *J Wrist Surg*. July 2019. doi:10.1055/s-0039-1693658

72. Amadio PC, Berquist TH, Smith DK, Ilstrup DM, Cooney WP, Linscheid RL. Scaphoid malunion. *J Hand Surg Am*. 1989;14(4):679-687. http://www.ncbi.nlm.nih.gov/pubmed/2787817. Accessed June 8, 2019.

73. Jiranek WA, Ruby LK, Millender LB, Bankoff MS, Newberg AH. Long-term results after Russe bone-grafting: the effect of malunion of the scaphoid. *J Bone Joint Surg Am*. 1992;74(8):1217-1228. http://www.ncbi.nlm.nih.gov/pubmed/1400550. Accessed June 8, 2019.

74. Bain GI, Bennett JD, MacDermid JC, Slethaug GP, Richards RS, Roth JH. Measurement of the scaphoid humpback deformity using longitudinal computed tomography: Intra- and interobserver variability using various measurement techniques. *J Hand Surg Am*. 1998;23(1):76-81. doi:10.1016/S0363-5023(98)80093-2

75. Ring D, Patterson JD, Levitz S, Wang C, Jupiter JB. Both Scanning Plane and Observer Affect Measurements of Scaphoid Deformity. *J Hand Surg Am*. 2005;30(4):696-701. doi:10.1016/J.JHSA.2005.03.001

76.	FORWARD DP, SINGH HP, DAWSON S, DAVIS TRC. The Clinical Outcome of Scaphoid Fracture Malunion at 1 Year. *J Hand Surg (European Vol.* 2009;34(1):40-46. doi:10.1177/1753193408093327

77.	Lee C-H, Lee K-H, Lee B-G, Kim D-Y, Choi W-S. Clinical outcome of scaphoid malunion as a result of scaphoid fracture nonunion surgical treatment: A 5-year minimum follow-up study. *Orthop Traumatol Surg Res.* 2015;101(3):359-363. doi:10.1016/j.otsr.2014.09.026

78.	Fernandez DL. *THE SCAPHOID: COMPLICATIONS AND TREATMENT SCAPHOID NON-UNION.* Vol 41.; 2004. https://pdfs.semanticscholar.org/872d/122fe3743f669a0d72320f030a1e387ec0f8.pdf. Accessed June 8, 2019.

79.	Birchard D, Pichora D. Experimental corrective scaphoid osteotomy for scaphoid malunion with abnormal wrist mechanics. *J Hand Surg Am.* 1990;15(6):863-868. doi:10.1016/0363-5023(90)90004-B

80.	Linscheid RL, Lynch NM. Scaphoid osteotomy for malunion. *Tech Hand Up Extrem Surg.* 1998;2(2):119-125. http://www.ncbi.nlm.nih.gov/pubmed/16609475. Accessed June 8, 2019.

81.	Sendher R, Ladd AL. The Scaphoid. *Orthop Clin North Am.* 2013;44(1):107-120. doi:10.1016/J.OCL.2012.09.003

82.	El-Karef EA. Corrective osteotomy for symptomatic scaphoid malunion. *Injury.* 2005;36(12):1440-1448. doi:10.1016/j.injury.2005.09.003

83.	Fernandez DL. A technique for anterior wedge-shaped grafts for scaphoid nonunions with carpal instability. *J Hand Surg Am.* 1984;9(5):733-737. http://www.ncbi.nlm.nih.gov/pubmed/6386956. Accessed June 8, 2019.

84.	Lee C-H, Lee K-H, Lee B-G, Kim D-Y, Choi W-S. Clinical outcome of scaphoid malunion as a result of scaphoid fracture nonunion surgical treatment: A 5-year minimum follow-up study. *Orthop Traumatol Surg Res.* 2015;101(3):359-363. doi:10.1016/J.OTSR.2014.09.026

85.	Barton NJ. The late consequences of scaphoid fractures. *J Bone Joint Surg Br.* 2004;86(5):626-630. http://www.ncbi.nlm.nih.gov/pubmed/15274253. Accessed June 8, 2019.

86.	Afshar A, Mohammadi A, Zohrabi K, Navaeifar N, Sami SH, Taleb H. Correlation of Reconstructed Scaphoid Morphology with Clinical Outcomes. *Arch bone Jt Surg.* 2015;3(4):244-249. http://www.ncbi.nlm.nih.gov/pubmed/26550587. Accessed June 8, 2019.

87.	Nellans KW, Kowalski E, Chung KC. The Epidemiology of Distal Radius Fractures. *Hand Clin.* 2012;28(2):113-125. doi:10.1016/j.hcl.2012.02.001

88.	Oestern HJ. Distal radius fractures. In: *Bone and Joint Injuries: Trauma Surgery III.* Springer Berlin Heidelberg; 2014:121-137. doi:10.1007/978-3-642-38388-5_13

89.	Meena S, Sharma P, Sambharia AK, Dawar A. Fractures of distal radius: an overview. *J Fam Med Prim care.* 2014;3(4):325-332. doi:10.4103/2249-4863.148101

90.	Karl JW, Olson PR, Rosenwasser MP. The epidemiology of upper extremity fractures in the United States, 2009. *J Orthop Trauma.* 2015;29(8):e242-e244. doi:10.1097/BOT.0000000000000312

91.	Naranje SM, Erali RA, Warner WC, Sawyer JR, Kelly DM. Epidemiology of Pediatric Fractures Presenting to Emergency Departments in the United States. *J Pediatr Orthop.* 2016;36(4):e45-e48. doi:10.1097/BPO.0000000000000595

92.	Wood AM, Robertson GA, Rennie L, Caesar BC, Court-Brown CM. The epidemiology of

sports-related fractures in adolescents. *Injury*. 2010;41(8):834-838. doi:10.1016/j.injury.2010.04.008

93. Baron JA, Karagas M, Barrett J, et al. Basic Epidemiology of Fractures of the Upper and Lower Limb... : Epidemiology. *Epidemiology*. 1996;7(6):612-618. doi:10.2307/3702912

94. Nellans KW, Kowalski E, Chung KC. The Epidemiology of Distal Radius Fractures. *Hand Clin*. 2012;28(2):113-125. doi:10.1016/j.hcl.2012.02.001

95. Quinn SF, Murray W, Watkins T, Kloss J. CT for determining the results of treatment of fractures of the wrist. *AJR Am J Roentgenol*. 1987;149(1):109-111. doi:10.2214/ajr.149.1.109

96. Chung KC, Shauver MJ, Birkmeyer JD. Trends in the United States in the treatment of distal radial fractures in the elderly. *J Bone Jt Surg - Ser A*. 2009;91(8):1868-1873. doi:10.2106/JBJS.H.01297

97. Mackenney PJ, McQueen MM, Elton R. Prediction of instability in distal radial fractures. *J Bone Jt Surg - Ser A*. 2006;88(9):1944-1951. doi:10.2106/JBJS.D.02520

98. McQueen MM, MacLaren A, Chalmers J. The value of remanipulating Colles' fractures. *J Bone Jt Surg - Ser B*. 1986;68(2):232-233. doi:10.1302/0301-620x.68b2.3958009

99. McKay SD, MacDermid JC, Roth JH, Richards RS. Assessment of complications of distal radius fractures and development of a complication checklist. *J Hand Surg Am*. 2001;26(5):916-922. doi:10.1053/jhsu.2001.26662

100. Bushnell BD, Bynum DK. Malunion of the distal radius. *J Am Acad Orthop Surg*. 2007;15(1):27-40. doi:10.5435/00124635-200701000-00004

101. Seigerman D, Lutsky K, Fletcher D, et al. Complications in the Management of Distal Radius Fractures: How Do We Avoid them? *Curr Rev Musculoskelet Med*. 2019;12(2):204-212. doi:10.1007/s12178-019-09544-8

102. Operative Techniques in Orthopaedic Trauma Surgery - Paul Tornetta, III - Google Books. https://books.google.ca/books?hl=en&lr=&id=fiwBCwAAQBAJ&oi=fnd&pg=PT365&ots=MEJeDaaV2d&sig=A2JeD1yHblzO5DGkqzu0k74KmBs&redir_esc=y#v=onepage&q&f=false. Accessed September 27, 2020.

103. Haase SC, Chung KC. Management of Malunions of the Distal Radius. *Hand Clin*. 2012;28(2):207-216. doi:10.1016/j.hcl.2012.03.008

104. Prommersberger KJ, Pillukat T, Mühldorfer M, Van Schoonhoven J. Malunion of the distal radius. *Arch Orthop Trauma Surg*. 2012;132(5):693-702. doi:10.1007/s00402-012-1466-y

105. Jenkins NH, Mintowt-Czyz WJ. Mal-union and dysfunction in Colles' fracture. *J Hand Surg Am*. 1988;13(3):291-293. doi:10.1016/0266-7681(88)90090-3

106. Evans BT, Jupiter JB. Best Approaches in Distal Radius Fracture Malunions. *Curr Rev Musculoskelet Med*. 2019;12(2):198-203. doi:10.1007/s12178-019-09540-y

107. Anzarut A, Johnson JA, Rowe BH, Lambert RGW. Radiologic and Patient-Reported Functional Outcomes in an Elderly Cohort With Conservatively Treated Distal Radius Fractures The Journal of Hand Surgery 1121. 2004. doi:10.1016/j.jhsa.2004.07.002

108. DL F. Malunion of the distal radius: current approach to management. *Instr Course Lect*. 1993;42:99-113.

109. Dias JJ, Wray CC, Jones JM. The radiological deformity of Colles' fractures. *Injury*. 1987;18(5):304-308. doi:10.1016/0020-1383(87)90047-7

110. Karnezis IA, Panagiotopoulos E, Tyllianakis M, Megas P, Lambiris E. Correlation between radiological parameters and patient-rated wrist dysfunction following fractures of the distal radius. *Injury*. 2005;36(12):1435-1439. doi:10.1016/j.injury.2005.09.005

111. Gliatis JD, Plessas SJ, Davis TRC. Outcome of distal radial fractures in young adults. *J Hand Surg Am*. 2000;25 B(6):535-543. doi:10.1054/jhsb.2000.0373

112. Souer JS, Lozano-Calderon SA, Ring D. Predictors of Wrist Function and Health Status After Operative Treatment of Fractures of the Distal Radius. *J Hand Surg Am*. 2008;33(2):157.e1-157.e8. doi:10.1016/j.jhsa.2007.10.003

113. Chung KC, Kotsis S V., Kim HM. Predictors of Functional Outcomes After Surgical Treatment of Distal Radius Fractures. *J Hand Surg Am*. 2007;32(1):76-83. doi:10.1016/j.jhsa.2006.10.010

114. Egol KA, Walsh M, Romo-Cardoso S, Dorsky S, Paksima N. Distal radial fractures in the elderly: Operative compared with nonoperative treatment. *J Bone Jt Surg - Ser A*. 2010;92(9):1851-1857. doi:10.2106/JBJS.I.00968

115. Arora R, Lutz M, Deml C, Krappinger D, Haug L, Gabl M. A prospective randomized trial comparing nonoperative treatment with volar locking plate fixation for displaced and unstable distal radial fractures in patients sixty-five years of age and older. *J Bone Jt Surg - Ser A*. 2011;93(23):2146-2153. doi:10.2106/JBJS.J.01597

116. Young BT, Rayan GM. Outcome following nonoperative treatment of displaced distal radius fractures in low-demand patients older than 60 years. *J Hand Surg Am*. 2000;25(1):19-28. doi:10.1053/jhsu.2000.jhsu025a0019

117. Brogren E, Hofer M, Petranek M, Wagner P, Dahlin LB, Atroshi I. Relationship between distal radius fracture malunion and arm-related disability: a prospective population-based cohort study with 1-year follow-up. *BMC Musculoskelet Disord*. 2011;12:9. doi:10.1186/1471-2474-12-9

118. De Smet L, Verhaegen F, Degreef I. Carpal malalignment in malunion of the distal radius and the effect of corrective osteotomy. *J Wrist Surg*. 2014;3(3):166-170. doi:10.1055/s-0034-1384823

119. Anzarut A, Johnson JA, Rowe BH, Lambert RGW, Blitz S, Majumdar SR. Radiologic and patient-reported functional outcomes in an elderly cohort with conservatively treated distal radius fractures. *J Hand Surg Am*. 2004;29(6):1121-1127. doi:10.1016/j.jhsa.2004.07.002

120. Jaremko JL, Lambert RGW, Rowe BH, Johnson JA, Majumdar SR. Do radiographic indices of distal radius fracture reduction predict outcomes in older adults receiving conservative treatment? *Clin Radiol*. 2007;62(1):65-72. doi:10.1016/J.CRAD.2006.08.013

121. Fujii K, Henmi T, Kanematsu Y, Mishiro T, Sakai T, Terai T. Fractures of the Distal End of Radius in Elderly Patients: A Comparative Study of Anatomical and Functional Results. *J Orthop Surg*. 2002;10(1):9-15. doi:10.1177/230949900201000103

122. Vogt MT, Cauley JA, Tomaino MM, Stone K, Williams JR, Herndon JH. Distal Radius Fractures in Older Women: A 10-Year Follow-Up Study of Descriptive Characteristics and Risk Factors. The Study of Osteoporotic Fractures. *J Am Geriatr Soc*. 2002;50(1):97-103. doi:10.1046/j.1532-5415.2002.50014.x

123. Kodama N, Takemura Y, Ueba H, Imai S, Matsusue Y. Acceptable parameters for alignment of distal radius fracture with conservative treatment in elderly patients. *J Orthop Sci*. 2014;19(2):292-297. doi:10.1007/s00776-013-0514-y

124. Batra S, Gupta A. The effect of fracture-related factors on the functional outcome at 1 year in distal radius fractures. *Injury*. 2002;33(6):499-502. doi:10.1016/S0020-1383(01)00174-7

125. Villar RN, Marsh D, Rushton N, Greatorex RA. Three years after Colles' fracture. A prospective review. *J Bone Jt Surg - Ser B*. 1987;69(4):635-638. doi:10.1302/0301-620x.69b4.3611172

126. Taleisnik J, Watson HK. Midcarpal instability caused by malunited fractures of the distal

radius. *J Hand Surg Am*. 1984;9(3):350-357. doi:10.1016/S0363-5023(84)80222-1

127. Brogren E, Wagner P, Petranek M, Atroshi I. Distal radius malunion increases risk of persistent disability 2 years after fracture: A prospective cohort study hand. *Clin Orthop Relat Res*. 2013;471(5):1691-1697. doi:10.1007/s11999-012-2767-8

128. Sasagawa K, Sakamoto M, Yoshida H, Kobayashi K, Tanabe Y. *Three-Dimensional Contact Analysis of Human Wrist Joint Using MRI*.

129. Moojen TM, Snel JG, Ritt MJPF, Venema HW, Kauer JMG, Bos KE. In vivo analysis of carpal kinematics and comparative review of the literature. *J Hand Surg Am*. 2003;28(1):81-87. doi:10.1053/jhsu.2003.50009

130. Pillai RR, Thoomukuntla B, Ateshian GA, Fischer KJ. MRI-based modeling for evaluation of in vivo contact mechanics in the human wrist during active light grasp. *J Biomech*. 2007;40(12):2781-2787. doi:10.1016/j.jbiomech.2006.12.019

131. Kobayashi M, Berger RA, Nagy L, et al. Normal kinematics of carpal bones: A three-dimensional analysis of carpal bone motion relative to the radius. *J Biomech*. 1997;30(8):787-793. doi:10.1016/S0021-9290(97)00026-2

132. Werner FW, Short WH, Fortino MD, Palmer AK. The relative contribution of selected carpal bones to global wrist motion during simulated planar and out-of-plane wrist motion. *J Hand Surg Am*. 1997;22(4):708-713. doi:10.1016/S0363-5023(97)80133-5

133. Wolfe SW, Crisco JJ, Katz LD. A non-invasive method for studying in vivo carpal kinematics. *J Hand Surg (British Eur Vol*. 1997;22(2):147-152. doi:10.1016/S0266-7681(97)80050-2

134. Burgess RC. The effect of a simulated scaphoid malunion on wrist motion. *J Hand Surg Am*. 1987;12(5 Pt 1):774-776. http://www.ncbi.nlm.nih.gov/pubmed/3655241. Accessed June 8, 2019.

135. de Roo MGA, Dobbe JGG, van der Horst CMAM, Streekstra GJ, Strackee SD. Carpal kinematic changes after scaphoid nonunion: an in vivo study with four-dimensional CT imaging. *J Hand Surg Eur Vol*. 2019;44(10):1056-1064. doi:10.1177/1753193419866598

136. Leventhal EL, Wolfe SW, Moore DC, Akelman E, Weiss APC, Crisco JJ. Interfragmentary Motion in Patients With Scaphoid Nonunion. *J Hand Surg Am*. 2008;33(7):1108-1115. doi:10.1016/j.jhsa.2008.03.008

137. Moritomo H, Murase T, Oka K, Tanaka H, Yoshikawa H, Sugamoto K. Relationship Between the Fracture Location and the Kinematic Pattern in Scaphoid Nonunion. *J Hand Surg Am*. 2008;33(9):1459-1468. doi:10.1016/j.jhsa.2008.05.035

138. Moore DC, Hogan KA, Crisco JJ, Akelman E, Dasilva MF, Weiss A-PC. Three-dimensional in vivo kinematics of the distal radioulnar joint in malunited distal radius fractures. *J Hand Surg Am*. 2002;27(2):233-242. http://www.ncbi.nlm.nih.gov/pubmed/11901382. Accessed June 8, 2019.

139. Lalone EA, Grewal R, King GW, MacDermid JC. Evaluation of an Image-Based Tool to Examine the Effect of Fracture Alignment and Joint Congruency on Outcomes after Wrist Fracture. *Open Orthop J*. 2015;9(1):168-178. doi:10.2174/1874325001509010168

140. Tarallo L, Mugnai R, Adani R, Catani F. Malunited extra-articular distal radius fractures: corrective osteotomies using volar locking plate. *J Orthop Traumatol*. 2014;15(4):285-290. doi:10.1007/s10195-014-0307-x

141. Stormont TJ, An KN, Morrey BF, Chao EY. Elbow joint contact study: Comparison of techniques. *J Biomech*. 1985;18(5):329-336. doi:10.1016/0021-9290(85)90288-X

142. Viegas SF, Tencer AF, Cantrell J, et al. Load transfer characteristics of the wrist. Part I. The normal joint. *J Hand Surg Am*. 1987;12(6):971-978. doi:10.1016/S0363-5023(87)80093-X

143. Pogue DJ, Viegas SF, Patterson RM, et al. Effects of distal radius fracture malunion on wrist joint mechanics. *J Hand Surg Am*. 1990;15(5):721-727. doi:10.1016/0363-5023(90)90143-F

144. Short WH, Werner FW, Green JK, Masaoka S. Biomechanical evaluation of ligamentous stabilizers of the scaphoid and lunate. *J Hand Surg Am*. 2002;27(6):991-1002. doi:10.1053/jhsu.2002.35878

145. Shaaban H, Giakas G, Bolton M, et al. Contact area inside the distal radioulnar joint: Effect of axial loading and position of the forearm. *Clin Biomech*. 2007;22(3):313-318. doi:10.1016/j.clinbiomech.2006.05.010

146. DESHMUKH SC, SHANAHAN D, COULTHARD D. Distal Radioulnar Joint Incongruity After Shortening of the Ulna. *J Hand Surg Am*. 2000;25(5):434-438. doi:10.1016/s0266-7681(00)80006-6

147. Marai GE, Laidlaw DH, Demiralp Ç, Andrews S, Grimm CM, Crisco JJ. Estimating Joint Contact Areas and Ligament Lengths from Bone Kinematics and Surfaces. *IEEE Trans Biomed Eng*. 2004;51(5):790-799. doi:10.1109/TBME.2004.826606

148. Cohen ZA, McCarthy DM, Kwak SD, et al. Knee cartilage topography, thickness, and contact areas from MRI: In- vitro calibration and in-vivo measurements. *Osteoarthr Cartil*. 1999;7(1):95-109. doi:10.1053/joca.1998.0165

149. Van Ginckel A, Roosen P, Almqvist KF, Verstraete K, Witvrouw E. Effects of in vivo exercise on ankle cartilage deformation and recovery in healthy volunteers: An experimental study. *Osteoarthr Cartil*. 2011;19(9):1123-1131. doi:10.1016/j.joca.2011.06.009

150. Lalone EA, McDonald CP, Ferreira LM, Peters TM, King GW, Johnson JA. Development of an image-based technique to examine joint congruency at the elbow. *Comput Methods Biomech Biomed Engin*. 2013;16(3):280-290. doi:10.1080/10255842.2011.617006

151. Gammon B, Lalone E, Nishiwaki M, Willing R, Johnson J, King GJW. Arthrokinematics of the Distal Radioulnar Joint Measured Using Intercartilage Distance in an In Vitro Model. *J Hand Surg Am*. 2018;43(3):283.e1-283.e9. doi:10.1016/j.jhsa.2017.08.010

152. Lalone EA, McDonald CP, Ferreira LM, Peters TM, King GW, Johnson JA. Development of an image-based technique to examine joint congruency at the elbow. *Comput Methods Biomech Biomed Engin*. 2013;16(3). doi:10.1080/10255842.2011.617006

153. Leahy RM, Clackdoyle R. *Computed Tomography*.; 2005.

154. Pruitt DL, Gilula LA, Manske PR, Vannier MW. Computed tomography scanning with image reconstruction in evaluation of distal radius fractures. *J Hand Surg Am*. 1994;19(5):720-727. doi:10.1016/0363-5023(94)90174-0

155. Leng S, Zhao K, Qu M, An K-N, Berger R, McCollough CH. Dynamic CT technique for assessment of wrist joint instabilities. *Med Phys*. 2011;38(S1):S50-S56. doi:10.1118/1.3577759

156. Kuo LC, Su FC, Chiu HY, Yu CY. Feasibility of using a video-based motion analysis system for measuring thumb kinematics. *J Biomech*. 2002;35(11):1499-1506. doi:10.1016/S0021-9290(02)00083-0

157. Tersi L, Fantozzi S, Stagni R. In Silico Evaluation. *EURASIP J Adv Signal Process*. 2010;2010. doi:10.1155/2010/142989

158. Davis T. Wrist Instability, Edited by U. Buchler. Martin Dunitz, London, 1996. ISBN L-85317-32-7. Price £49.95. . *J Hand Surg Am*. 1996;21(5):702-702. doi:10.1016/s0266-7681(96)80170-7

159. Carelsen B, Bakker NH, Strackee SD, et al. 4D rotational x-ray imaging of wrist joint dynamic motion. *Med Phys*. 2005;32(9):2771-2776. doi:10.1118/1.2000647

160. Protas JM, Jackson WT. Evaluating carpal instabilities with fluoroscopy. *Am J Roentgenol*. 1980;135(1):137-140. doi:10.2214/ajr.135.1.137
161. Choi YS, Lee YH, Kim S, Cho HW, Song HT, Suh JS. Four-dimensional real-time cine images of wrist joint kinematics using dual source CT with minimal time increment scanning. *Yonsei Med J*. 2013;54(4):1026-1032. doi:10.3349/ymj.2013.54.4.1026
162. Cole RJ, Bindra RR, Evanoff BA, Gilula LA, Yamaguchi K, Gelberman RH. Radiographic evaluation of osseous displacement following intra- articular fractures of the distal radius: Reliability of plain radiography versus computed tomography. *J Hand Surg Am*. 1997;22(5):792-800. doi:10.1016/S0363-5023(97)80071-8
163. Rozental TD, Bozentka DJ, Katz MA, Steinberg DR, Beredjiklian PK. Evaluation of the sigmoid notch with computed tomography following intra-articular distal radius fracture. *J Hand Surg Am*. 2001;26(2):244-251. doi:10.1053/jhsu.2001.22930
164. Dahlen HC, Franck WM, Sabauri G, Amlang M, Zwipp H. Fehlklassifikation extraartikulärer distaler radiusfrakturen in konventionellen röntgenaufnahmen: Vergleichende untersuchung der frakturmorphologie zwischen biplanarer röntgendiagnostik und CT. *Unfallchirurg*. 2004;107(6):491-498. doi:10.1007/s00113-004-0747-5
165. Welling RD, Jacobson JA, Jamadar DA, Chong S, Caoili EM, Jebson PJL. MDCT and Radiography of Wrist Fractures: Radiographic Sensitivity and Fracture Patterns. *Am J Roentgenol*. 2008;190(1):10-16. doi:10.2214/AJR.07.2699
166. Fotiadou A, Patel A, Morgan T, Karantanas AH. Wrist injuries in young adults: The diagnostic impact of CT and MRI. *Eur J Radiol*. 2011;77(2):235-239. doi:10.1016/j.ejrad.2010.05.011
167. Gilley E, Puri S, Trehan SK, Hearns KA, Weiland AJ, Carlson MG. Importance of Computed Tomography in Determining Displacement of Scaphoid Fractures. *J Hand Surg Am*. 2015;40(9):e9-e10. doi:10.1016/j.jhsa.2015.06.022
168. Stevenson JD, Morley D, Srivastava S, Willard C, Bhoora IG. Early CT for suspected occult scaphoid fractures. *J Hand Surg Eur Vol*. 2012;37(5):447-451. doi:10.1177/1753193411428993
169. Langhoff O, Andersen JL. Consequences of late immobilization of scaphoid fracture. *J Hand Surg Am*. 1988;13(1):77-79. doi:10.1016/0266-7681(88)90058-7
170. Guitton TG, Ring D. Interobserver reliability of radial head fracture classification: Two-dimensional compared with three-dimensional CT. *J Bone Jt Surg - Ser A*. 2011;93(21):2015-2021. doi:10.2106/JBJS.J.00711
171. Andersen DJ, Blair WF, Steyers J, Adams BD, El-Khouri GY, Brandser EA. Classification of distal radius fractures: An analysis of interobserver reliability and intraobserver reproducibility. *J Hand Surg Am*. 1996;21(4):574-582. doi:10.1016/S0363-5023(96)80006-2
172. Christersson A, Nysjö J, Berglund L, et al. Comparison of 2D radiography and a semi-automatic CT-based 3D method for measuring change in dorsal angulation over time in distal radius fractures. *Skeletal Radiol*. doi:10.1007/s00256-016-2350-6
173. de Muinck Keizer RJO, Lechner KM, Mulders MAM, Schep NWL, Eygendaal D, Goslings JC. Three-dimensional virtual planning of corrective osteotomies of distal radius malunions: a systematic review and meta-analysis. *Strateg Trauma Limb Reconstr*. 2017;12(2):77-89. doi:10.1007/s11751-017-0284-8
174. Carelsen B, Jonges R, Strackee SD, et al. Detection of in vivo dynamic 3-D motion patterns in the wrist joint. *IEEE Trans Biomed Eng*. 2009;56(4):1236-1244. doi:10.1109/TBME.2008.2009069

175. Foumani M, Strackee SD, Jonges R, et al. In-vivo three-dimensional carpal bone kinematics during flexion-extension and radio-ulnar deviation of the wrist: Dynamic motion versus step-wise static wrist positions. *J Biomech*. 2009;42(16):2664-2671. doi:10.1016/j.jbiomech.2009.08.016

176. Marai GE, Crisco JJ, Laidlaw DH. A kinematics-based method for generating cartilage maps and deformations in the multi-articulating wrist joint from CT images. In: *Annual International Conference of the IEEE Engineering in Medicine and Biology - Proceedings*. ; 2006:2079-2082. doi:10.1109/IEMBS.2006.259742

177. Kwong Y, Mel AO, Wheeler G, Troupis JM. Four-dimensional computed tomography (4DCT): A review of the current status and applications. *J Med Imaging Radiat Oncol*. 2015;59(5):545-554. doi:10.1111/1754-9485.12326

178. Wassilew GI, Janz V, Heller MO, et al. Real time visualization of femoroacetabular impingement and subluxation using 320-slice computed tomography. *J Orthop Res*. 2013;31(2):275-281. doi:10.1002/jor.22224

179. Edirisinghe Y, Troupis JM, Patel M, Smith J, Crossett M. Dynamic motion analysis of dart throwers motion visualized through computerized tomography and calculation of the axis of rotation. *J Hand Surg Eur Vol*. 2014;39(4):364-372. doi:10.1177/1753193413508709

180. Shapeero LG, Dye SF, Lipton MJ, Gould RG, Galvin EG, Genant HK. Functional dynamics of the knee joint by ultrafast, cine-CT. *Invest Radiol*. 1988;23(2):118-123. doi:10.1097/00004424-198802000-00007

181. Shaw CB, Foster BH, Borgese M, et al. Real-time three-dimensional MRI for the assessment of dynamic carpal instability. *PLoS One*. 2019;14(9). doi:10.1371/journal.pone.0222704

182. Wright TW, Dobyns JH, Linscheid RL, Macksoud W, Siegert J. Carpal instability non-dissociative. *J Hand Surg Am*. 1994;19(6):763-773. doi:10.1016/0266-7681(94)90255-0

183. Schmitt R, Froehner S, Coblenz G, Christopoulos G. Carpal instability. *Eur Radiol*. 2006;16(10):2161-2178. doi:10.1007/s00330-006-0161-1

184. Cerezal L, Del Piñal F, Abascal F, García-Valtuille R, Pereda T, Canga A. Imaging findings in ulnar-sided wrist impaction syndromes. *Radiographics*. 2002;22(1):105-121. doi:10.1148/radiographics.22.1.g02ja01105

185. Watanabe A, Souza F, Vezeridis PS, Blazar P, Yoshioka H. Ulnar-sided wrist pain. II. Clinical imaging and treatment. *Skeletal Radiol*. 2010;39(9):837-857. doi:10.1007/s00256-009-0842-3

186. Kim JP, Park MJ. Assessment of Distal Radioulnar Joint Instability After Distal Radius Fracture: Comparison of Computed Tomography and Clinical Examination Results. *J Hand Surg Am*. 2008;33(9):1486-1492. doi:10.1016/j.jhsa.2008.05.017

187. Crisco JJ, Moore DC, Marai GE, et al. Effects of distal radius malunion on distal radioulnar joint mechanics—an in vivo study. *J Orthop Res*. 2007;25(4):547-555. doi:10.1002/jor.20322

188. Werner F, St-Amand H, Moritomo H, Sutton L, Short W. The Effect of Scaphoid Fracture Site on Scaphoid Instability Patterns. *J Wrist Surg*. 2015. doi:10.1055/s-0035-1570396

189. Dias JJ, Singh HP, Dias J J, Singh P. Displaced fracture of the waist of the scaphoid. *J Bone Jt Surg Br*. 2011;93(11):93-1433. doi:10.1302/0301-620X.93B11

190. Gillette BP, Amadio PC, Kakar S. Long-Term Outcomes of Scaphoid Malunion. *Hand (N Y)*. 2017;12(1):26-30. doi:10.1177/1558944716643295

191. Modaresi S, Kallem MS, Lee P, McIff TE, Toby EB, Fischer KJ. Evaluation of midcarpal capitate contact mechanics in normal, injured and post-operative wrists. *Clin Biomech*

(Bristol, Avon). 2017;47:96-102. doi:10.1016/j.clinbiomech.2017.06.008

192. Belhaouane R, Lebeau N, Maes-Clavier C, et al. Reproducibility of X-rays and CT arthrography in SLAC, SNAC, SCAC wrists. *Hand Surg Rehabil*. 2016. doi:10.1016/j.hansur.2016.08.006

193. Bain G, Bennett J, Richards R, Slethaug G, Roth J. Longitudinal computed tomography of the scaphoid: a new technique. *Skeletal Radiol*. 1995;24(4). doi:10.1007/BF00198413

194. Kellgren JH, Lawrence JS. Radiological Assessment of Osteo-Arthrosis. *Ann Rheum Dis*. 1957;16(4):494-502. doi:10.1136/ard.16.4.494

195. Pollock J, O'Toole R V., Nowicki SD, Eglseder WA. Articular Cartilage Thickness at the Distal Radius: A Cadaveric Study. *J Hand Surg Am*. 2013;38(8):1477-1481. doi:10.1016/j.jhsa.2013.04.037

196. Catalano LW, Cole RJ, Gelberman RH, Evanoff BA, Gilula LA, Borrelli J. Displaced intra-articular fractures of the distal aspect of the radius. Long-term results in young adults after open reduction and internal fixation. *J Bone Joint Surg Am*. 1997;79(9):1290-1302. http://www.ncbi.nlm.nih.gov/pubmed/9314391. Accessed February 1, 2019.

197. Andriacchi TP, Mündermann A, Smith RL, Alexander EJ, Dyrby CO, Koo S. A framework for the in vivo pathomechanics of osteoarthritis at the knee. *Ann Biomed Eng*. 2004;32(3):447-457. http://www.ncbi.nlm.nih.gov/pubmed/15095819. Accessed September 10, 2019.

198. Johnson JE, Lee P, McIff TE, Toby EB, Fischer KJ. Effectiveness of surgical reconstruction to restore radiocarpal joint mechanics after scapholunate ligament injury: An in vivo modeling study. *J Biomech*. 2013;46(9):1548-1553. doi:10.1016/j.jbiomech.2013.03.020

199. Boe CC, Amadio PC, Kakar S. The Management of the Healed Scaphoid Malunion: What to Do? *Hand Clin*. 2019;35(3):373-379. doi:10.1016/J.HCL.2019.03.008

200. Dias JJ, Singh HP. Displaced fracture of the waist of the scaphoid. *J Bone Joint Surg Br*. 2011;93-B(11):1433-1439. doi:10.1302/0301-620X.93B11.26934

201. Zhao K, Breighner R, Holmes D, Leng S, McCollough C, An K-N. A Technique for Quantifying Wrist Motion Using Four-Dimensional Computed Tomography: Approach and Validation. *J Biomech Eng*. 2015. doi:10.1115/1.4030405

202. Jupiter JB. *Current Conce, Pts Review Fractures of the Distal. End of the Radius*.; 1991. http://sites.surgery.northwestern.edu/reading/Documents/curriculum/Box 01/11000299.pdf. Accessed June 8, 2019.

203. Cole JM, Obletz BE. Comminuted fractures of the distal end of the radius treated by skeletal transfixion in plaster cast. An end-result study of thirty-three cases. *J Bone Joint Surg Am*. 1966;48(5):931-945. http://www.ncbi.nlm.nih.gov/pubmed/5942809. Accessed June 8, 2019.

204. Giannoudis P V., Tzioupis C, Papathanassopoulos A, Obakponovwe O, Roberts C. Articular step-off and risk of post-traumatic osteoarthritis. Evidence today. *Injury*. 2010;41(10):986-995. doi:10.1016/j.injury.2010.08.003

205. Foumani M, Strackee SD, van de Giessen M, Jonges R, Blankevoort L, Streekstra GJ. In-vivo dynamic and static three-dimensional joint space distance maps for assessment of cartilage thickness in the radiocarpal joint. *Clin Biomech*. 2013;28(2):151-156. doi:10.1016/j.clinbiomech.2012.11.005

206. Rainbow MJ, Wolff AL, Crisco JJ, Wolfe SW. Functional kinematics of the wrist. *J Hand Surg (European Vol*. 2016;41(1):7-21. doi:10.1177/1753193415616939

207. Tay SC, Primak AN, Fletcher JG, et al. Four-dimensional computed tomographic imaging in the wrist: Proof of feasibility in a cadaveric model. *Skeletal Radiol*. 2007.

doi:10.1007/s00256-007-0374-7

208. Miyake J, Murase T, Yamanaka Y, Moritomo H, Sugamoto K, Yoshikawa H. Comparison of three dimensional and radiographic measurements in the analysis of distal radius malunion. *J Hand Surg (European Vol*. 2013;38(2):133-143. doi:10.1177/1753193412451383

209. Kihara H, Palmer AK, Werner FW, Short WH, Fortino MD. The effect of dorsally angulated distal radius fractures on distal radioulnar joint congruency and forearm rotation. *J Hand Surg Am*. 1996;21(1):40-47. doi:10.1016/S0363-5023(96)80152-3

210. Haus BM, Jupiter JB. Intra-articular fractures of the distal end of the radius in young adults: reexamined as evidence-based and outcomes medicine. *J Bone Joint Surg Am*. 2009;91(12):2984-2991. doi:10.2106/JBJS.I.00269

211. Buzzatti L, Keelson B, Apperloo J, et al. Four-dimensional CT as a valid approach to detect and quantify kinematic changes after selective ankle ligament sectioning. *Sci Rep*. 2019;9(1):1-9. doi:10.1038/s41598-018-38101-5

212. Kelbauskas L, Shetty R, Cao B, et al. Optical computed tomography for spatially isotropic four-dimensional imaging of live single cells. *Sci Adv*. 2017;3(12):e1602580. doi:10.1126/sciadv.1602580

213. Zhao K, Breighner R, Holmes D, et al. A technique for quantifying wrist motion using four-dimensional computed tomography: approach and validation. *J Biomech Eng*. 2015;137(7):0745011. doi:10.1115/1.4030405

214. Müller ME, Koch P, Nazarian S, et al. Principles of the Classification of Fractures. In: *The Comprehensive Classification of Fractures of Long Bones*. Springer Berlin Heidelberg; 1990:4-7. doi:10.1007/978-3-642-61261-9_2

215. Jayakumar P, Teunis T, Giménez B, Verstreken F, Di Mascio L, Jupiter J. AO Distal Radius Fracture Classification: Global Perspective on Observer Agreement. *J Wrist Surg*. 2016;06(01):046-053. doi:10.1055/s-0036-1587316

216. Rainbow MJ, Kamal RN, Leventhal E, et al. In Vivo Kinematics of the Scaphoid, Lunate, Capitate, and Third Metacarpal in Extreme Wrist Flexion and Extension. *J Hand Surg Am*. 2013;38(2):278-288. doi:10.1016/j.jhsa.2012.10.035

217. Lee DJ, Elfar JC. Carpal Ligament Injuries, Pathomechanics, and Classification. *Hand Clin*. 2015;31(3):389-398. doi:10.1016/j.hcl.2015.04.011

218. Lalone EA, McDonald CP, Ferreira LM, Peters TM, King GW, Johnson JA. Development of an image-based technique to examine joint congruency at the elbow. *Comput Methods Biomech Biomed Engin*. 2013;16(3):280-290. doi:10.1080/10255842.2011.617006

219. van den Borne MPJ, van't Hof BWL, Prins HJ, Vincken KL, Schuurman AH, Castelein RM. The distal radio-ulnar joint: Persisting deformity in well reduced distal radius fractures in an active population. *Inj Extra*. 2007;38(11):377-383. doi:10.1016/j.injury.2007.02.034

Appendix A — Glossary

Active Motion	Muscle forces move a joint
Arthritis	A degenerative disorder affecting a joint
Biomechanics	The study of forces produced
Computed Tomography	Three-dimensional medical imaging method
Distal	Away from origin or attachment point
Dynamic	Images in motion (real-time)
Extension	Increases the angle between two body parts
Flexion	Decreases the angle between two body parts
Humpback	The lateral intrascaphoid angle increased due to the shortening of the palmar cortical length
In-Vitro	Experiment conducted within a living body
In-Vivo	Experiment conducted outside a living body
Joint Congruency	Relative positions of two bone surfaces articulating in a joint
Kinematics	The study of motion
Kinetics	The study of forces
Malunion	Healing of a fracture in a non-anatomical position
Passive	External forces move a joint
Static	Contains one-time frame
Union	Healing of a fracture

PUNEET RANOTA

EDUCATION

MESc in Biomedical Engineering   2019 to 2020
The University of Western Ontario, London, ON

BMSc in Medical Sciences   2014 to 2018
The University of Western Ontario, London, ON

AWARDS

Western Research Graduate Scholarship	2019 to 2020
CMHR Transdisciplinary Bone & Joint Training Award	2019 to 2020
Dean's Honor List	2014, 2017
Entrance Scholarship of Excellence	2014

RELATED WORK EXPERIENCE

Teaching Assistant for Foundations of Engineering Practice   2019 to 2020
 Faulty of Engineering, Western University, London, Ontario
- Collaborated with a fellow TA for course grading, preparation, and classroom management
- Motivated and engaged students in course materials

Summer Student Mentor   2019 to 2020
Human Biomechanics Lab, London, Ontario
- Mentored research assistants, ensuring proper understanding of concepts and completion of assigned roles

Teaching Assistant for Biology for Sciences II   2020
 Faulty of Science, Western University, London, Ontario
- Aided students with experiment completion and understanding by demonstrating proper lab techniques and relating concepts back to lecture

Teaching Assistant for Applied Industrial Organic Chemistry   2019
 Faulty of Engineering, Western University, London, Ontario
- Led laboratory sections, graded weekly lab reports and provided constructive criticism to improve students' writing ability

Western Engineering Summer Academy Instructor   2019
Western University, London, Ontario
- Designed Biomedical Engineering lecture series in a team that resulted in achieving high participation and engagement from high school students

3rd Slicer Project Week   2019
Western University, London, Ontario
- Learned to use the 3DSlicer software, modified existing data analysis methods to meet research project objectives, and trained lab members

Medical Sciences Laboratory Student 2017
Western University, London, Ontario
- Conducted a research study (investigating the relationship between metformin and Alzheimer's Disease) from design to analysis and reported conclusions in a detailed report and poster presentation

Volunteer Research Assistant 2016 to 2017
Anatomy and Cell Biology Lab, London, Ontario
- Applied molecular biology techniques (PCR, western blot, etc.)
- Worked alongside graduate students in experiment execution and obtaining data, and presented findings in weekly lab meetings

PRESENTATIONS AND PUBLICATIONS

Ranota, P., Holdsworth D., MacDermid J., Suh N., Lalone E. (2020). The Effect of Distal Radius Fractures on Joint Mechanics, Osteoarthritis, and Patient Outcomes. Presented at Western's Bone & Joint Institute Showcase (Virtual), September 15.

Ranota, P., Lee T., Suh N., Lalone E. (2020). Four-Dimensional Computed Tomography (4DCT) to Measure Distal-radial and Radio-carpal Joint Congruency Following Wrist Fracture. Poster presented at Canadian Orthopaedic Association Annual Meeting (Virtual), June 19-20.

Ranota, P., Lee T., Suh N., Lalone E. (2020). 4DCT to Examine Joint Congruency Following Wrist Fracture. Podium presented at Canadian Bone and Joint Conference (Virtual), June 11-13.

Ranota, P., Suh N., Lalone E. (2020). 4DCT to Measure Distal Radial-Ulnar and Radio-Carpal Joint Congruency Following Distal Radius Fractures (submitted in May to the *Journal of Orthopaedic Research*).

Ranota, P., Lee T., Suh N., Lalone E. (2020). 4DCT to Measure Distal-radial and Radio-carpal Joint Congruency Following Wrist Fracture. Podium presented at Imaging Network Ontario Symposium (Virtual), March 26-27.

Ranota, P., Lee T., Suh N., Lalone E. (2020). 4DCT to Measure Distal-radial and Radio-carpal Joint Congruency Following Wrist Fracture. Poster presented at Orthopaedic Research Society Annual Meeting, Phoenix, Arizona, February 8-11.

Ranota, P., Seltser A., Grewal R., Suh N., Lalone E. (2019). The Effect of Scaphoid Malunion on Contact Mechanics. (submitted in November to the *Journal of Hand Surgery*).

Ranota, P., Riddle M., Lee T., Suh N., Lalone E. (2019). 4DCT to Examine Wrist Contact Mechanics. Poster presented at the Ontario Biomechanics Conference, Alliston, Ontario, March 8-10.

Ranota, P., Riddle M., Lee T., Suh N., Lalone E. (2019). 4DCT to Examine Wrist Contact Mechanics. Poster presented at the Annual Imaging Network Ontario Symposium, London, Ontario, March 28-29.